HEALTH AND MEDICINE

Distinct roles of ORAI1 in T cell–mediated allergic airway inflammation and immunity to influenza A virus infection

Yin-Hu Wang[1]†, Lucile Noyer[1]†, Sascha Kahlfuss[1]†‡, Dimitrius Raphael[1], Anthony Y. Tao[1], Ulrike Kaufmann[1]§, Jingjie Zhu[1], Marisa Mitchell-Flack[1], Ikjot Sidhu[1], Fang Zhou[1], Martin Vaeth[1]||, Paul G. Thomas[2], Sean P. Saunders[3], Kenneth Stauderman[4], Maria A. Curotto de Lafaille[3]¶, Stefan Feske[1]*

T cell activation and function depend on Ca^{2+} signals mediated by store-operated Ca^{2+} entry (SOCE) through Ca^{2+} release–activated Ca^{2+} (CRAC) channels formed by ORAI1 proteins. We here investigated how SOCE controls T cell function in pulmonary inflammation during a T helper 1 (T_H1) cell–mediated response to influenza A virus (IAV) infection and T_H2 cell–mediated allergic airway inflammation. T cell–specific deletion of *Orai1* did not exacerbate pulmonary inflammation and viral burdens following IAV infection but protected mice from house dust mite–induced allergic airway inflammation. ORAI1 controlled the expression of genes including p53 and E2F transcription factors that regulate the cell cycle in T_H2 cells in response to allergen stimulation and the expression of transcription factors and cytokines that regulate T_H2 cell function. Systemic application of a CRAC channel blocker suppressed allergic airway inflammation without compromising immunity to IAV infection, suggesting that inhibition of SOCE is a potential treatment for allergic airway disease.

INTRODUCTION

T cell activation depends on Ca^{2+} signals following T cell receptor (TCR) engagement. Ca^{2+} signals regulate many aspects of T cell function including gene expression, cytokine production, metabolism, and proliferation (*1*, *2*). Ca^{2+} influx after antigen binding to the TCR is mediated by the highly Ca^{2+}-selective Ca^{2+} release–activated Ca^{2+} (CRAC) channel in the plasma membrane (*3*, *4*). In T cells, CRAC channels are formed by ORAI1 and its homolog ORAI2, which are tetraspanning membrane proteins that assemble as hexameric complexes and form the pore of the channel (*5*). CRAC channels are bound and opened by stromal interaction molecule 1 (STIM1) and STIM2, two single-pass membrane protein in the endoplasmic reticulum (ER). The activation of STIM proteins follows the release of Ca^{2+} from the ER through inositol 1,4,5-trisphosphate (IP_3) receptors, which are Ca^{2+}-permeable channels in the ER membrane that open upon TCR stimulation, activation of phospholipase C–γ, and production of IP_3. Because the activation of STIM and ORAI proteins is regulated by the Ca^{2+} concentration in the ER, this form of Ca^{2+} influx is called store-operated Ca^{2+} entry (SOCE). Complete lack of SOCE due to inherited mutations in *ORAI1* and *STIM1* genes causes combined immunodeficiency (CID) defined by recurrent infections with viral, bacterial, and fungal pathogens in human patients (*6*). In mice, combined deletion of both *Orai1* and *Orai2* or *Stim1* and *Stim2* genes in T cells is necessary to abolish SOCE and to impair immunity to infection with viral and fungal pathogens (*7*–*9*). T cell–specific deletion of *Orai1* or *Stim1* alone, by contrast, reduces SOCE only partially and does not impair immunity to infection with lymphocytic choriomeningitis virus (LCMV) (*8*, *10*). Deletion of *Orai1* or *Stim1* in T cells protects mice from T cell–mediated autoimmunity in rodent models of inflammatory bowel disease (IBD), experimental autoimmune encephalomyelitis (EAE), graft-versus-host disease (GvHD), and psoriasiform skin inflammation (*8*, *11*–*16*). Protection is due to impaired production of T helper 1 (T_H1) and T_H17 cytokines including interferon-γ (IFN-γ), interleukin-17A (IL-17A), and granulocyte-macrophage colony-stimulating factor; attenuated expression of the T_H17 cell–specific transcription factor RAR-related orphan receptor gamma t (RORγt); and defects in the metabolic function of T_H17 cells. The role of SOCE in the differentiation and function of T_H2 cells is not well understood. The Ca^{2+}-regulated transcription factor nuclear factor of activated T cells (NFAT), however, is well known to control the expression of the T_H2 cytokines IL-4, IL-5, and IL-13, by binding to the promoters of all three genes (*17*).

Allergic asthma (AA) is a chronic inflammatory airway disease, which, in 50 to 70% of patients, is characterized by type 2 inflammation with increased levels of T_H2 cytokines, enhanced immunoglobulin E (IgE) production, and eosinophilia (*18*). Airway inflammation in AA is triggered by a plethora of aeroallergens, including house dust mite (HDM) feces, which stimulate the release of cytokines such as IL-33, IL-25, and thymic stromal lymphopoietin (TSLP) from airway epithelial cells (AECs) (*19*). These mediators recruit T_H2 cells that produce cytokines including IL-4, which triggers B cell maturation and IgE production, and IL-5, which enhances IgE production and mobilizes eosinophils from the bone marrow. T_H2 cells are characterized by the expression of the transcription factor GATA-binding protein 3 (GATA3) and the type 2 cytokines IL-4, IL-5, and IL-13 (*20*). Little is known about the role of SOCE in T_H2 cells

[1]Department of Pathology, New York University Grossman School of Medicine, New York, NY 10016, USA. [2]St. Jude's Children's Research Hospital, Memphis, TN 38105, USA. [3]Division of Pulmonary, Critical Care and Sleep Medicine, Departments of Medicine and Cell Biology, New York University Grossman School of Medicine, NY 10016, USA. [4]CalciMedica Inc., La Jolla, CA 92037, USA.
*Corresponding author. Email: feskes01@nyumc.org
†These authors contributed equally to this work.
‡Present address: Institute of Molecular and Clinical Immunology, Institute of Medical Microbiology and Hospital Hygiene, Medical Faculty, Otto-von-Guericke-University, Magdeburg, Germany.
§Present address: Genentech, South San Francisco, CA 94080, USA.
||Present address: Max Planck Research group for Systems Immunology, Julius Maximilians University, Wuerzburg, Germany.
¶Present address: Icahn School of Medicine at Mount Sinai, New York, NY 10029, USA.

and type 2 immune responses. The expression of IL-4 is reduced in SOCE-deficient murine T cells (*8*, *21*–*23*) and in T cells of patients with loss-of-function mutations in *STIM1* and *ORAI1* (*24*). By contrast, ectopic expression of STIM1 or STIM2 elevated IL-4 production in murine $CD4^+$ T cells in vitro (*23*). Treatment of mice with two different CRAC channel inhibitors prevented ovalbumin (OVA)–induced, late-phase asthmatic responses in animal models (*25*–*27*). However, whether these effects were due to altered T cell function remains unknown because CRAC channels and SOCE were also shown to mediate cytokine production in AECs treated with HDM allergens (*28*, *29*).

Influenza A viruses (IAVs) cause annual epidemics with high mortality especially in infants and elderly (*30*, *31*). Immunity against IAV is mediated by $CD4^+$ and $CD8^+$ T cells as well as neutralizing antibodies. $CD4^+$ T cells differentiate into T_H1 cells that express proinflammatory cytokines such as IFN-γ and tumor necrosis factor–α (TNF-α) and may differentiate into lung-resident memory T cells that control influenza infection (*32*–*34*). $CD4^+$ T cell help is also required for an effective $CD8^+$ T cell memory response during IAV infection (*35*). In addition, $CD4^+$ T follicular helper (T_{fh}) cells promote humoral immunity by providing costimulation to B cells in germinal centers (GCs) and helping them mature into antibody-producing long-lived plasma cells or memory B cells (*36*). This function of T_{fh} cells is mediated by molecules such as CD40L and ICOS (inducible T cell costimulator) and cytokines such as IL-4 and IL-21. T_{fh} cell differentiation requires CRAC channels because mice with T cell–specific deletion of *Stim1* and *Stim2* and abolished SOCE have strongly decreased numbers of T_{fh} cells and GC B cells and lack class-switched, antigen-specific antibodies after viral infection (*9*). SOCE controls the differentiation of T_{fh} cells and the expression of CD40L, ICOS, IL-4, IL-21, and other factors required for T_{fh} cell function. Only complete deletion of SOCE in mice with T cell–specific deletion of either *Orai1* and *Orai2* or *Stim1* and *Stim2* compromises T_{fh} cell function and antiviral immunity (*8*, *9*), whereas no defects are observed after deletion of *Orai1* or *Stim1* alone (*8*, *10*). The quantitative requirements of SOCE for adaptive immunity to IAV infection are not known.

Given the SOCE-dependent role of T cells in adaptive immunity to viral and other infections on one hand and the protective effects of SOCE inhibition in autoimmune disease models on the other, the question arises whether CRAC channel inhibition is a possible treatment for autoimmune and allergic inflammation without compromising immunity to infection. To address this question, we compared how genetic and pharmacological suppression of CRAC channel function affects immunity to IAV infection and inflammation in HDM-induced AA. We found that T cell–specific deletion of *Orai1* leaves immunity to the H3N2 strain of IAV largely intact because viral burdens and pulmonary inflammation were comparable to wild-type (WT) controls. By contrast, deletion of *Orai1* protected mice from HDM-induced allergic airway inflammation, which was due to impaired antigen-specific expansion, differentiation, and function of T_H2 cells. These defects, in turn, were associated with altered expression of genes that regulate cell cycle progression and are required for establishing and maintaining the T_H2 cell differentiation program including the transcription factors GATA3, interferon regulatory factor 4 (IRF4), and basic leucine zipper ATF-like transcription factor (BATF) and cytokines IL-2 and IL-4. Treatment of mice with the CRAC channel inhibitor CM4620 suppressed allergic airway inflammation but did not compromise immunity to IAV infection. Collectively, our data suggest that T_H2 cell–mediated airway inflammation is more dependent on CRAC channels than T_H1 cell–mediated antiviral immunity. These findings may have important implications for the treatment of AA and other T cell–dependent inflammatory diseases.

RESULTS

T cell–specific deletion of *Orai1* does not exacerbate IAV infection

Given the important role of SOCE in T cell–mediated immunity to infection in humans and mice (*1*), we speculated that deletion of *Orai1*, the dominant CRAC channel homolog in T cells, may result in compromised immune responses to IAV infection. To test this hypothesis, we infected $Orai1^{fl/fl}Cd4Cre$ and WT control mice intranasally with a single dose of the laboratory strain A/HK/x31 (Hkx31, H3N2) of IAV that was engineered to express $OVA_{323–339}$ (IAV^{OVA}) (Fig. 1A) (*37*). Note that both $CD4^+$ and $CD8^+$ T cells of $Orai1^{fl/fl}Cd4Cre$ mice lack ORAI1 protein (fig. S1A) and have reduced (but not abolished) SOCE (fig. S1B) because of *Cd4Cre* expression at the $CD4^+$ $CD8^+$ double-positive stage of T cell development in the thymus. All infected WT and $Orai1^{fl/fl}Cd4Cre$ mice survived and experienced a similar ~10% reduction in body weight at day 7 before starting to recover (Fig. 1B). The histological analysis of lungs from mice at day 9 postinfection (p.i.) showed comparable pulmonary inflammation and total alveolar volume fraction between *Orai1*-deficient and WT mice (Fig. 1, C to E). IAV burdens in the lungs of mice were analyzed by quantitative real-time polymerase chain reaction (qRT-PCR) of viral genome segments as previously described (*38*, *39*) and showed no significant differences between WT and $Orai1^{fl/fl}Cd4Cre$ mice at day 9 p.i. (Fig. 1F and fig. S1C).

Normal humoral immune response in IAV infected *Orai1*-deficient mice

Immunity to pulmonary infection with IAV is mediated by several T cell subsets including $CD8^+$ cytotoxic T lymphocytes and $CD4^+$ T_H1 and T_{fh} cells (*40*). To understand the effects of *Orai1* deletion on T cells in the lung during IAV infection, we analyzed the mediastinal lymph nodes (mLNs) and lungs of $Orai1^{fl/fl}Cd4Cre$ and WT littermate mice after infection with IAV^{OVA}. We observed moderately higher frequencies but normal total numbers of $CD4^+$ T cells in the lungs of $Orai1^{fl/fl}Cd4Cre$ mice at day 9 p.i. compared to WT littermates, whereas frequencies of *Orai1*-deficient $CD8^+$ T cells were normal (fig. S1D). The frequencies and total numbers of all $CD4^+CD44^+CD62L^-$ effector T cells in the lungs of *Orai1*-deficient and WT mice were comparable, with moderate but significant reduction in the frequencies of IAV-specific $CD4^+CD44^+CD62L^-NP_{311–325}{}^+$ effector T cells in $Orai1^{fl/fl}Cd4Cre$ mice (fig. S1E). Moreover, the frequencies and total numbers of $CD8^+$ naïve, effector, and effector memory T cells were similar in both cohorts of mice (fig. S1F). Likewise, the frequencies and numbers of $CD4^+$ and $CD8^+$ tissue-resident memory T cells in the lungs of $Orai1^{fl/fl}Cd4Cre$ and WT mice were comparable. Overall, these data show that lack of ORAI1 and reduced SOCE in T cells does not grossly affect the composition of the IAV-specific T cell compartment.

We had previously reported that complete abolition of SOCE in *Orai1/Orai2*- or *Stim1/Stim2*-deficient T cells impairs T_{fh} cell differentiation and function and thus humoral immunity to LCMV infection (*8*, *9*). We therefore analyzed the numbers of IAV-specific T_{fh} cells ($CD4^+CD44^+PD\text{-}1^+CXCR5^+NP_{311–325}{}^+$) in the mLNs of $Orai1^{fl/fl}Cd4Cre$ mice. Whereas the frequencies of IAV-specific T_{fh} cells were slightly reduced in the absence of ORAI1, their total numbers were comparable to WT mice (Fig. 1G). The frequencies and numbers of

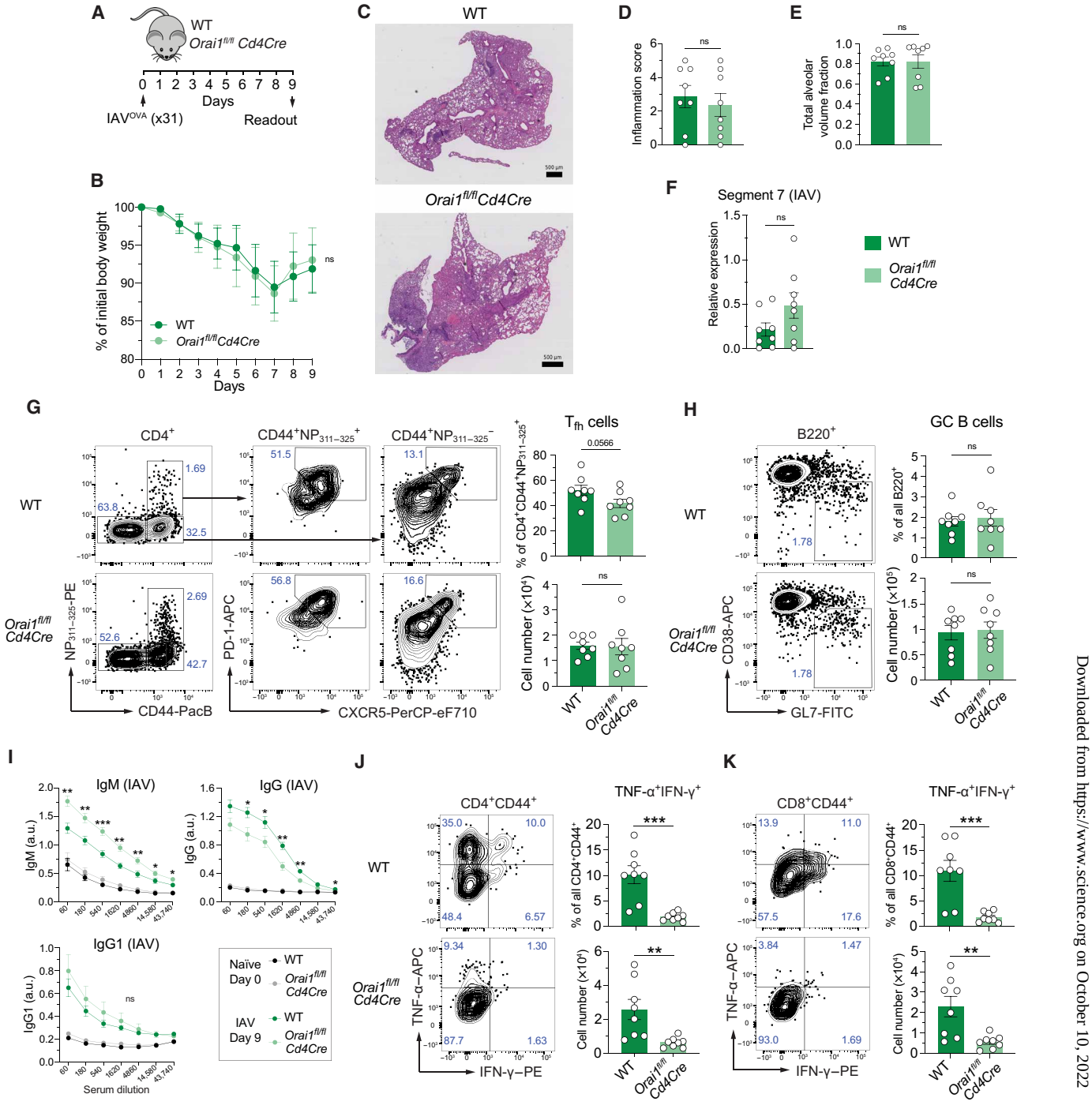

Fig. 1. Deletion of *Orai1* in T cells does not attenuate pulmonary inflammation and antibody production after infection with IAV. (**A**) Mouse model of x31 (H3N2) IAV infection. (**B**) Body weight of WT versus *Orai1*$^{fl/fl}$*Cd4Cre* mice after infection with IAV, shown as weight normalized to day 0. (**C**) Representative hematoxylin and eosin (H&E) stains of lungs from WT and *Orai1*$^{fl/fl}$*Cd4Cre* mice at day 9 after infection with x31 influenza A. Scale bar, 500 μm. (**D**) Inflammation score calculated from the lungs of WT and *Orai1*$^{fl/fl}$*Cd4Cre* mice at day 9 following IAV infection. (**E**) Total alveolar volume fraction of lungs from WT and *Orai1*$^{fl/fl}$*Cd4Cre* mice. (**F**) qRT-PCR analysis of IAV (segment 7) levels in total lung tissue from WT versus *Orai1*$^{fl/fl}$*Cd4Cre* mice at day 9 after infection. (**G**) Representative flow cytometry plots of IAV-specific CXCR5^{+}PD-1^{+} T$_{fh}$ cells, their frequencies (%), and absolute numbers in mediastinal lymph nodes (mLNs) from WT and *Orai1*$^{fl/fl}$*Cd4Cre* mice 9 days after IAV infection. (**H**) Representative flow cytometry plots of B220^{+}CD38^{-}GL7^{+} GC B cells, their frequencies (%), and absolute numbers in mLNs from WT and *Orai1*$^{fl/fl}$*Cd4Cre* mice 9 days after IAV infection. FITC, fluorescein isothiocyanate. (**I**) IAV (x31)–specific IgM, IgG, and IgG1 levels in the serum of WT and *Orai1*$^{fl/fl}$*Cd4Cre* mice before (day 0) and after (day 9) IAV infection. a.u., arbitrary units. (**J** and **K**) Analysis of TNF-α– and IFN-γ–producing CD4^{+}CD44^{+} (J) and CD8^{+}CD44^{+} (K) T cells from mLNs of WT and *Orai1*$^{fl/fl}$*Cd4Cre* mice at day 9 after IAV infection. Representative flow cytometry plots, frequencies (%), and total numbers of T cells. Data in (A) to (K) are the means ± SEM of eight WT and eight *Orai1*$^{fl/fl}$*Cd4Cre* mice and two independent experiments. Statistical analysis is performed by unpaired Student's *t* test with the following significance levels: ***$P < 0.001$; **$P < 0.01$; *$P < 0.05$. ns, not significant.

$B220^+CD38^-GL7^+$ GC B cells were similar in IAV-infected WT and *Orai1*$^{fl/fl}$*Cd4Cre* mice (Fig. 1H). In line with slightly reduced T_{fh} cell frequencies in mLNs, we observed moderately lower levels of IAV-specific IgG antibodies in the serum of *Orai1*$^{fl/fl}$*Cd4Cre* mice, whereas IAV-specific IgG1 antibodies were comparable to WT mice. Conversely, IAV-specific IgM titers were higher in *Orai1*-deficient mice, suggesting that lack of ORAI1 in T cells results in a moderate decrease in Ig class switching or differentiation of plasma cells (Fig. 1I). IAV infection induces the production of IFN-γ and TNF-α by T cells, which contribute to immunity to IAV and cause tissue damage, respectively (*41*–*43*). We measured the numbers of effector $CD4^+$ and $CD8^+$ T cells producing both cytokines 9 days after IAV infection. The percentages and absolute numbers of TNF-α^+IFN-γ^+ double-producing $CD4^+CD44^+$ and $CD8^+CD44^+$ effector T cells were significantly reduced in *Orai1*$^{fl/fl}$*Cd4Cre* compared to WT mice (Fig. 1, J and K). To further validate our findings, we tested the effects of *Orai1* deletion in T cells in another viral infection model by inoculating *Orai1*$^{fl/fl}$*Cd4Cre* and WT mice with the Armstrong strain of LCMV. Ten days after LCMV infection, the frequencies of T_{fh} cells and GC B cells in the spleen and mesenteric lymph nodes of WT and *Orai1*-deficient mice were comparable, and robust GC formation was observed in both strains (fig. S2, A to C). Furthermore, the numbers of $CD4^+CXCR5^{hi}PD\text{-}1^{hi}CD44^{hi}Foxp3^+$ T follicular regulatory cells, which are involved in controlling the GC reaction, were similar in LCMV-infected WT and *Orai1*$^{fl/fl}$*Cd4Cre* mice (fig. S2D). Consistent with the above observations, the levels of IgM and class-switched Igs were largely normal, although a moderate reduction in total IgG and IgE levels was found in the serum of *Orai1*-deficient mice (fig. S2E). Together, our findings show that T cell–specific deletion of *Orai1* does not significantly impair immune responses to viral infection, notably IAV.

T cell–specific deletion of *Orai1* protects mice from HDM-induced allergic airway inflammation

We had previously reported that deletion of *Orai1* in T cells significantly attenuates the severity of T cell–mediated inflammation in the EAE model of multiple sclerosis (*12*) and GvHD (*8*). To directly compare the role of ORAI1 in T cell–mediated immunity to IAV infection and inflammation in the same organ, we chose to induce allergic airway inflammation in *Orai1*-deficient mice. To this end, we sensitized WT and *Orai1*$^{fl/fl}$*Cd4Cre* mice intranasally with HDM extract on three consecutive days and rechallenged them with HDM 8 days later (Fig. 2A). Inflammation and cellular and humoral immune responses were investigated 1 day after the last rechallenge by analyzing the lungs, mLNs, bronchoalveolar lavage (BAL) fluid, and blood of mice. To characterize airway inflammation, we stained the lungs of WT and *Orai1*$^{fl/fl}$*Cd4Cre* mice treated with HDM or phosphate-buffered saline (PBS) as control with hematoxylin and eosin (H&E). HDM-challenged WT mice showed severe pulmonary inflammation, which was characterized by peribronchial inflammation, a hallmark of AA, and moderate perivascular cellular infiltrates (Fig. 2, B and C). Peribronchial inflammation was significantly attenuated in HDM-challenged *Orai1*$^{fl/fl}$*Cd4Cre* mice compared to WT littermates. In addition, we found that the increased airway smooth muscle thickness in HDM-treated WT mice was significantly attenuated in HDM-challenged *Orai1*$^{fl/fl}$*Cd4Cre* mice (Fig. 2D). Whereas HDM-induced airway inflammation in WT mice was accompanied by strong mucus production by bronchial epithelial cells identified by periodic acid–Schiff (PAS) staining, a similar increase in mucus production was absent in *Orai1*-deficient mice (Fig. 2E). A common feature of AA is elevated serum IgE levels. We detected significantly lower levels of IgE in the serum of *Orai1*$^{fl/fl}$*Cd4Cre* than WT mice after HDM sensitization and rechallenge (Fig. 2F). Consistent with the pulmonary inflammation in HDM-treated WT mice, we observed significantly elevated numbers of $CD4^+$ T cells as well as B cells in their BAL fluid, which were absent in the BAL of HDM-challenged *Orai1*$^{fl/fl}$*Cd4Cre* mice (Fig. 2G). Similarly, the numbers of $CD4^+$ T cells and B cells in the mLNs of HDM-treated *Orai1*$^{fl/fl}$*Cd4Cre* mice were decreased compared to HDM-treated WT littermates (Fig. 2G). A hallmark of AA is the recruitment of eosinophils to the airways where they play important roles in asthma exacerbation (*44*, *45*). We detected significantly increased frequencies of eosinophils in the BAL fluid of WT mice after HDM immunization, whereas eosinophil frequencies in HDM-treated *Orai1*$^{fl/fl}$*Cd4Cre* mice were significantly lower than those in WT mice (Fig. 2H). Eosinophils express the C-C motif chemokine 3 (CCR3), which is required for their recruitment to the lung (*46*). CCR3 responds to a variety of chemokines, including eotaxin [C-C motif chemokine ligand 11 (CCO11)], eotaxin-3 (CCL26), monocyte-chemotactic protein 3 [MCP-3 (CCL7)], MCP-4 (CCL13), and RANTES [regulated upon activation, normal T cell expressed and secreted (CCL5)] whose production is stimulated by T_H2 cytokines (*47*, *48*). We found that mRNA levels of *Eotaxin1*, *Rantes*, *Mcp3*, and *Mcp1* were significantly lower in the lungs of HDM-treated *Orai1*$^{fl/fl}$*Cd4Cre* mice compared to WT littermates (Fig. 2I), providing a likely explanation for reduced eosinophil frequencies in the absence of ORAI1. Together, our findings demonstrate that the deletion of *Orai1* in T cells significantly attenuates allergic airway inflammation following sensitization and rechallenge with HDM allergen.

Lack of ORAI1 in OVA-specific T cells protects from HDM/OVA-induced airway inflammation without impairing immunity to IAV^{OVA} infection

Because deletion of *Orai1* in T cells protected mice from HDM-induced allergic airway inflammation while maintaining immunity to IAV infection, we investigated the mechanisms underlying this dichotomy. To rule out that the difference is due to different strengths of TCR signaling induced by HDM- and IAV-derived antigens, we generated *Orai1*$^{fl/fl}$*Cd4Cre* OT-II mice whose $CD4^+$ T cells express a transgenic TCR that is specific for OVA. Naïve $CD4^+$ T cells from *Orai1*$^{fl/fl}$*Cd4Cre* OT-II and WT OT-II mice were injected into T cell–deficient TCR$\alpha^{-/-}$ host mice, which were either infected with IAV^{OVA} (Fig. 3A) or immunized with OVA and HDM extract (HDM/OVA) (Fig. 3B). In this model, only the TCR-transgenic, transferred T cells with fixed antigen specificity mediate antiviral and allergic immunity. Following infection with IAV^{OVA}, the lungs of host mice showed similar frequencies and total numbers of *Orai1*$^{fl/fl}$*Cd4Cre* OT-II and WT OT-II donor T cells (Fig. 3C). By contrast, the numbers of *Orai1*$^{fl/fl}$*Cd4Cre* OT-II cells in the lungs of host mice after HDM/OVA immunization and rechallenge were significantly reduced compared to control OT-II cells (Fig. 3D). Pulmonary inflammation after x31 IAV^{OVA} infection was similar in host mice that had received WT OT-II or *Orai1*$^{fl/fl}$*Cd4Cre* OT-II donor T cells (Fig. 3, E and G). By contrast, the lungs of host mice transferred with *Orai1*$^{fl/fl}$*Cd4Cre* OT-II donor cells showed significantly less peribronchial inflammation than recipients of WT OT-II cells after immunization and rechallenge with HDM/OVA (Fig. 3, F and I). The analysis of serum antibodies following x31 IAV^{OVA} infection showed similar titers of IAV^{OVA}-specific

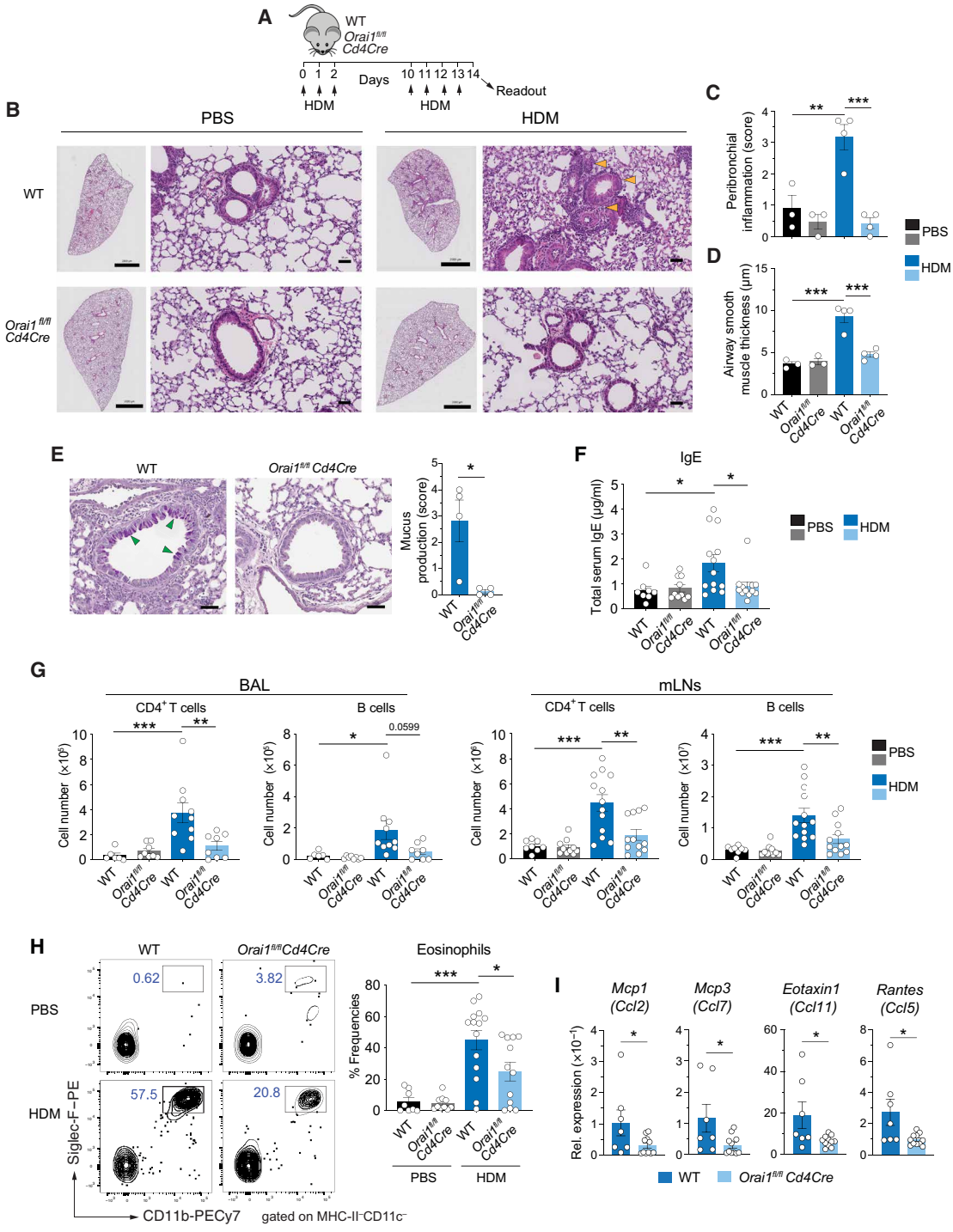

Fig. 2. ORAI1 is essential for T cell–dependent allergic airway inflammation in response to HDM exposure. (**A**) Mouse model of sensitization and rechallenge of mice with HDM extract to induce allergic airway inflammation. (**B**) Representative H&E stains of lungs from WT and *Orai1*$^{fl/fl}$*Cd4Cre* mice at day 14. Scale bars, 2000 μm (right) and 50 μm (left). (**C** and **D**) Analysis of peribronchial inflammation (C) and airway smooth muscle layer thickness (D) of WT and *Orai1*$^{fl/fl}$*Cd4Cre* mice at day 14. (**E**) Representative PAS stains of lungs and quantitative analysis of mucus production of WT and *Orai1*$^{fl/fl}$*Cd4Cre* mice at day 14. Scale bars, 50 μm. (**F**) Total IgE levels in the serum of WT and *Orai1*$^{fl/fl}$*Cd4Cre* mice at day 14. (**G**) Numbers of CD4$^+$ and B220$^+$ B cells in the BAL fluid (left) and mLNs (right) of mice at day 14. (**H**) Representative flow cytometry plots and summary bar graphs showing the frequencies of Cd11b$^+$Siglec-F$^+$ eosinophils within MHC-II$^-$CD11c$^-$ cells in the BAL fluid of WT and *Orai1*$^{fl/fl}$*Cd4Cre* mice at day 14. (**I**) Relative mRNA expression of chemokines in whole lung tissue (qRT-PCR). Data in (C) to (E) are the means ± SEM of three to four mice per group. Data in (F) are the means ± SEM from 8 to 13 mice per cohort. Data in (G) are the means ± SEM from 6 to 13 mice per cohort. Data in (H) are the means ± SEM of 8 to 14 mice per cohort. Data in (I) are the means ± SEM of 7 to 11 mice per cohort. Data are from at least two independent experiments; statistical analysis in (C), (D), and (F) to (H) is performed by one-way analysis of variance (ANOVA) (Tukey's multiple comparisons test) and that in (E) and (I) is performed by unpaired Student's *t* test. ***$P < 0.001$; **$P < 0.01$; *$P < 0.05$.

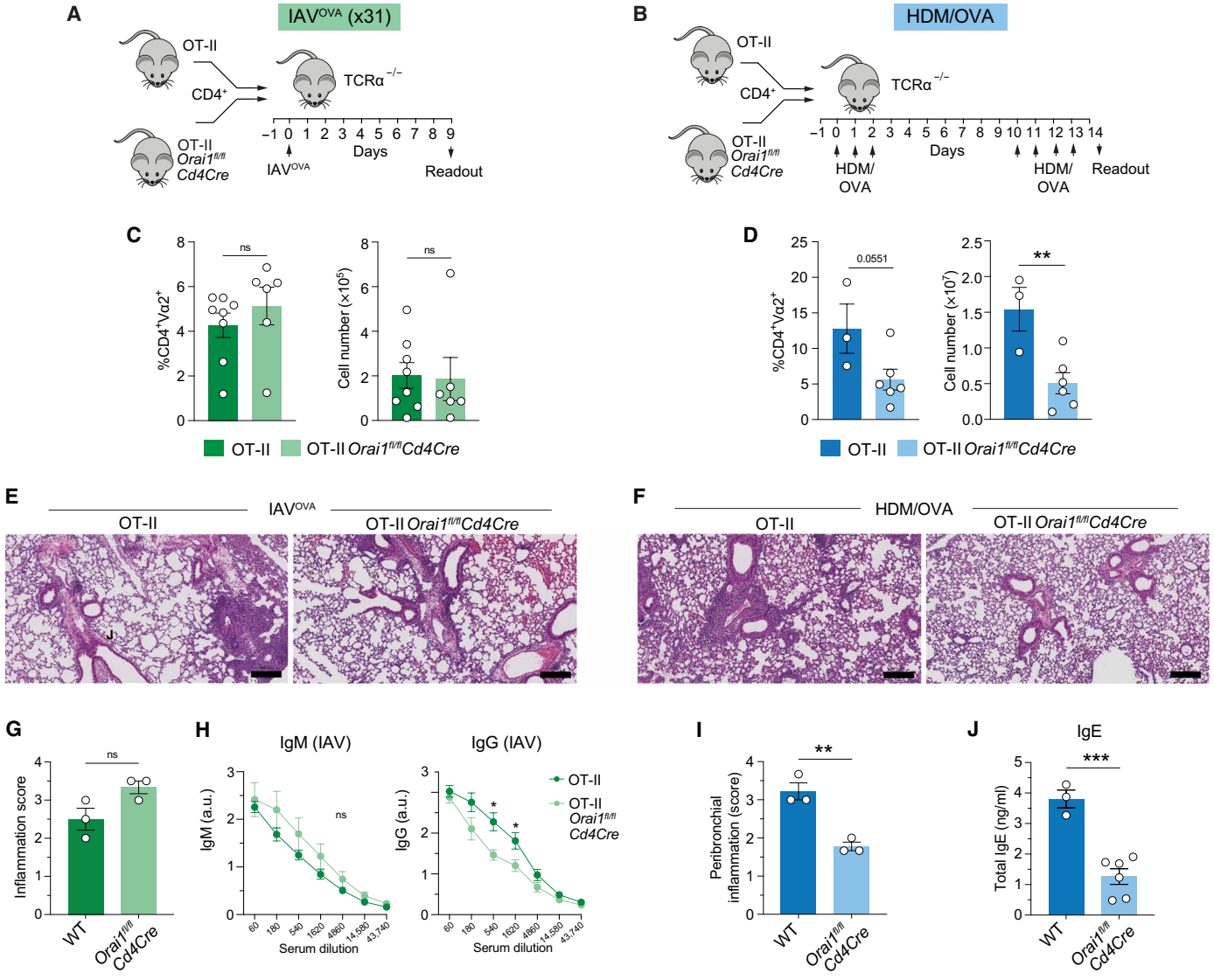

Fig. 3. Deletion of *Orai1* in antigen-specific T cells protects from allergic airway inflammation without compromising immunity to IAV infection. (**A** and **B**) Experimental protocols to study antigen-specific T cell responses to pulmonary infection with 10^5 median tissue culture infectious dose ($TCID_{50}$) IAV^{OVA} (x31) (A) and allergic airway inflammation after immunization and rechallenge with HDM/OVA (B) following adoptive transfer of OVA-specific $CD4^+$ T cells from WT OT-II and *Orai1*$^{fl/fl}$*Cd4Cre* OT-II mice into T cell–deficient *TCRα*$^{-/-}$ mice. (**C** and **D**) Frequencies and total numbers of donor OT-II T cells in the lungs of *TCRα*$^{-/-}$ recipient mice at day 9 after IAV infection (C) and at day 14 after HDM/OVA immunization and rechallenge (D). (**E** and **F**) Representative H&E stains of lungs of mice at day 9 after IAV^{OVA} infection (E) and at day 14 after sensitization and rechallenge with HDM/OVA (F). Scale bars, 200 μm. (**G** and **I**) Quantification of lung inflammation of three *TCRα*$^{-/-}$ recipient mice per cohort at day 9 after IAV^{OVA} infection (G) and at day 14 after sensitization and rechallenge with HDM/OVA (I). (**H**) IAV-specific IgM and IgG titers in the serum of *TCRα*$^{-/-}$ mice at day 9 after transfer of WT and *Orai1*$^{fl/fl}$*Cd4Cre* OT-II T cells and IAV^{OVA} infection. (**J**) Total IgE levels in the serum of the serum of *TCRα*$^{-/-}$ mice at day 14 after transfer of WT and *Orai1*$^{fl/fl}$*Cd4Cre* OT-II T cells and sensitization and rechallenge with HDM/OVA. Data in (C) and (D) are the means ± SEM of six to eight (C) and three to six (D) *TCRα*$^{-/-}$ recipient mice per cohort. Data in (G) and (I) are the means ± SEM of three *TCRα*$^{-/-}$ recipient mice per cohort. Data in (H) are from five to six *TCRα*$^{-/-}$ recipient mice per cohort. Data in (J) are from three to six *TCRα*$^{-/-}$ recipient mice per cohort. Statistical analysis is performed by unpaired Student's *t* test. ***$P < 0.001$; **$P < 0.01$; *$P < 0.05$.

IgM and a slight decrease in IAV^{OVA}-specific IgG in mice injected with *Orai1*$^{fl/fl}$*Cd4Cre* OT-II donor cells compared to WT OT-II (Fig. 3H). This was in contrast to the significantly reduced total IgE levels in the serum of HDM/OVA-challenged *TCRα*$^{-/-}$ host mice that had been injected with *Orai1*$^{fl/fl}$*Cd4Cre* OT-II compared to WT OT-II T cells (Fig. 3J). Together, these data show that deletion of *Orai1* in T cells expressing the same TCR has distinct effects on their ability to mount an antiviral immune response to IAV^{OVA} and to mediate airway inflammation against HDM/OVA.

Differential regulation of cell cycle pathways in T cells after HDM-induced allergic airway inflammation compared to IAV infection

To understand why T cell–specific *Orai1* deletion attenuates allergic airway inflammation but not immunity to IAV infection, we compared T cell activation and gene expression in donor WT OT-II and *Orai1*$^{fl/fl}$*Cd4Cre* OT-II cells isolated from the lungs of *TCRα*$^{-/-}$ host mice after IAV^{OVA} infection or HDM/OVA challenge (Fig. 3, A and B). Principal components analysis (PCA) of RNA sequencing

(RNA-seq) data showed that WT OT-II T cells isolated from HDM/OVA-immunized and IAV^{OVA}-infected mice clearly segregated, suggesting that both treatments induce a different T cell response despite the shared TCR specificity (fig. S3, A and B). To elucidate specific differences in gene expression in WT OT-II T cells following HDM immunization and IAV infection, we analyzed differentially expressed genes (DEGs) and conducted Kyoto Encyclopedia of Genes and Genomes (KEGG) pathway analysis. Several pathways were differentially regulated after HDM/OVA challenge and IAV^{OVA} infection including TCR signaling, influenza A, and T_H1/T_H2 differentiation (fig. S3, C and D). Whereas several negative regulators of T cell activation such as *Pdcd1*, *Ctla4*, and *Il-10* were differentially up-regulated in HDM/OVA-stimulated T cells, proinflammatory genes such as *Ifng* and positive regulators of T cell signaling such as *Jun*, *Nfatc3*, and *Ppp3ca* were differentially up-regulated after IAV^{OVA} infection. In the influenza A pathway, most of the genes were significantly up-regulated in OT-II cells only after IAV^{OVA} infection. In addition, as expected, several T_H1-associated genes were significantly increased only after IAV^{OVA} infection, but not HDM/OVA stimulation, including *Ifng*, *Il12rb2*, and *Stat4* (fig. S3C). Other pathways that were differentially regulated in HDM/OVA compared to IAV^{OVA}-treated WT OT-II T cells were cell cycle, FoxO signaling, and p53 signaling (fig. S3D). The differential regulation of the KEGG cell cycle pathway was confirmed using BioCarta and Gene Ontology, which both revealed G_2-M and cell cycle G_2-M among the top identified pathways (fig. S3E). Within these pathways, 65 to 100% of genes were specifically up-regulated in HDM/OVA-stimulated compared to IAV^{OVA}-stimulated OT-II T cells. Among the up-regulated genes were key regulators of the cell cycle including *Cdk1*, *Mcm6*, and *Bub1* (fig. S3F). Many of these genes are also part of the p53 signaling pathway. Together, the comparison of differentially regulated KEGG pathways in OT-II T cells suggests that HDM/OVA stimulation results in stronger induction of cell cycle regulatory genes than IAV^{OVA} infection.

ORAI1 controls the expression of cell cycle regulators and T cell proliferation during allergic airway inflammation

We next investigated how ORAI1 affects gene expression in OT-II T cells after HDM/OVA immunization compared to IAV^{OVA} infection to understand why *Orai1*$^{fl/fl}$*Cd4Cre* mice are protected from allergic airway inflammation but have normal T cell responses to IAV infection. To elucidate the molecular mechanisms behind this dichotomy, we compared DEG and pathways in $CD4^+$ T cells from *Orai1*$^{fl/fl}$*Cd4Cre* OT-II and WT OT-II mice that had been adoptively transferred to host mice immunized and rechallenged with HDM/OVA or infected with IAV^{OVA}. A total of 362 genes were differentially up- or down-regulated in WT versus *Orai1*-deficient T cells after IAV^{OVA} infection compared to 1690 genes after HDM/OVA immunization and rechallenge (Fig. 4A). Of these 1690 genes, 934 were down-regulated and 756 were up-regulated in the absence of ORAI1. Further assessment of these DEGs using Ingenuity Pathway Analysis (IPA), BioCarta, Gene Ontology, and KEGG pathway analysis identified a preponderance of deregulated pathways in *Orai1*-deficient T cells that are related to cell cycle regulation, cell division, and DNA replication (Fig. 4B). Gene set enrichment analysis (GSEA) confirmed these results and showed that expression of cell cycle and G_2-M checkpoint–related genes was reduced in *Orai1*$^{fl/fl}$*Cd4Cre* OT-II cells (Fig. 4C). In-depth analysis of the KEGG pathways cell cycle and DNA replication revealed significantly reduced expression of genes that promote cell cycle progression, DNA synthesis, and replication in *Orai1*-deficient compared to WT T cells after HDM/OVA immunization. Among these genes were *Bub1*, *Cdk1*, *Mcm6*, *Mcm4*, *Orc6*, *Mad2l1*, *Prim1*, *Rpa3*, and *Ccna2* (Fig. 4D). By contrast, no difference in expression of these genes was observed between *Orai1*$^{fl/fl}$*Cd4Cre* OT-II and WT OT-II cells after infection with IAV^{OVA}. These data suggest that ORAI1 is required for the regulation of cell cycle progression in the context of allergen challenge but not viral infection.

To identify ORAI1-dependent regulators of DEGs after HDM/OVA immunization, we used two independent approaches, the IPA upstream regulator analysis and epigenetic Landscape In Silico deletion Analysis (LISA) (*49*). Of all upstream regulators detected by IPA, a number of transcription factors, kinases, and other proteins regulating cell cycle progression such as cyclin-dependent kinase (CDK) inhibitor 1A (CDKN1A), tumor suppressor protein TP53, and the E2F transcription factor 4 (E2F4) and E2F1 were among those detected at the highest level of significance (Fig. 4E). Whereas activation *Z* scores of TP53, its downstream target CDKN1A and E2F4, which mediate cell cycle arrest, were up in *Orai1*-deficient OT-II T cells, those for E2F1, which promotes proliferation, were down. Accordingly, almost all CDKN1A target genes were suppressed in the absence of ORAI1 (fig. S4A). Moreover, GSEA further revealed that the expression of E2F target genes was strongly depleted in *Orai1*$^{fl/fl}$*Cd4Cre* compared to WT OT-II T cells (Fig. 4F and fig. S4, B and C), which was consistent with impaired proliferation of *Orai1*-deficient T cells. IPA's definition of upstream transcriptional regulator is broad and includes transcription factors, kinases, and signaling molecules that can affect gene expression. By contrast, LISA compares lists of genes with chromatin immunoprecipitation sequencing datasets to identify transcription factors and chromatin regulators that are directly responsible for the perturbation of a DEG set (*49*). Comparison of DEG in *Orai1*$^{fl/fl}$*Cd4Cre* and WT OT-II T cells by LISA identified E2F4 as a potential direct regulator of cell cycle progression in the context of HDM/OVA-induced allergic airway inflammation (Fig. 4G). Other ORAI1-dependent transcription factors identified by LISA included signal transducer and activator of transcription 6 (STAT6) and STAT5A, which mediate IL-4 and IL-2 receptor signaling, respectively, and thus T_H2 differentiation. LISA also identified IRF4 and BATF as regulators of DEGs in *Orai1*-deficient T cells, which was intriguing because both transcription factors are required for efficient T_H2 differentiation (*50*–*53*). To test whether dysregulation of cell cycle gene expression in *Orai1*-deficient T cells indeed affects T cell proliferation, we immunized WT and *Orai1*$^{fl/fl}$*Cd4Cre* mice with HDM/OVA and measured proliferation by 5-bromo-2′-deoxyuridine (BrdU) incorporation (Fig. 4, H to J). We observed significantly reduced frequencies of HDM-specific, proliferative ($BrdU^+$) effector $CD4^+CD44^+$ T cells in the mLNs of *Orai1*$^{fl/fl}$*Cd4Cre* mice compared to their WT littermates. These results strongly suggest that ORAI1 regulates the expression of genes regulating cell cycle progression and proliferation in antigen-specific T cells during allergic airway inflammation (Fig. 4K).

To investigate the effects of *Orai1* deletion on the proliferation of T_H2 cells further, we differentiated $CD4^+$ T cells from WT and *Orai1*$^{fl/fl}$*Cd4Cre* mice in T_H2 cells in vitro. *Orai1*-deficient T_H2 cells had significantly reduced SOCE compared to WT T_H2 cells following passive store depletion with thapsigargin or TCR cross-linking with anti-CD3 antibodies (fig. S5, A and B). The extent of the SOCE defect in the absence of ORAI1 was comparable in T_H2 and T_H1 cells.

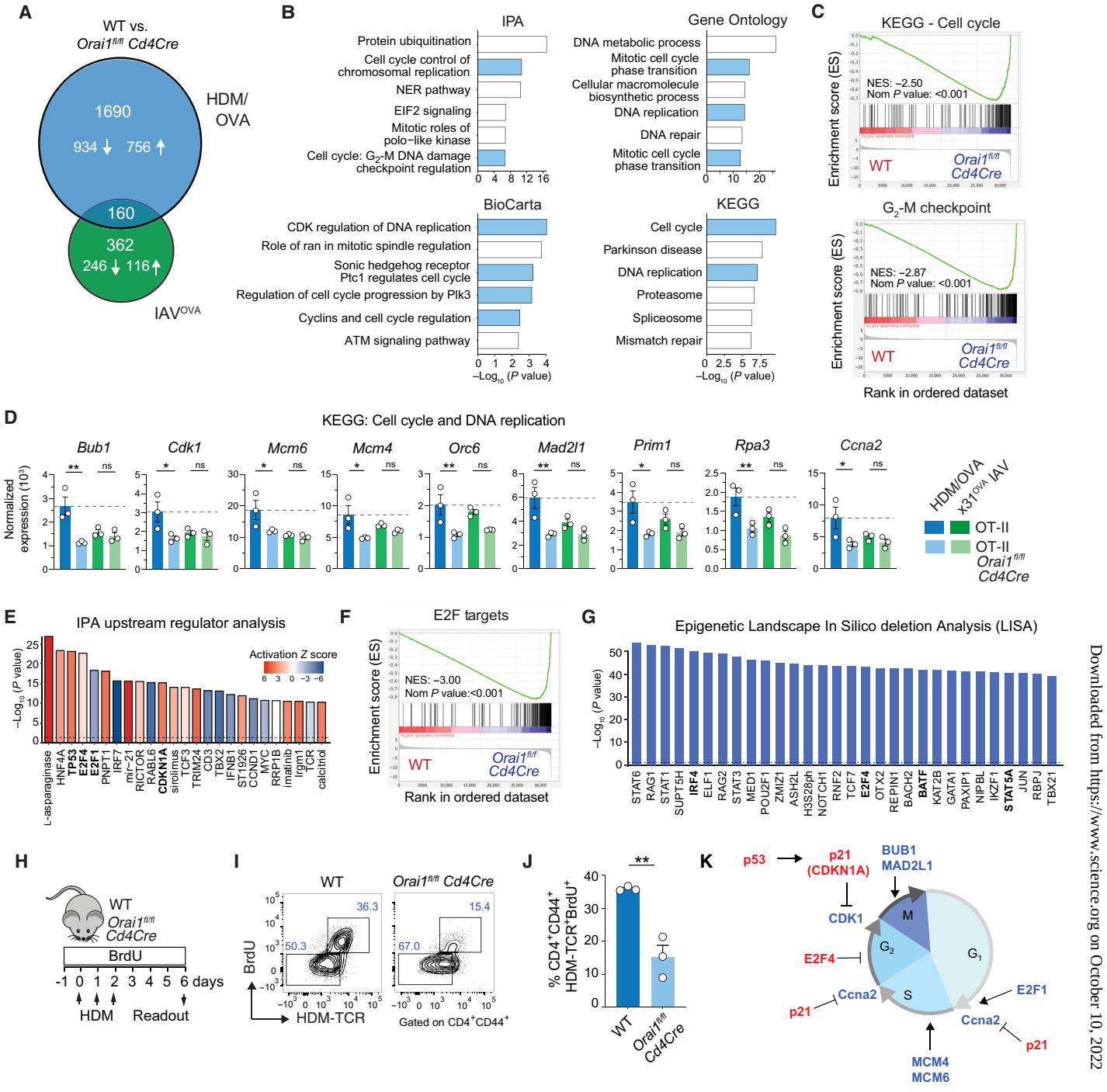

Fig. 4. ORAI1 controls the expression of cell cycle regulators and T cell proliferation during allergic airway inflammation. (**A**) Numbers of up-regulated (↑) or down-regulated (↓) DEGs in OT-II T cells of WT and *Orai1*$^{fl/fl}$*Cd4Cre* mice at days 9 and 14 after IAV^{OVA} (x31) infection and HDM/OVA treatment, respectively (Fig. 3, A and B). (**B** and **C**) Analysis of WT and *Orai1*$^{fl/fl}$*Cd4Cre* T cells at day 14 of HDM/OVA treatment (Fig. 3B). (B) Top six dysregulated pathways obtained by IPA, BioCarta, Gene Ontology, and KEGG, ranked by *P* values. Cell cycle–related pathways are shown in blue. ATM, ataxia telangiectasia mutated; NER, nucleotide excision repair; NES, normalized enrichment score; Plk3, Polo-like kinase 3. (C) GSEA of KEGG cell cycle (M7963) and hallmark G_2-M checkpoint (M5901). (**D**) Normalized RNA-seq–based gene expression from the KEGG pathways cell cycle and DNA replication in T cells after IAV^{OVA} infection and HDM/OVA treatment. (**E** to **G**) Analysis of WT and *Orai1*$^{fl/fl}$*Cd4Cre* T cells at day 14 of HDM/OVA treatment. (E) IPA upstream regulator analysis of DEG ranked by *P* value. Colors indicate the activation *Z* score. Key regulators are highlighted in bold. (F) GSEA of E2F targets (M5925). (G) Epigenetic Landscape In Silico deletion Analysis (LISA) of transcriptional regulators of DEG ranked by *P* value. Key regulators are highlighted in bold. (**H** to **J**) Antigen-specific T cell proliferation after HDM treatment. (H) Experimental protocol. (I) Representative flow cytometry plot of CD4$^+$CD44$^+$ T cells after BrdU incorporation and staining with I-A^b tetramers (HDM-TCR$^+$). (J) Frequencies of CD4$^+$CD44$^+$BrdU$^+$HDM-TCR$^+$ T cells from three WT and three *Orai1*$^{fl/fl}$*Cd4Cre* mice. (**K**) Control of cell cycle progression by ORAI1. Inhibitors are highlighted in red, activators in blue. Statistical analysis in (B) and (E) is performed by Fisher's exact test: $P < 0.1$; that in (D) is performed by ANOVA (Sidak's multiple comparisons); that in (F) is performed by a Wilcoxon rank sum test; and that in (I) is performed by unpaired Student's *t* test. $^{**}P < 0.01$; $^{*}P < 0.05$.

T_H2, but not T_H1, cells showed significantly reduced expression of regulators of cell cycle progression including *Cdk1*, *Mcm6*, *Bub1*, and *Ccna2* (fig. S5C). When we stimulated T_H2 cells by anti-CD3/CD28 cross-linking in vitro, we observed significantly reduced frequencies of cells in the G_2-M phase (fig. S5D) and a moderate but significant proliferation defect (fig. S5E) in *Orai1*-deficient T_H2 cells compared to WT controls. These data are consistent with the proliferation defect and dysregulated cell cycle gene expression of *Orai1*$^{fl/fl}$*Cd4Cre* $CD4^+$ T cells in vivo after HDM immunization (Fig. 4).

By contrast, we did not observe differential expression of genes or pathways related to cell cycle regulation in *Orai1*$^{fl/fl}$*Cd4Cre* OT-II T cells in the context of IAV^{OVA} infection (fig. S6, A and B). Neither did an IPA upstream regulator analysis reveal genes controlling the cell cycle to be dysregulated in the absence of ORAI1 (fig. S6C). Instead, KEGG pathway analysis showed aberrant regulation of several other pathways in *Orai1*$^{fl/fl}$*Cd4Cre* OT-II T cells following IAV^{OVA} infection. These included influenza A, T_H1 and T_H2 cell differentiation, and retinoic acid-inducible gene I (RIG-1)–like signaling pathways (fig. S6, A and B), which was consistent with the reported roles of T_H1 cells and RIG-I in antiviral immunity to influenza infection (*54*, *55*). Furthermore, the IPA upstream regulator analysis showed strongly reduced activation scores for the T_H1-associated cytokines IL-12 and IFN-γ (fig. S6C). Overall, however, the deletion of *Orai1* did not have a strong impact on the expression of T_H1 genes because only 5% of known T_H1 signature genes were either up- or down-regulated in *Orai1*$^{fl/fl}$*Cd4Cre* OT-II T cells after IAV infection (fig. S6D). Collectively, our data demonstrate that ORAI1 plays a specific role in regulating cell cycle progression in T_H2 cells in vitro and during allergic airway inflammation in vivo.

ORAI1 promotes T_H2 cell effector functions in HDM-induced allergic airway inflammation

AA is characterized by type 2 inflammation that is associated with increased IgE production, eosinophilia, and increased levels of T_H2 cytokines. When we compared DEGs in OT-II T cells of WT and *Orai1*$^{fl/fl}$*Cd4Cre* mice following HDM/OVA immunization to previously reported T_H2 gene signatures, we found that expression of all genes belonging to a T_H2 signature gene set was down-regulated in *Orai1*-deficient compared to WT T cells (Fig. 5A). GSEA confirmed that most T_H2 signature genes were depleted in *Orai1*$^{fl/fl}$*Cd4Cre* compared to WT OT-II T cells after HDM/OVA immunization (Fig. 5B). Given the role of ORAI1 in promoting gene expression in T_H2 cells, we investigated the production of T_H2 cytokines by $CD4^+$ T cells in the lungs of $TCR\alpha^{-/-}$ mice that had been injected with T cells from WT OT-II or *Orai1*$^{fl/fl}$*Cd4Cre* OT-II mice and immunized with HDM extract using the same protocol as shown in Fig. 3B. We found significantly reduced numbers of *Orai1*-deficient $CD4^+$ T cells in the lungs of mice that are able to produce IL-4 and IL-13 compared to $CD4^+$ WT T cells (Fig. 5C). Similarly, *Il4* and *Il13* mRNA levels were reduced in lung tissue of *Orai1*$^{fl/fl}$*Cd4Cre* mice after HDM rechallenge (fig. S7A). To further investigate the role of ORAI1 for T_H2 cell function, we differentiated $CD4^+$ T cells of WT and *Orai1*$^{fl/fl}$*Cd4Cre* mice into T_H2 cells in vitro. Stimulation of T_H2 cells with anti-CD3/CD28 resulted in the production of IL-4 and IL-13 protein, which was significantly impaired in *Orai1*-deficient T_H2 cells (fig. S7, B and C). IL-5 expression by human T_H2 cells requires several rounds of antigen stimulation in vitro and is a hallmark of differentiated T_H2 cells (*56*). IL-5–producing $CD4^+$ T cells were undetectable even in HDM-immunized WT mice by intracellular cytokine staining, but a more sensitive analysis by cytometric bead array showed that IL-5 production by *Orai1*-deficient $CD4^+$ T cells isolated from the lungs of HDM-treated mice was significantly reduced compared to WT $CD4^+$ T cells (Fig. 5D). As expected, $CD4^+$ T cells polarized into T_H1 cells for comparison did not produce IL-4 or IL-13 but expressed IFN-γ, whose levels were strongly reduced in *Orai1*-deficient T_H1 cells (fig. S8, A and B). Reduced cytokine production was not limited to T_H2 cytokines as *Tnfa* mRNA levels were moderately reduced in the lungs of HDM-treated *Orai1*$^{fl/fl}$*Cd4Cre* mice compared to WT controls (fig. S7A); moreover, protein levels of TNF-α, IL-10, and IL-2 were reduced in both T_H1 and T_H2 cells of *Orai1*$^{fl/fl}$*Cd4Cre* mice (fig. S8, A and B). Collectively, these findings demonstrate that ORAI1 is an important regulator of T_H2 responses in allergic airway inflammation.

ORAI1 regulates T_H2 cell differentiation and function

T_H2 responses are dependent on the transcription factor GATA3, which is essential for T_H2 cell differentiation, proliferation, and function (*57*). GATA3 directly binds to several regions in the T_H2 cytokine gene locus and regulates expression of the T_H2 signature cytokines IL-4, IL-5, and IL-13 (*58*). Given the reduced expression of IL-4 and IL-13 and attenuated T_H2 responses in vivo after HDM sensitization and rechallenge, we analyzed the expression of GATA3 in $CD4^+$ T cells isolated from mLNs of WT and *Orai1*$^{fl/fl}$*Cd4Cre* mice that were sensitized and rechallenged with HDM. We observed reduced numbers of $GATA3^+CD4^+$ T cells in *Orai1*-deficient mice compared to WT littermates (Fig. 5E). We next investigated the effects of *Orai1* deletion on the expression levels of GATA3 in $CD4^+$ T cells that were polarized into T_H2 cells in the presence of IL-4 in vitro. Whereas T_H2 cells from WT mice showed robust GATA3 expression, GATA3 mRNA and protein levels were significantly attenuated in *Orai1*-deficient T_H2 cells at day 5 of differentiation (Fig. 5, F and G, and fig. S8C). Besides GATA3, we also observed reduced expression of IRF4 protein, and *Irf4* and *Batf* mRNA in *Orai1*-deficient T_H2 cells in vitro (fig. S9, A and B). Both transcription factors are expressed by various $CD4^+$ T cell subsets and induced after TCR stimulation and IL-4 receptor (IL-4R) signaling (*59*). IRF4 and BATF are considered to be pioneer factors that mediate the remodeling and accessibility of chromatin (*60*). IRF4 is required for T_H2 differentiation by promoting the expression of GATA3 (*50*) and IL-4 (*51*). Note that the levels of GATA3, IRF4, and BATF were reduced in *Orai1*-deficient T cells only at day 5, and not yet at day 3, of T_H2 differentiation. These findings suggest that deletion of *Orai1* and partial reduction of SOCE do not interfere with the induction of IRF4 and BATF but their maintenance in T_H2 cells.

ORAI1 regulates HDM-induced airway inflammation through IL-2R expression and IL-2 signaling

The expression of GATA3 requires IL-4 signaling, which is mediated by the IL-4R and the transcription factor STAT6 (*61*, *62*). The expression of IL-4 and IL-4R, in turn, depends on IL-2 signaling via STAT5 (fig. S9C) (*63*). We therefore hypothesized that impaired IL-2 and IL-4 production by *Orai1*-deficient $CD4^+$ T cells may contribute to the impaired maintenance of GATA3 expression and T_H2 differentiation. Further analysis of DEG and signaling pathways that are dysregulated in *Orai1*-deficient T cells after HDM/OVA immunization revealed a strong depletion of genes belonging to the IL-2/STAT5A signaling pathway (Fig. 6A). STAT5A and its homolog

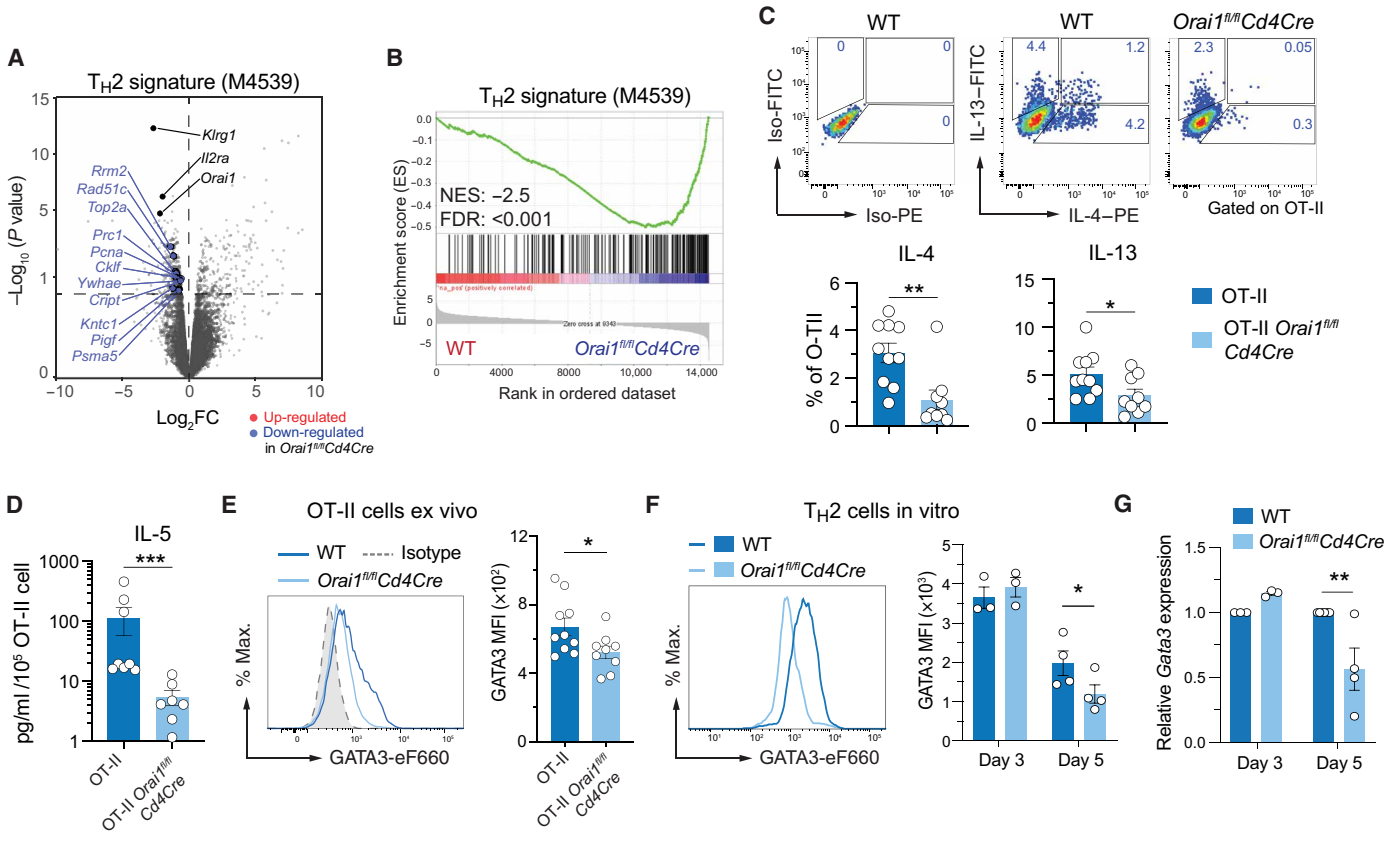

Fig. 5. ORAI1 regulates T_H2 cell differentiation and function. (**A** to **E**) Analysis of RNA-seq data from T cells of WT and *Orai1*$^{fl/fl}$*Cd4Cre* mice at day 14 of HDM/OVA treatment (Fig. 3B). (A and B) Volcano plot (A) and GSEA plot (B) of DEGs in *Orai1*-deficient versus WT CD4$^+$ T cells that belong to the gene set naïve CD4 T cell versus 48h act T_H2 down (M4529) (*115*). FC, fold change. (C) Representative flow cytometry plots and frequencies of IL-4– and IL-13–producing WT and *Orai1*$^{fl/fl}$*Cd4Cre* donor OT-II CD4$^+$ T cells isolated from the lungs of TCR$\alpha^{-/-}$ host mice day 14 after HDM/OVA treatment. Cells were stimulated with phorbol 12-myristate 13-acetate (PMA)/ionomycin for 4 hours in vitro. (D) IL-5 production by donor OT-II T cells isolated from the lungs of TCR$\alpha^{-/-}$ host mice at day 14 after HDM/OVA treatment and restimulated in vitro with anti-CD3 for 24 hours. IL-5 concentration was measured in the cell culture supernatants by cytometric bead array and normalized to T cell numbers. (E) Representative flow cytometry plots and quantification of GATA3 mean fluorescence intensity (MFI) in OT-II cells isolated from lungs of mice at day 14 after HDM/OVA treatment. (**F** and **G**) GATA3 expression by CD4$^+$ T cells polarized into T_H2 cells for 3 to 5 days in vitro. GATA3 protein (F) and mRNA (G) expression measured by flow cytometry and qRT-PCR, respectively. mRNA levels were normalized to *Rpl32* housekeeping gene and WT T cells. Data in (C) to (E) are the means ± SEM of 9 to 10 mice from two independent experiments. Data in (F) and (G) are the means ± SEM of three to four mice from at least two independent experiments. Statistical analysis in (C) is performed by unpaired Student's *t* test; that in (D) and (E) is performed by Mann-Whitney test; that in (F) is performed by paired Student's *t* test; and that in (G) is performed by two-way ANOVA (Sidak's multiple comparison). ***$P < 0.001$; **$P < 0.01$; *$P < 0.05$.

STAT5B are critical mediators of IL-2R signaling, which controls the differentiation and homeostasis of many T cell subsets (*64*). One of the most significantly reduced genes in *Orai1*$^{fl/fl}$*Cd4Cre* compared to WT OT-II T cells was *Il2ra*, which encodes the α chain of the IL-2 receptor (CD25) (Fig. 6B). A similar reduction was not observed in *Orai1*-deficient OT-II T cells after IAV^{OVA} infection. IL-2 has been shown to enhance airway inflammation in response to inhaled allergen (*65*, *66*). To assess the significance of reduced IL-2/STAT5 pathway expression in *Orai1*-deficient T cells for allergic airway inflammation, we tested whether exogenous IL-2 restores lung inflammation in *Orai1*$^{fl/fl}$*Cd4Cre* mice. To this end, *Orai1*$^{fl/fl}$*Cd4Cre* mice were sensitized with HDM and injected with exogenous IL-2 at the time of HDM rechallenge (Fig. 6C). Whereas *Orai1*$^{fl/fl}$*Cd4Cre* mice had significantly reduced peribronchial inflammation compared to WT mice, *Orai1*$^{fl/fl}$*Cd4Cre* mice treated with IL-2 showed a similar degree of pulmonary inflammation as WT mice (Fig. 6, D and E). Given the reduced GATA3 expression in *Orai1*-deficient T cells (Fig. 5, E to G), we measured GATA3 levels in T cells isolated from the lungs of *Orai1*$^{fl/fl}$*Cd4Cre* mice that were injected with IL-2 at the time of HDM challenge. GATA3 expression was significantly increased in *Orai1*-deficient CD4$^+$ T cells following IL-2 injection compared to untreated *Orai1*-deficient mice (Fig. 6F). Collectively, these data show that ORAI1 regulates IL-2/STAT5 signaling in CD4$^+$ T cells, which is required to maintain T_H2 cell differentiation and allergic airway inflammation.

Pharmacological CRAC channel inhibition reduces asthmatic airway inflammation without compromising immunity to IAV infection

To test whether pharmacological inhibition of CRAC channels could be an effective approach to treating allergic airway inflammation, we used the selective CRAC channel blocker CM4620 (*67*). CM4620 has passed two phase 2 clinical trials for COVID-19 (coronavirus disease 2019)–associated pulmonary inflammation (NCT04661540)

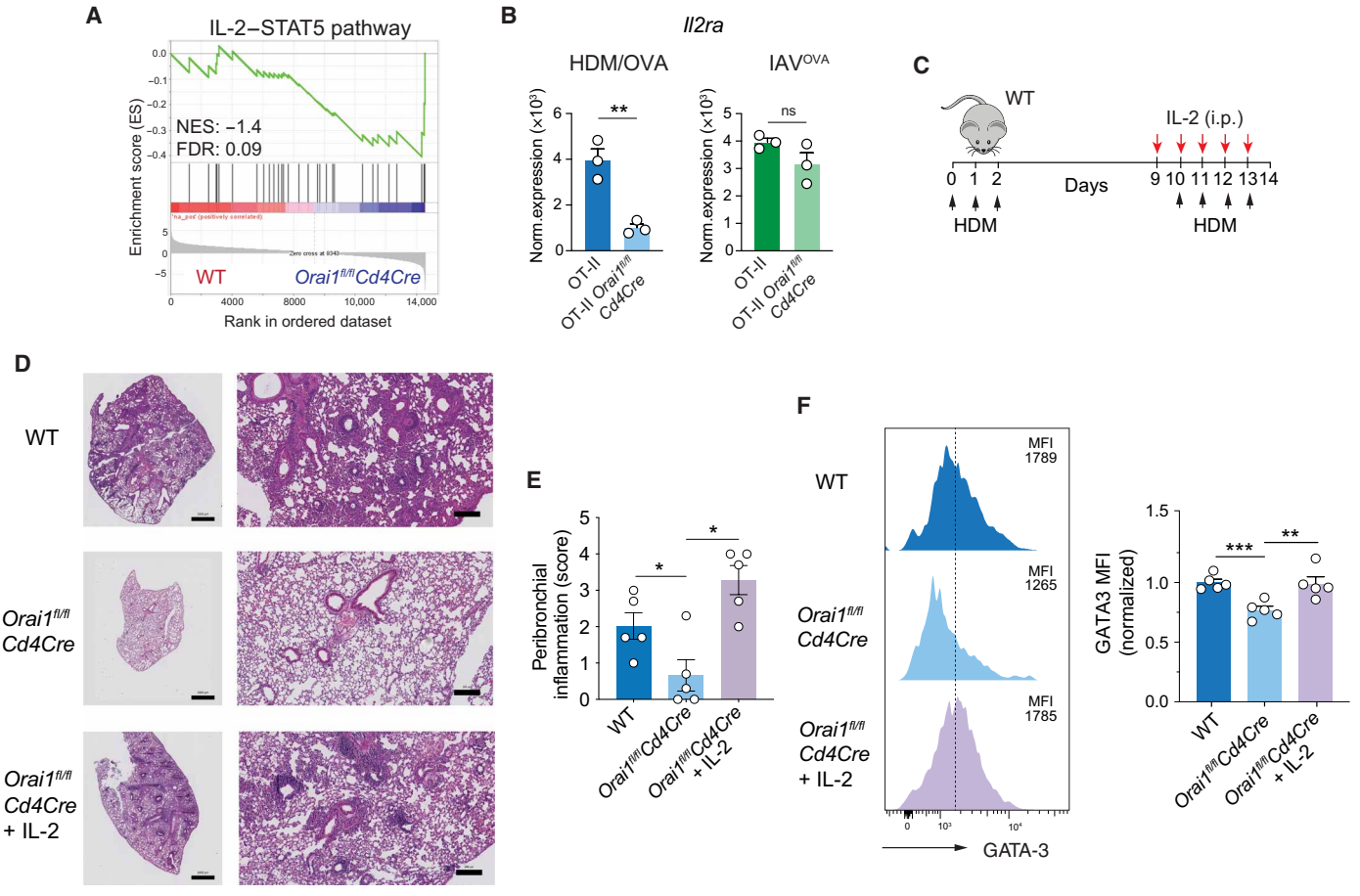

Fig. 6. ORAI1 regulates HDM-induced airway inflammation through IL-2R expression and IL-2 signaling. (**A**) GSEA plot of DEGs that belong to the gene set IL-2/STAT5 pathway (M234) (*116*) in OT-II CD4$^+$ T cells from WT and *Orai1*$^{fl/fl}$*Cd4Cre* at day 14 after HDM/OVA treatment (Fig. 3B). (**B**) Normalized *Il2ra* mRNA expression in CD4$^+$ OT-II T cells from mice after IAV^{OVA} infection or HDM/OVA treatment from RNA-seq (Fig. 3, A and B). (**C** to **F**) IL-2 treatment restores HDM-induced airway inflammation in *Orai1*-deficient mice. (C) Experimental protocol. WT and *Orai1*$^{fl/fl}$*Cd4Cre* mice were immunized and challenged with HDM; some *Orai1*-deficient mice received recombinant human IL-2 (1.5×10^5 IU/day, i.p.) during HDM challenge from days 9 to 13. (D) Representative H&E stains of lungs. Scale bars, 1000 μm (left) and 50 μm (right). (E) Peribronchial inflammation scores. (F) Representative flow cytometry plots and MFI of GATA3 expression in CD4$^+$ T cells isolated from the lungs normalized to levels in WT mice. Data in (B) are the means ± SEM of three mice per cohort. Data in (E) and (F) are the means ± SEM of five mice per cohort from two independent experiments. Statistical analysis in (B) and (F) is performed by unpaired Student's *t* test; that in (E) is performed by Mann-Whitney test. ***$P < 0.001$; **$P < 0.01$; *$P < 0.05$.

and acute pancreatitis (NCT03401190). Treatment of CD4$^+$ T cells from WT mice with 0.5 or 1 μM CM4620 resulted in significant inhibition of the rate of increase of $[Ca^{2+}]_i$ after thapsigargin stimulation (which is an indirect readout for CRAC channel function) and the integrated Ca^{2+} signal over time (Fig. 7A). To test the effects of systemic SOCE inhibition on allergic airway inflammation, we sensitized WT mice with HDM and treated them orally with CM4620 at the time of HDM rechallenge (Fig. 7B). Serum concentrations of CM4620 were confirmed by liquid chromatography–mass spectrometry (LC-MS) at the end of the treatment period and ranged from 6.76 to 10.17 μM, equivalent to 25.7 to 38.7 nM free compound levels (Fig. 7C). Mice treated with vehicle alone showed severe peribronchial inflammation and mucus production, whereas allergic airway inflammation was significantly reduced in mice that had been treated with CM4620 (Fig. 7, D and E). Reduced airway inflammation was associated with lower frequencies of IL-4– and IL-13–producing CD4$^+$ T cells in the lungs of CM4620-treated mice compared to controls (Fig. 7F) and reduced expression of GATA3 (Fig. 7G). In addition, mRNA levels of proinflammatory cytokines including *Il4*, *Il5*, *Il13*, and *Il6* were reduced in the lungs of mice treated with the CRAC channel inhibitor compared to vehicle injected mice (Fig. 7H). Notably, the administration of CM4620 at the time of HDM rechallenge had no effects on the frequencies of T_{fh} cells and GC B cells in the mLNs (Fig. 7, I and J). Accordingly, the titers of Der p 1-specific IgE antibodies were comparable in mice treated with the CRAC inhibitor and vehicle alone (Fig. 7K). The anti-inflammatory effects of CRAC channel inhibition on HDM-induced allergic airway inflammation are consistent with the attenuated inflammation observed in *Orai1*$^{fl/fl}$*Cd4Cre* compared to WT mice.

To investigate whether CRAC channel inhibition is associated with an increased susceptibility to IAV infection because of impaired antiviral immunity, we infected WT mice with the x31 strain of IAV and treated them with CM4620 on four consecutive days after infection (fig. S10A). Serum concentrations of CM4620 in the median inhibitory concentration range were confirmed by LC-MS at the end of the treatment period and ranged from 7.1 to 13.0 μM (free

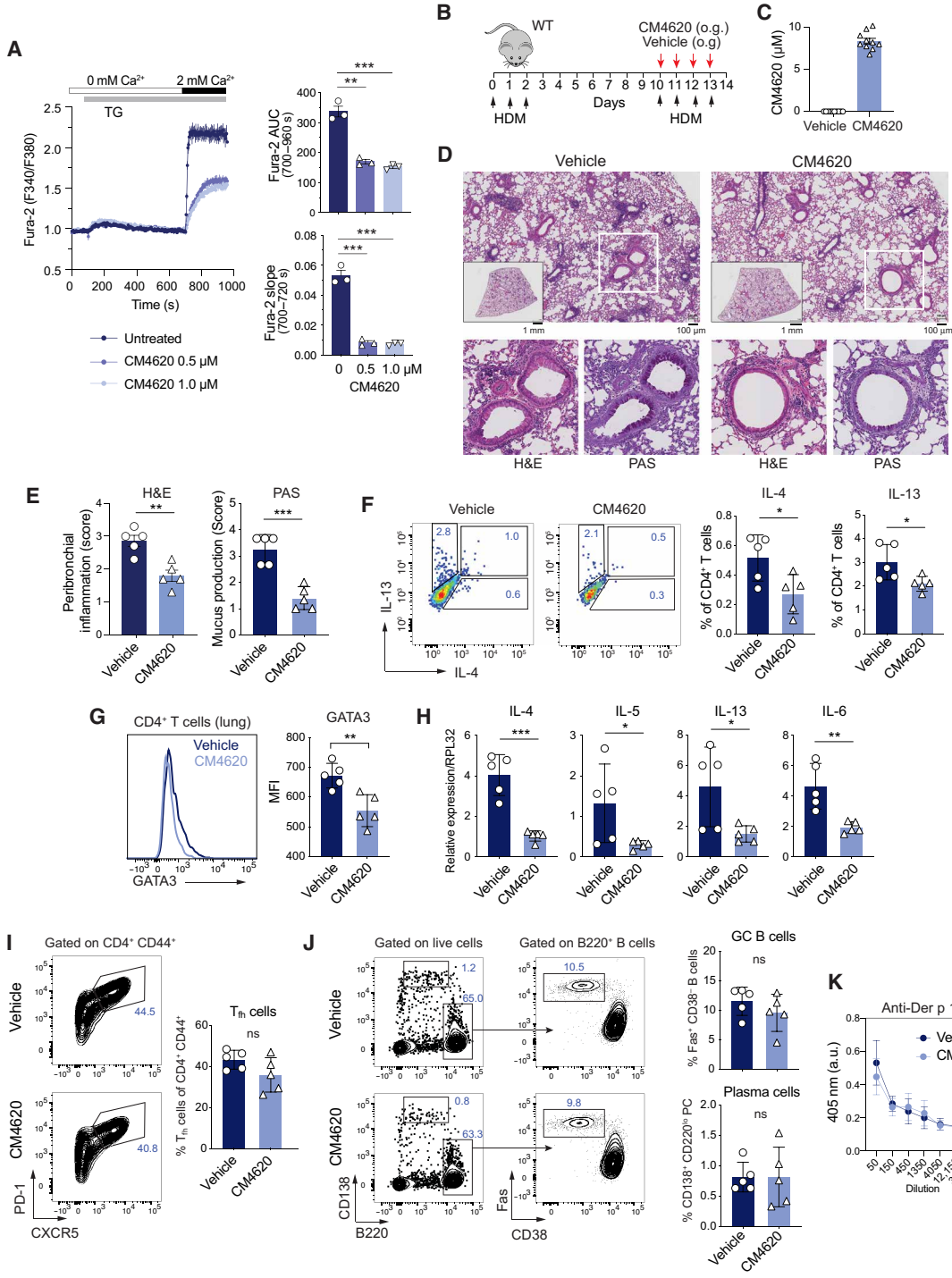

Fig. 7. Pharmacological CRAC channel inhibition alleviates asthmatic airway inflammation. (**A**) Intracellular Ca^{2+} levels ($[Ca^{2+}]_i$) in WT naïve $CD4^+$ T cells treated with 0.5 or 1 μM CM4620. Cells were stimulated with 1 μM thapsigargin in Ca^{2+}-free Ringer solution, followed by perfusion with 2 mM extracellular Ca^{2+}. Quantification of the area under the curve (AUC) and slope following Ca^{2+} readdition. (**B**) Experimental protocol for HDM sensitization/rechallenge. WT mice were treated with CM4620 (25 mg/kg) or vehicle by oral gavage (o.g.) on days 10 to 13, analyzed at day 14. (**C**) Concentrations of CM4620 in the serum of mice measured by LC-MS. (**D** and **E**) Representative H&E and PAS stains (D) and peribronchial inflammation and mucus production (E) in the lungs. (**F**) Representative flow cytometry plots and frequencies of IL-4– and IL-13–producing $CD4^+$ T cells isolated from the lungs of mice treated with vehicle or CM4620 and stimulated with PMA/ionomycin for 4 hours in vitro. (**G**) GATA3 expression in $CD4^+$ T cells from the lungs of vehicle or CM4620-treated mice by flow cytometry. (**H**) Cytokine mRNA levels in total lung tissues of mice by qRT-PCR. (**I**) Representative flow cytometry plots and quantification of $CXCR5^+PD\text{-}1^+$ T_{fh} cells in mLNs. (**J**) Representative flow cytometry plots and quantification of Fas^+CD38^- GC B cells and $CD138^+B220^{lo}$ plasma cells in mLNs of mice treated with vehicle or CM4620. (**K**) Der p 1-specific IgE levels in the serum of mice analyzed by enzyme-linked immunosorbent assay (ELISA). Data in (A) are the means ± SEM from three mice and independent experiments. Data in (C) to (K) are the means ± SEM from five mice per cohort. Statistical analysis is performed by unpaired Student's *t* test. ***$P < 0.001$; **$P < 0.01$; *$P < 0.05$.

compound levels, 26.9 to 49.5 nM) (fig. S10B). IAV infection resulted in similar degrees of pulmonary inflammation (fig. S10, C and D) and had no effect on the viral burdens detected in the lungs of CM4620-treated mice compared to littermates injected with vehicle only (fig. S10E). However, the numbers of $CD4^+$ T cells isolated from the lungs of CM4620-treated mice at day 14 of IAV infection producing the cytokines IL-2, IFN-γ, and TNF-α were reduced compared to controls (fig. S10F), indicating that the CRAC channel inhibitor treatment indeed suppresses T cell function. Because humoral immunity is required to control IAV infection, we measured the frequencies and total numbers of $CXCR5^+PD\text{-}1^+$ T_{fh} cells, $Fas^+GL\text{-}7^+$ GC B cells, and $CD138^+$ plasma cells in mLNs. Treatment of IAV-infected mice with CM4620 had no effect on the frequencies of either cell population compared to the vehicle control group (fig. S10, G and H). Accordingly, the levels of IAV-specific IgM and IgG antibodies in the serum of CM4620 and vehicle-treated mice were comparable (fig. S10I). Collectively, our data demonstrate that pharmacological CRAC channel inhibition suppresses the airway inflammation associated with HDM allergen challenge without dampening antiviral immunity to IAV infection.

DISCUSSION

We here investigated the role of ORAI1 and SOCE in allergic airway inflammation and pulmonary infection with IAV. Deletion of *Orai1* in T cells strongly attenuated HDM-induced type 2 airway inflammation evident from reduced peribronchial immune cell infiltration, eosinophils in the BAL, production of T_H2 cytokines, and IgE levels. The effects of *Orai1* deletion were intrinsic to T cells because the adoptive transfer of allergen-specific $CD4^+$ T cells to lymphopenic host mice had similar protective effects against HDM-induced allergic airway inflammation. Moreover, pharmacological inhibition of SOCE with a selective CRAC channel inhibitor attenuated HDM-induced allergic airway inflammation and T_H2 responses. At the molecular level, protection from AA was associated with impaired IL-2–dependent maintenance of T_H2 differentiation and a T_H2 cell–specific defect in cell cycle progression and proliferation.

By contrast, *Orai1* deletion in T cells did not significantly impair T cell–mediated antiviral immunity to IAV infection because pulmonary inflammation, viral titers, IAV-specific antibody levels, and the frequencies of IAV-specific T_{fh} cells and GC B cells were comparable in $Orai1^{fl/fl}Cd4Cre$ and WT mice. The only strong defect we were able to detect following IAV infection was a reduction in the frequencies of IFN-γ– and TNF-α–producing $CD4^+$ T cells in $Orai1^{fl/fl}Cd4Cre$ mice or WT mice treated with the CRAC channel blocker CM4620. The role of IFN-γ and TNF-α in immunity to IAV infection is complex. TNF-α has mostly an immune regulatory role in immunity to IAV and its reduction might enhance, rather than impair, $CD8^+$ T cell responses to IAV (*68*, *69*). IFN-γ was shown by some studies (*70*, *71*) to be critical for antiviral immunity to IAV, whereas others observed no protective role or reported increased susceptibility to IAV infection (*72*, *73*). In addition, note that T cells are not the only producers of IFN-γ because natural killer cells and type 1 innate lymphoid cells are also able to secrete IFN-γ. Because only T cells lack IFN-γ in $Orai1^{fl/fl}Cd4Cre$ mice, this defect may be compensated by other immune cells. We conclude that partially reduced SOCE following deletion on *Orai1* in T cells or pharmacological CRAC channel inhibition does not compromise immunity to IAV infection despite reduced TNF-α and IFN-γ production by T cells.

Protection from HDM-induced allergic airway inflammation in mice with T cell–specific deletion of *Orai1* or WT mice treated with a CRAC channel inhibitor was accompanied by reduced frequencies and numbers of IL-4– and IL-13–producing effector $CD4^+$ T cells in the lung after sensitization and rechallenge with HDM allergen. Similar defects were observed in vitro in *Orai1*-deficient $CD4^+$ T cells after polarization into T_H2 cells. Moreover, the expression of a variety of chemokines known to be induced by IL-4 and IL-13 such as *Mcp1*, *Mcp3*, *Eotaxin1*, and *Rantes* was reduced in $Orai1^{fl/fl}Cd4Cre$ mice after HDM sensitization and rechallenge, providing an explanation for the attenuated pulmonary eosinophil infiltration, a hallmark of asthmatic airway inflammation in humans and mice (*74*). Consistent with the attenuated type 2 inflammation, RNA-seq of $CD4^+$ T cells isolated from the lungs of HDM-immunized $Orai1^{fl/fl}Cd4Cre$ mice identified a significant down-regulation of T_H2 signature genes (*75*). Moreover, we observed reduced expression of the T_H2 transcription factor GATA3 in *Orai1*-deficient $CD4^+$ T cells isolated from the lungs of HDM-sensitized mice and in *Orai1*-deficient $CD4^+$ T cells polarized into T_H2 cells in vitro. GATA3 cooperates with other transcription factors, including the Ca^{2+}-regulated NFAT to promote IL-4 expression and T_H2 differentiation (*76*). Note that naïve *Orai1*-deficient $CD4^+$ T cells were initially able to induce GATA3 after TCR stimulation and polarization under T_H2 conditions but failed to maintain GATA3 expression at day 5 after polarization. Besides GATA3, the expression of two other transcription factors required for T_H2 function, IRF4 and BATF, was impaired in *Orai1*-deficient T cells. RNA-seq and LISA showed that both factors regulate gene expression in T cells of HDM-immunized mice in an ORAI1-dependent manner. Although IRF4 is not selectively expressed in T_H2 cells, it is necessary for proper T_H2 differentiation through the induction of GATA3 and IL-4 (*50*, *51*). Likewise, BATF is required for T_H2 differentiation (*52*), and together with IRF4 and IL-4, it is part of a positive feedback loop during T_H2 cell polarization (*53*).

The fact that GATA3, IRF4, and BATF were induced at similar levels in *Orai1*-deficient and WT T cells suggested that their initial expression in T_H2 cells, although reported to be reduced after strong suppression of SOCE (*9*, *16*), is not sensitive to the partial reduction of SOCE found in T cells of $Orai1^{fl/fl}Cd4Cre$ mice. By contrast, the maintenance of GATA3 expression and that of IRF4 and BATF was impaired in *Orai1*-deficient T_H2 cells in vitro. We reasoned that sustained GATA3 expression indirectly requires the Ca^{2+}-dependent production of cytokines and cytokine receptors. It is well established that IL-4 induces T_H2 polarization via IL-4R and STAT6 signaling and the induction of GATA3 expression (*77*). LISA of RNA-seq data from *Orai1*-deficient T cells of HDM-immunized mice identified STAT6 as a potential regulator of DEGs. T_H2 differentiation also depends (besides IL-4) on IL-2 and IL-2R signaling via STAT5, which regulate the expression of IL-4 and the IL-4R (*63*, *78*). Moreover, IL-2 signals directly induce the expression of IRF4 in T_H9 cells (*79*). We hypothesized that impaired IL-2 production may be responsible for the failed maintenance of GATA3 expression and T_H2 differentiation in the absence of ORAI1 for the following reasons: (i) IL-2 expression depends on SOCE (*8*, *14*, *80*); (ii) the IL-2/STAT5 signaling pathway was strongly deregulated in T cells isolated from HDM-immunized $Orai1^{fl/fl}Cd4Cre$ mice; and (iii) the expression of *Il2ra* encoding the α chain of the IL-2R (CD25) was strongly decreased in $CD4^+$ T cells of $Orai1^{fl/fl}Cd4Cre$ OT-II mice following HDM immunization. Restoring IL-2 levels in $Orai1^{fl/fl}Cd4Cre$ mice

by injection of IL-2 during HDM rechallenge resulted in a significantly more pronounced peribroncheal inflammation compared to untreated *Orai1*$^{fl/fl}$*Cd4Cre* mice. IL-2 injection also normalized the expression of GATA3 in *Orai1*-deficient T cells to levels comparable to those in WT T cells. These results indicate that IL-2 is required for sustaining T_H2 cell differentiation and their proinflammatory function in the context of AA.

Immunity to IAV infection is mediated in large part by neutralizing IgG antibodies against hemagglutinin that block the interaction between the virus and host cells. In AA, IgE antibodies mediate the activation of mast cells and airway inflammation. We reasoned that protection from HDM-induced airway inflammation may be due to reduced IgE levels, whereas preserved immunity to IAV infection may in part be explained by normal levels of flu-specific IgG. The production of IAV-specific IgG antibodies was not significantly impaired in IAV infected *Orai1*$^{fl/fl}$*Cd4Cre* mice or WT mice treated with the CRAC channel blocker CM4620. Moreover, we observed comparable numbers of T_{fh} cells in *Orai1*$^{fl/fl}$*Cd4Cre* mice or CM4620-treated WT mice following infection with IAV or LCMV. These observations are in line with our previous findings that the differentiation and function of T_{fh} cells following LCMV infection are only decreased when SOCE is abolished completely in O*rai1*/*Orai2*-deficient or *Stim1*/*Stim2*-deficient T cells but not by a partial reduction of SOCE in *Orai1*- or *Stim1*-deficient T cells (*8*, *9*). The preserved differentiation of T_{fh} cells and production of virus-specific IgG antibodies in IAV-infected *Orai1*$^{fl/fl}$*Cd4Cre* mice provide a compelling explanation why viral titers and pulmonary inflammation were not increased compared to WT mice.

By contrast, ORAI1 appears to have a slightly different function with regard to the ability of T cells to promote IgE production in response to allergen exposure. We observed reduced serum IgE levels in HDM-sensitized and rechallenged *Orai1*$^{fl/fl}$*Cd4Cre* mice compared to WT controls. Similarly, IgE levels were decreased in TCR$\alpha^{-/-}$ mice injected with $CD4^+$ T cells from *Orai1*$^{fl/fl}$*Cd4Cre* OT-II mice compared to mice that had received WT OT-II T cells. Recently, IL-13–producing T_{fh} cells were identified to be critical for allergen-specific IgE production and allergic airway inflammation (*81*). IL-13 expression was reduced in *Orai1*-deficient $CD4^+$ T cells isolated from HDM immunized mice, which provides a potential explanation for decreased IgE levels. In contrast to *Orai1*$^{fl/fl}$*Cd4Cre* mice, however, the treatment of HDM-immunized WT mice with the CRAC channel blocker CM4620 at the time of HDM rechallenge had no effects on the levels of HDM-specific IgE antibodies and the numbers of T_{fh} cells despite reduced IL-13 production. A likely explanation for the different effects of genetic deletion and pharmacological inhibition of ORAI1 on IgE levels and T_{fh} cell numbers is the timing of SOCE suppression. Whereas $CD4^+$ T cells from *Orai1*$^{fl/fl}$*Cd4Cre* mice lack SOCE during both the immunization and rechallenge with HDM, $CD4^+$ T cells from CM4620-treated WT mice had attenuated SOCE only during rechallenge with HDM. These data suggest that ORAI1 and SOCE are required for the differentiation of allergen-specific T_{fh} cells and IgE production upon first allergen encounter. It is presently unclear why *Orai1* deletion impairs the production of IgE but not IgG antibodies. IL-4 produced by T_{fh} cells promotes class switching to IgE, whereas IL-21 fosters class switching to IgG subtypes (*82*, *83*) and inhibits class switching to IgE (*84*, *85*). SOCE is required, however, for the production of both IL-4 and IL-21 (*9*).

Besides impaired production of T_H2 cytokines, we observed a significant reduction of *Orai1*-deficient $CD4^+$ T cells in the lungs, BAL, and mLNs of mice after HDM immunization. The analysis of T cell proliferation by BrdU incorporation in vivo following HDM immunization revealed a pronounced decrease in the numbers of HDM-specific, proliferating T cells in the absence of *Orai1*. A similar proliferation defect was observed in *Orai1*-deficient T_H2 cells in vitro, which was associated with a reduction of T_H2 cells in the G_2-M phase. These findings suggested that Ca^{2+} influx through ORAI1 promotes cell cycle progression of T_H2 cells. RNA-seq of *Orai1*-deficient T cells showed that some of the most significantly deregulated genes and pathways were those related to cell cycle regulation. Numerous genes and pathways positively regulating the cell cycle and G_2-M checkpoint were decreased in *Orai1*-deficient $CD4^+$ T cells from HDM immunized (but not IAV infected) mice including *Bub1*, *Cdk1*, *Mcm6*, *Mcm4*, *Orc6*, *Mad2l1*, *Prim1*, *Rpa3*, and *Ccna2*.

To identify ORAI1- and Ca^{2+}-regulated transcription factors that control cell cycle gene expression, we used IPA upstream regulator analysis and LISA, which showed a down-regulation of several transcription factors and cyclins that promote cell cycle progression such as E2F1, MYC, and Cyclin D1 in *Orai1*-deficient $CD4^+$ T cells. Conversely, transcription factors and CDK inhibitors that suppress cell cycle progression such as E2F4, p53, and p21 (CDKN1A) were up-regulated. Accordingly, the expression of p21, E2F4, and E2F1 target genes was strongly and almost uniformly down-regulated in *Orai1*-deficient T cells. Whereas regulation of E2F4 by Ca^{2+} has not been reported, the expression and phosphorylation of E2F1 were shown to be regulated by extracellular Ca^{2+} levels in keratinocytes (*86*). The Ca^{2+} dependence of E2F4 and E2F1 in *Orai1*-deficient T cells from HDM immunized mice is reminiscent of the down-regulation of other E2F family members (E2F2, E2F3) in SOCE-deficient regulatory T (T_{reg}) cells of *Stim1*$^{fl/f}$*Stim2*$^{fl/fl}$*Cd4Cre* mice reported earlier (*87*).

In addition to E2F4, the expression of two other inhibitors of cell cycle progression, p53 and p21, was up-regulated in *Orai1*-deficient T cells. p21 inhibits the activity of CDK1 at the G_2-M transition and that of CDK2 at the G_1-S and S-G_2 transition (*88*). The function of p21 is controlled by the tumor suppressor p53, whose effects on cell cycle arrest are dependent on p21. TCR signaling results in down-regulation of p53, thereby enabling the antigen-specific, cytokine-driven proliferation of T cells (*89*). How Ca^{2+} regulates the expression of p53 and p21 is not well understood. A general role of Ca^{2+} in controlling cell cycle progression has been reported and occurs at several transition points, for instance, at the G_0-G_1 checkpoint after mitogenic stimulation and at the G_1-S boundary (*90*). Cell cycle regulation by Ca^{2+} is mediated by the Ca^{2+} binding protein calmodulin (CaM), which, in turn, regulates CaM kinases and the phosphatase calcineurin. Inhibition of calcineurin in human T cells was shown to lead to cell cycle arrest in G_1, which was associated with increased expression of transforming growth factor–β and an accumulation of p21 (*91*). Because ORAI1 is the main source of Ca^{2+} influx in T cells, it is likely that at least some of its effects on cell cycle progression are mediated through calcineurin.

Our study shows that Ca^{2+} influx via ORAI1 channels is critical for the differentiation, proliferation, and function of T_H2 cells. As a consequence, *Orai1*$^{fl/fl}$*Cd4Cre* mice are protected from allergic airway inflammation. *Orai1*$^{fl/fl}$*Cd4Cre* mice have preserved immunity to infection with IAV, suggesting that SOCE in T cells is of particular importance for type 2 inflammation in allergic airway disease. What explains these different requirements for ORAI1 in

T cell–mediated immune responses in the same organ? One explanation is that a single infection with IAV^{OVA} results in weaker TCR signaling than repeated HDM exposure during sensitization and rechallenge with HDM. This explanation seems unlikely, however, because the transcriptomic analysis of OVA-specific WT T cells showed a robust up-regulation of TCR signaling genes, indicating that IAV infection is associated with sustained TCR signaling even 9 days after IAV infection. This conclusion is consistent with the prolonged presentation of influenza antigens weeks after viral clearance, which was sufficient to generate highly differentiated $CD4^+$ effector T cells (*92*). Another potential explanation is that deletion of *Orai1* has different effects on Ca^{2+} influx in T_H1 and T_H2 cells. We did, however, observe similar defects in SOCE in T_H1 and T_H2 cells from *Orai1*$^{fl/fl}$*Cd4Cre* mice. We favor instead a model in which T_H2 cells are more sensitive to a partial reduction of SOCE than T_H1 cells because the expression of IL-2 and IL-4 is Ca^{2+} dependent, which, in turn, is required for the maintenance of GATA3, IRF4, and BATF expression. In this context, note that SOCE is not only important for the differentiation of T_H2 cells but also important for the differentiation of other $CD4^+$ T cell subsets including T_{fh}, T_H17, and induced T_{reg} cells (*9*, *16*, *93*), although their Ca^{2+} signaling requirements differ. All $CD4^+$ T_H cell subsets have in common that their ability to produce signature cytokines depends on SOCE, including IFN-γ (T_H1), IL-4, IL-13 (T_H2), and IL-17A (T_H17), which explains, at least in part, the protection of mice with T cell–specific deletion of *Orai1* and *Stim1* from autoimmune, inflammatory diseases such as EAE, IBD, GvHD, and psoriasiform skin inflammation (*8*, *11*–*14*). Our findings in this study indicate that SOCE has a comparable role in T_H2 cells and allergic airway inflammation.

The role of ORAI1 and SOCE in human asthma is not well understood. A study in Japanese and Taiwanese populations has identified single-nucleotide polymorphisms (SNPs) in *ORAI1* that are associated with susceptibility of atopic dermatitis (AD) (*94*). One of these SNPs (rs3741596) results in a missense mutation (ORAI1 p.S218G), which, when overexpressed, was later shown to disrupt Ca^{2+} influx and Ca^{2+}-dependent gene expression (*95*). AD is one of the most common pediatric inflammatory skin disorders that is characterized by a T_H2-dominant immune response. Many clinical studies have reinforced the concept of an "atopic march" during which the occurrence of AD in infancy is followed by an increased risk of developing one or more disorders characterized by type 2 inflammation including AA (*96*). It is unclear at present how the ORAI1 p.S218G polymorphism and decreased Ca^{2+} influx contribute to increased AD susceptibility and if this or other polymorphisms are also associated with an increased risk for developing AA.

Several studies have explored the effects of SOCE inhibition on T cells from asthma patients. The CRAC channel blocker Synta66 inhibited anti-CD2/CD3/CD28–induced production of IL-2, IL-7, IL-13, and IFN-γ in a concentration-dependent manner in healthy and severe asthma donors (*26*). Using an OVA-driven rat model of AA, the same study found a reduction of inflammatory cytokines in the lungs and eosinophils in the BAL of Synta66-treated rats, which was associated with attenuated airway obstruction. Similar observations were made using three other CRAC channel inhibitors, YM-58483 (BTP2), 3-fluoropyridine-4-carboxylic acid, and SKF 96365, which reduced cytokine production, airway inflammation, and airway remodeling in a guinea pig model of AA (*25*, *27*, *97*). The anti-inflammatory effects of these CRAC channel inhibitors on AA are not limited to T_H2 cells. Mast cells are critical mediators of airway hyperresponsiveness in AA, and their proinflammatory function is dependent on CRAC channels. Studies of mast cells isolated from nasal polyps of patients have shown that CRAC channel blockers, alone or in combination with a leukotriene receptor antagonist, potently suppress CRAC channel activation (*98*). AECs are potent producers of inflammatory mediators that regulate bronchomotor tone and immune cell recruitment following stimulation by airway allergens. Ca^{2+} influx in AECs is mediated by ORAI1 channels, and their inhibition was shown to suppress the production of TSLP, IL-6, IL-8, and prostaglandin E2 (*29*). Collectively, these studies demonstrate that CRAC channels are required for the function of numerous cell types involved in the pathogenesis of AA, and their inhibition may be a feasible approach for AA therapy (*99*). Our finding that deletion of *Orai1* in T cells attenuates AA without compromising adaptive immunity to IAV infection suggests that suppression of type 2 inflammation in AA by inhibition of CRAC channels is not associated with an increased risk or severity of viral infection. Given the still rising incidence of AA worldwide, identifying safe targets for AA therapy without compromising immunity to infection is critical.

METHODS

Mice

The generation of *Orai1*$^{fl/fl}$ mice has been described before (*100*). Mice were crossed to *Cd4-Cre* mice [The Jackson Laboratory (JAX) strain 017336] and further to OT-II mice [*B6.Cg-Tg(TcraTcrb)425Cbn/J*, JAX strain 004194]. *TCRα*$^{-/-}$ mice (*B6.129S2-Tcra*^{tm1Mom}*/J*) were purchased from JAX (strain 002116). Sex-matched male and female mice were used between 6 and 12 weeks of age. Mice were maintained under specific pathogen–free conditions. All experiments were conducted in accordance with protocols approved by the Institutional Animal Care and Use Committee of at New York University School of Medicine.

HDM-induced airway inflammation

To induce allergic airway inflammation, *Orai1*$^{fl/fl}$*Cd4Cre* mice and Cre-negative *Orai1*$^{fl/fl}$ littermate controls (WT) were anesthetized with isoflurane and intranasally sensitized with 15 μg of crude extract from HDM *Dermatophagoides pteronyssinus* (Greer Laboratories, NC9756554) on three consecutive days (days 0 to 2), followed by rechallenge with 15 μg of HDM extract for 4 days (days 10 to 13). Control mice received PBS intranasally on days 0 to 2 and days 10 to 13. On day 14, serum and BAL fluid were collected. Following cervical dislocation, mice were perfused intracardially with 10 ml of ice-cold PBS containing 2 mM EDTA. mLNs and lungs were harvested and processed for histology and cell isolation. For IL-2 rescue experiments, *Orai1*$^{fl/fl}$*Cd4Cre* mice were injected intraperitoneally (i.p.) with 1.5×10^5 IU of recombinant human IL-2 on days 9 to 13. Both male and female mice were used for the HDM-induced airway inflammation as sex-dependent differences in lung inflammation were reported in the HDM model (*101*, *102*).

IAV infection

Orai1$^{fl/fl}$*Cd4Cre* and WT control mice were anesthetized and infected intranasally with the laboratory strain A/HK/x31 (x31-IAV) of the IAV subtype H3N2. The $OVA_{323–339}$ peptide that binds $H2I\text{-}A^b$ was engineered into the globular head of the hemagglutinin molecule of

x31-IAV (IAV^{OVA}) as previously described (*37*). The viral titers of the stocks were determined via median tissue culture infectious dose ($TCID_{50}$) assay in Madin-Darby canine kidney cells as previously described (*103*). The virus infectious dose used in all experiments was 10^5 $TCID_{50}$ per mouse. The body weight of mice was monitored daily, and 9 days p.i., lungs were isolated for histology after intracardial perfusion. Lungs and mLNs were used to prepare single-cell suspensions, followed by flow cytometric analysis. Viral burdens in the lungs were measured by qRT-PCR using oligonucleotide primers against different regions of IAV isolated from total lung mRNA (primer sequences are listed in table S1).

Adoptive T cell transfer

For some IAV infection and HDM immunization experiments, naïve $CD4^+$ T cells were isolated from WT OT-II or *Orai1*$^{fl/fl}$ *Cd4Cre* OT-II mice, followed by retro-orbital injection of 10^6 cells into *TCRα*$^{-/-}$ recipient mice. One day later, mice were infected intranasally with 10^5 $TCID_{50}$ of IAV^{OVA}. Alternatively, mice were sensitized intranasally with a mixture of 15 μg of HDM extract and 25 μg of OVA (Sigma-Aldrich, A5503) for three consecutive days, followed on days 10 to 13 by intranasal rechallenge of mice with the same HDM and OVA mixture according to published protocols (*104*).

Histology

Lungs of the HDM-immunized and IAV-infected mice were fixed with 4% paraformaldehyde, embedded in paraffin, and cut at 5 μm. Sample slides were stained with H&E or PAS in 95% ethanol using standard methods. Images were acquired using an AT2 (Leica) or Nanozoomer (Hamamatsu) whole slide scanner and visualized using the OMERO Plus imaging software (Glencoe Software). Inflammation in the lungs of IAV-infected mice was quantified using the following scoring system: 0, no inflammation; 1, only moderate peribronchial Inflammation; 2, <10% inflamed lung tissue; 3, 10 to 25% inflamed lung tissue; 4, 25 to 50% inflamed lung tissue; 5, >50% inflamed lung tissue according to a scoring system reported in (*105*). Scoring was performed independently by two investigators, whose scores were averaged. The total alveolar volume fraction was determined using the following procedure: (i) Regions representing empty space were acquired by setting a color threshold in ImageJ (*106*); (ii) to calculate the total alveolar volume fraction, the area of empty space was divided by the total lung area using MATLAB (v2018a). Peribronchial inflammation in the lungs of mice that had been sensitized and rechallenged with HDM was determined using the following scoring system as previously reported (*107*): 0, normal; 1, few cells; 2, a ring of inflammatory cells of one cell layer deep; 3, a ring of inflammatory cells of two to four cell layers deep; 4, a ring of inflammatory cells of >4 cell layers deep. The scores of three representative bronchiole sections per mouse were averaged. Mucus production in the airways of HDM-treated mice was determined using the following method as previously reported (*107*, *108*): 0, no stained cells per bronchiole; 1, <25% stained cells; 2, 25 to 50% stained cells; 3, 50 to 75% stained cells; 4, >75% stained cells. Peribronchial inflammation was determined in a blinded manner by a pulmonary pathologist.

Bronchioalveolar lavage

Anesthetized mice were intubated with a tracheal cannula, and BAL fluid was recovered by gently flushing the airways three times with 200 μl of Hanks' balanced salt solution/EDTA buffer upon thoracic massage. The three BAL fractions from each mouse were pooled and analyzed by antibody staining and flow cytometry for immune cell populations.

Single-cell preparation of lung tissue and mLNs

Lungs were cut into 8 to 10 pieces and incubated for 45 min at 37°C with Liberase TL (15 mg/ml; Roche, 5401020001) in complete RPMI1640 medium supplemented with 10% fetal bovine serum (FBS). Following enzymatic digestion, samples were passed through a 70-μm cell strainer, which was flushed twice with PBS supplemented with 2% FBS. Cells were spun at 800*g* for 5 min, resuspended in complete RPMI1640 medium, and stained with antibodies as described below. Single-cell suspensions of mLNs prepared similar to lung tissue but without prior enzymatic digestion. Cells isolated from mLNs, lungs, and BAL were counted using trypan blue or precision counting beads (BioLegend, catalog no. 424902) and prepared for either flow cytometric analysis or restimulation to measure cytokine production.

T cell culture in vitro

Mouse $CD4^+$ T cells were isolated from spleens using the MagniSort Mouse $CD4^+$ T cell enrichment kit (Invitrogen, 8804-6821-74) following the manufacturer's instructions. Cells were maintained in complete RPMI1640 medium (Corning, 10-040-CV) containing 10% FBS, 2 mM L-glutamine, 50 U/ml penicillin-streptomycin, and 5.5 μM β-mercaptoethanol. For T_H2 cell differentiation, naïve $CD4^+$ T cells isolated from WT and *Orai1*$^{fl/fl}$*Cd4Cre* mice were stimulated with anti-CD3 (2.5 ng/ml; clone 2C11) and anti-CD28 antibodies (1 μg/ml; clone 37.51) (both Bio X Cell) on flat-bottom plates coated with rabbit anti-hamster IgG (25 μg/ml; MP Biomedicals, catalog no. MP0855398) in the presence of IL-4 (50 ng/ml; PeproTech) and anti-IFN-γ (5 μg/ml; eBioscience, clone 11B11) for 2 days. For T_H1 differentiation, $CD4^+$ T cells were stimulated with anti-CD3 (1 μg/ml) and anti-CD28 (1 μg/ml) antibodies on IgG-coated plates as described above in the presence of IL-12 (20 ng/ml; PeproTech) and anti-IL-4 (5 μg/ml; eBioscience, clone 11B11). On day 2, cells were detached and expanded in RPMI1640 medium supplemented or not with T_H1 or T_H2 cytokines as described above and hIL-2 (20 U/ml; PeproTech, 200-02). Cells were analyzed on days 3 to 5.

T cell proliferation, cell cycle, and apoptosis in vitro

Naïve $CD4^+$ T cells were stained with CellTrace Violet (Invitrogen, C34557) according to the manufacturer's instructions and stimulated with anti-CD3/28 Dynabeads (Gibco, 11456D) at a 1:4 ratio (Dynabead:T cell) under T_H2-polarizing conditions as described above for 3 and 4 days. Cells were then stained for surface markers and annexin V–Alexa Fluor 647 (BioLegend, 640912) in annexin V staining buffer (BioLegend, 422201) for 10 min and analyzed by flow cytometry. For cell cycle analysis, cells were fixed with 70% ethanol at −20°C. Cells were then washed in PBS, treated with ribonuclease cocktail (1:500; Invitrogen) for 15 min, and stained with propidium iodide (0.5 mg/ml; Sigma-Aldrich) for 30 min. Cells were resuspended in PBS and analyzed by flow cytometry.

Flow cytometry

Cells isolated from lungs and lymphoid organs or T cells cultured in vitro were washed and prepared in PBS containing 3% FBS and 2 mM EDTA. To prevent unspecific antibody binding, cells were first incubated with anti-CD16/CD32 antibodies (Fc block) for 10 min. For staining of surface markers, cells were incubated with fluorescently

labeled antibodies on ice for 15 min in the dark. For intracellular cytokine staining, cells were stimulated with 1 μM ionomycin (Sigma-Aldrich, 407952) and 20 nM phorbol 12-myristate 13-acetate (PMA; Calbiochem, 524400) for 4 hours in the presence of 5 μM brefeldin A (eBioscience, 00-4506-51). Cells were then fixed with an intracellular fixation kit (Invitrogen, 88-8824-00) for 30 min, permeabilized with Permeabilization Buffer (eBioscience, 00-8333-56), and incubated with anti-cytokine antibodies for 30 min. For staining of transcription factors, cells were incubated with antibodies against surface antigens, labeled with LIVE/DEAD Fixable Blue Dead Cell Stain (Thermo Fisher Scientific, L23105) following the manufacturer's instructions, and fixed/permeabilized with Foxp3 Transcription Factor Staining Buffer Set (eBioscience, 00-5523-00). Cells were subsequently incubated with antibodies against intracellular antigens for 30 min. The specificity of antibody binding was tested using isotype control antibodies and fluorescence minus one controls to correct for the spread of fluorophores into other detection channels (figs. S7 and S8). A complete list of antibodies and their fluorophore conjugates can be found in table S2. For the detection of IAV and HDM-specific T cells, we incubated cells with an IAV nucleocapsid protein-specific I-A^b tetramer ($NP_{311–325}$, QVYSLIRPNENPAHK) conjugated with allophycocyanin (APC) and an HDM-specific I-A^b tetramer (Der p $1_{217–227}$; CQIYPPNVNKI) conjugated with phycoerythrin (PE) or APC. All tetramers were obtained from the National Institutes of Health (NIH) Tetramer Core Facility (Emory University, Atlanta, GA). A complete list of tetramers and their respective fluorescent conjugates can be found in table S3. Samples were acquired on an LSR II or LSRFortessa flow cytometer (BD Biosciences) and analyzed using FlowJo software (TreeStar, versions 9.3.2 and 10.5.3.).

Cytometric bead array

To measure IL-5 production by pulmonary T cells, total lymphocytes isolated from the lungs of HDM-treated mice were stimulated with anti-CD3 (0.5 μg/ml; Bio X Cell, clone 145-2C11) in complete RPMI1640 medium containing 10% FBS for 24 hours, followed by the collection of cell culture supernatant. IL-5 levels were measured by cytometric bead array using the Mouse IL-5 Enhanced Sensitivity Flex Set (BD Biosciences, catalog no. 562234) and Mouse Enhanced Sensitivity Master Buffer Kit (BD Biosciences, catalog no. 562248) following the manufacturer's instructions. The concentrations of IL-5 were normalized to the number of T cells to evaluate the cytokine production capacity.

BrdU analysis

For the duration of 7 days, BrdU (0.8 mg/ml) was provided into the drinking water, to which experimental mice had access ad libitum. BrdU-supplemented drinking water was renewed daily. One day after starting BrdU treatment, mice were sensitized intranasally for 3 days with 15 μg of HDM extract. On day 3, mice were euthanized, and HDM-specific T cells isolated from their lungs and mLNs were analyzed for BrdU incorporation. Specifically, single-cell suspensions of the lungs and mLNs were washed with PBS and 2% FBS and fixed and permeabilized for 45 min at 4°C using the Foxp3 staining buffer kit (eBioscience, 00-5523-00). Cells were treated with 30 μg of deoxyribonuclease (DNase) for 45 min at 37°C; incubated with anti-CD16/CD32 antibody mix (eBioscience, 2.4G2) for 20 min at room temperature; stained with anti-BrdU antibody (eBioscience, catalog no. 11-5071-42), HDM-specific I-A(b) tetramer conjugated to PE or APC (as described above), and antibodies against surface and intracellular proteins; and subsequently analyzed by flow cytometry.

Enzyme-linked immunosorbent assay

To measure IAV-specific antibodies, high-binding enzyme-linked immunosorbent assay (ELISA) plates (Corning, 9018) were coated with heat-inactivated x31-IAV overnight at 4°C. ELISA plates were blocked with 20% FBS in PBS at 37°C for 1 hour, followed by washing three times with wash buffer [0.05% (v/v) Tween-20 in PBS]. Plates were incubated with serial dilutions of sera from WT and *Orai1*$^{fl/fl}$*Cd4Cre* mice for 1 hour at 37°C, followed by incubation with alkaline phosphatase goat anti-mouse IgM, IgG, and IgG1 secondary antibodies (SouthernBiotech, 1021-04, 1036-04, and 1071-04, respectively) at 37°C for 2 hours. After addition of substrate solution, absorption was measured at 405 nm using a FlexStation 3 plate reader (Molecular Devices). Measurements of total serum IgE levels were conducted using the IgE Mouse Uncoated ELISA Kit (Invitrogen, 88-50460-88) according to the manufacturer's protocol.

Synthesis of cDNA and qRT-PCR

Total RNA was extracted from cells using TRIzol reagent (Invitrogen, 15596026) as previously described (*109*). cDNA was synthesized using the Superscript II RT kit (Invitrogen, 18080-044) or the iScript kit (Bio-Rad, 1708891BUN) following the manufacturer's instructions. qRT-PCR was performed using the Maxima SYBR Green Master Mix (Applied Biosystems, 4309155) and the QuantStudio5 RT-PCR system (Applied Biosystems). Transcript levels were normalized to the expression of housekeeping genes using the $2^{-\Delta Ct}$ method. A complete list of primers used in this study can be found in table S1.

RNA sequencing

For RNA-seq, we prepared single-cell suspensions of lungs from TCR$\alpha^{-/-}$ recipient mice that had been injected with $CD4^+$ T cells from WT OT-II or *Orai1*$^{fl/fl}$ *Cd4Cre* OT-II mice and subsequently infected with IAV^{OVA} or sensitized and challenged with HDM/OVA. $CD4^+V\alpha2^+$ donor T cells were enriched to at least 83% purity by flow cytometric cell sorting using a FACSAriaII (BD Biosciences). Total RNA was extracted using the RNeasy Mini RNA Isolation Kit (QIAGEN, 74104), and RNA quality and quantity were analyzed using a Bioanalyzer 2100 (Agilent) and PICO chips. RNA libraries were prepared using the TruSeq RNA sample prep v2 kit (Illumina) using 100 ng of total RNA treated with DNase I (QIAGEN) following the manufacturer's protocol and 15 cycles of PCR amplification. The libraries were purified with AMPure beads (Beckman Coulter), quantified using a Qubit 2.0 fluorometer (Life Technologies), and visualized with an Agilent Tapestation 2200. Libraries prepared from different samples were pooled equimolarly and run on the HiSeq 4000 sequencing system to generate 50–base pair paired-end reads. Reads per sample FASTQ files were generated using the bcl2fastq2 Conversion software (v2.20). Adaptor sequences were trimmed using the Trimmomatic (v0.39) tool (*110*), and resulting reads were mapped to the mouse reference genome mm10 using STAR (v2.7.3a) (*111*). The read count matrix for the genomic features was generated using the R package Subread (Bioconductor v2.0.0). The DESeq2 package (Bioconductor v3.10) was used for differential gene expression analysis among groups of samples with three replicates each and for PCA. A statistical cutoff of false discovery rate (FDR) of <0.10 was used to determine statistically significant differences in gene expression.

The RNA-seq has been deposited in the Gene Expression Omnibus database under accession number GSE184228.

Bioinformatic pathway analysis

GSEA was performed using GSEA software (Broad Institute, v4.0.0) (*112*). Pathway analyses were performed using IPA (QIAGEN) and the EnrichR Bioinformatics tool (*113*). A statistical cutoff of $P < 0.10$ was used to determine significantly expressed pathways. The open-source software LISA was used to identify upstream regulators of individual DEGs (http://lisa.cistrome.org/). An upstream regulator analysis was conducted using IPA, with a statistical significance cutoff of P (adjusted) < 0.05. Activation Z score values were calculated using an asymptotic Gaussian approximation (*114*).

Treatment with CRAC channel inhibitor

The selective CRAC channel inhibitor CM4620 was provided by CalciMedica (La Jolla, CA) (*67*). The inhibitor was solubilized in vehicle composed of 0.5% methylcellulose (w/w) with a viscosity of 400 cP (Sigma-Aldrich, M0262-250G) and 1% (w/w) Tween 80 (Thermo Fisher Scientific, BP338-500) in double-distilled H_2O. The active form of CM4620 was administered by oral gavage at 25 mg/kg of body weight (25% loading) and 75 mg/kg of body weight of hypromellose acetate succinate (HPMCAS) bead carrier formulated in vehicle for four consecutive days. Control mice were treated with HPMCAS carrier alone. CM4620 concentrations in mouse plasma were determined using a high-sensitivity method developed by BioAgilytix, San Diego (formerly MicroConstants). The method uses high-performance liquid chromatography with tandem MS detection and is suitable for measuring concentrations ranging from 1 to 1000 ng/ml using 25.0 μl of mouse plasma extracted using a liquid-liquid approach.

Intracellular Ca^{2+} measurements

Naïve $CD4^+$ T cells as well as T_H1 and T_H2 cells from WT and *Orai1*$^{fl/fl}$*Cd4Cre* mice were loaded with 1 μM Fura-2-AM (Molecular Probes, F1221) for 30 min at room temperature, washed, and attached to 96-well plates (BD Falcon, 353219) coated with 0.01% (v/v) poly-L-Lysine (Sigma-Aldrich, P8920). At the beginning of each experiment, cells were kept in Ca^{2+}-free Ringer solution [155 mM NaCl, 4.5 mM KCl, 3 mM $MgCl_2$, 10 mM D-glucose, and 5 mM Na-Hepes (pH 7.4)], followed by treatment with 1 μM thapsigargin (Sigma-Aldrich, 586005) to deplete ER Ca^{2+} stores. Cells were subsequently perfused with Ca^{2+}-containing Ringer solution [155 mM NaCl, 4.5 mM KCl, 2 mM $CaCl_2$, 1 mM $MgCl_2$, 10 mM D-glucose, and 5 mM Na-Hepes (pH 7.4)] at the indicated time points to induce SOCE. Alternatively, cells were stimulated with anti-CD3 (1 μg/ml; clone 2C11) for 30 min during the loading with Fura-2-AM. Cells were then washed and kept in Ca^{2+}-free Ringer solution at the beginning of the recording, followed by CD3 cross-linking with rabbit anti-hamster IgG (1 μg/ml; MP Biomedicals, MP0855398), and addition of Ca^{2+}-containing Ringer solution. Fura-2 fluorescence was measured at an emission wavelength of 510 nm after excitation at 340 nm and 380 nm using FlexStation 3 (Molecular Devices) and plotted as baseline-normalized F340/F380 emission ratio.

Statistical analyses

All results are means with or without the SEM. The statistical significance of differences between experimental groups was determined by paired or unpaired Student's t test, Mann-Whitney test, one-way analysis of variance (ANOVA) with Tukey's or Sidak's multiple comparison test, or two-way ANOVA with Sidak multiple comparison test, as indicated in the figure legends. Differences were considered significant for $^*P < 0.05$, $^{**}P < 0.01$, and $^{***}P < 0.001$. The number of mice per experimental group is indicated in the respective figure legends. The statistical significance for DEGs was determined through DESeq2 using the Wald test. Differences were considered significant for an FDR of <0.10. Significantly expressed pathways through EnrichR and IPA were determined using Fisher's exact test, with significance being defined for $P < 0.10$. The statistical significance for transcription factors in the LISA was determined using the one-sided Wilcoxon rank sum test statistic (*49*).

SUPPLEMENTARY MATERIALS

Supplementary material for this article is available at https://science.org/doi/10.1126/sciadv.abn6552

View/request a protocol for this paper from *Bio-protocol*.

REFERENCES AND NOTES

1. M. Vaeth, S. Kahlfuss, S. Feske, CRAC channels and calcium signaling in T cell-mediated immunity. *Trends Immunol.* **41**, 878–901 (2020).
2. Y. Wang, A. Tao, M. Vaeth, S. Feske, Calcium regulation of T cell metabolism. *Curr. Opin. Physiol.* **17**, 207–223 (2020).
3. S. Feske, Calcium signalling in lymphocyte activation and disease. *Nat. Rev. Immunol.* **7**, 690–702 (2007).
4. M. Trebak, J. P. Kinet, Calcium signalling in T cells. *Nat. Rev. Immunol.* **19**, 154–169 (2019).
5. M. Prakriya, R. S. Lewis, Store-operated calcium channels. *Physiol. Rev.* **95**, 1383–1436 (2015).
6. R. S. Lacruz, S. Feske, Diseases caused by mutations in ORAI1 and STIM1. *Ann. N. Y. Acad. Sci.* **1356**, 45–79 (2015).
7. S. Kahlfuss, U. Kaufmann, A. R. Concepcion, L. Noyer, D. Raphael, M. Vaeth, J. Yang, P. Pancholi, M. Maus, J. Muller, L. Kozhaya, A. Khodadadi-Jamayran, Z. Sun, P. Shaw, D. Unutmaz, P. B. Stathopulos, C. Feist, S. B. Cameron, S. E. Turvey, S. Feske, STIM1-mediated calcium influx controls antifungal immunity and the metabolic function of non-pathogenic Th17 cells. *EMBO Mol. Med.* **12**, e11592 (2020).
8. M. Vaeth, J. Yang, M. Yamashita, I. Zee, M. Eckstein, C. Knosp, U. Kaufmann, P. Karoly Jani, R. S. Lacruz, V. Flockerzi, I. Kacskovics, M. Prakriya, S. Feske, ORAI2 modulates store-operated calcium entry and T cell-mediated immunity. *Nat. Commun.* **8**, 14714 (2017).
9. M. Vaeth, M. Eckstein, P. J. Shaw, L. Kozhaya, J. Yang, F. Berberich-Siebelt, R. Clancy, D. Unutmaz, S. Feske, Store-operated Ca^{2+} entry in follicular T cells controls humoral immune responses and autoimmunity. *Immunity* **44**, 1350–1364 (2016).
10. P. J. Shaw, C. Weidinger, M. Vaeth, K. Luethy, S. M. Kaech, S. Feske, $CD4^+$ and $CD8^+$ T cell-dependent antiviral immunity requires STIM1 and STIM2. *J. Clin. Invest.* **124**, 4549–4563 (2014).
11. U. Kaufmann, S. Kahlfuss, J. Yang, E. Ivanova, S. B. Koralov, S. Feske, Calcium signaling controls pathogenic Th17 cell-mediated inflammation by regulating mitochondrial function. *Cell Metab.* **29**, 1104–1118.e6 (2019).
12. U. Kaufmann, P. J. Shaw, L. Kozhaya, R. Subramanian, K. Gaida, D. Unutmaz, H. J. McBride, S. Feske, Selective ORAI1 inhibition ameliorates autoimmune central nervous system inflammation by suppressing effector but not regulatory T cell function. *J. Immunol.* **196**, +573–+585 (2016).
13. J. Ma, C. A. McCarl, S. Khalil, K. Luthy, S. Feske, T-cell-specific deletion of STIM1 and STIM2 protects mice from EAE by impairing the effector functions of Th1 and Th17 cells. *Eur. J. Immunol.* **40**, 3028–3042 (2010).
14. C. A. McCarl, S. Khalil, J. Ma, M. Oh-hora, M. Yamashita, J. Roether, T. Kawasaki, A. Jairaman, Y. Sasaki, M. Prakriya, S. Feske, Store-operated Ca2+ entry through ORAI1 is critical for T cell-mediated autoimmunity and allograft rejection. *J. Immunol.* **185**, 5845–5858 (2010).
15. M. K. Schuhmann, D. Stegner, A. Berna-Erro, S. Bittner, A. Braun, C. Kleinschnitz, G. Stoll, H. Wiendl, S. G. Meuth, B. Nieswandt, Stromal interaction molecules 1 and 2 are key regulators of autoreactive T cell activation in murine autoimmune central nervous system inflammation. *J. Immunol.* **184**, 1536–1542 (2010).
16. K. D. Kim, S. Srikanth, Y. V. Tan, M. K. Yee, M. Jew, R. Damoiseaux, M. E. Jung, S. Shimizu, D. S. An, B. Ribalet, J. A. Waschek, Y. Gwack, Calcium signaling via Orai1 is essential for induction of the nuclear orphan receptor pathway to drive Th17 differentiation. *J. Immunol.* **192**, 110–122 (2014).

17. N. Hermann-Kleiter, G. Baier, NFAT pulls the strings during CD4$^+$ T helper cell effector functions. *Blood* **115**, 2989–2997 (2010).
18. D. F. Choy, K. M. Hart, L. A. Borthwick, A. Shikotra, D. R. Nagarkar, S. Siddiqui, G. Jia, C. M. Ohri, E. Doran, K. M. Vannella, C. A. Butler, B. Hargadon, J. C. Sciurba, R. L. Gieseck, R. W. Thompson, S. White, A. R. Abbas, J. Jackman, L. C. Wu, J. G. Egen, L. G. Heaney, T. R. Ramalingam, J. R. Arron, T. A. Wynn, P. Bradding, T_H2 and T_H17 inflammatory pathways are reciprocally regulated in asthma. *Sci. Transl. Med.* **7**, 301ra129 (2015).
19. B. N. Lambrecht, H. Hammad, J. V. Fahy, The cytokines of asthma. *Immunity* **50**, 975–991 (2019).
20. K. Hirahara, A. Poholek, G. Vahedi, A. Laurence, Y. Kanno, J. D. Milner, J. J. O'Shea, Mechanisms underlying helper T-cell plasticity: Implications for immune-mediated disease. *J. Allergy Clin. Immunol.* **131**, 1276–1287 (2013).
21. Y. Gwack, S. Srikanth, M. Oh-Hora, P. G. Hogan, E. D. Lamperti, M. Yamashita, C. Gelinas, D. S. Neems, Y. Sasaki, S. Feske, M. Prakriya, K. Rajewsky, A. Rao, Hair loss and defective T- and B-cell function in mice lacking ORAI1. *Mol. Cell. Biol.* **28**, 5209–5222 (2008).
22. M. Oh-Hora, X. Lu, M. Shiokawa, H. Takayanagi, S. Yamasaki, Stromal interaction molecule deficiency in T cells promotes spontaneous follicular helper T cell development and causes type 2 immune disorders. *J. Immunol.* **202**, 2616–2627 (2019).
23. M. Oh-Hora, M. Yamashita, P. G. Hogan, S. Sharma, E. Lamperti, W. Chung, M. Prakriya, S. Feske, A. Rao, Dual functions for the endoplasmic reticulum calcium sensors STIM1 and STIM2 in T cell activation and tolerance. *Nat. Immunol.* **9**, 432–443 (2008).
24. S. Feske, R. Draeger, H. H. Peter, K. Eichmann, A. Rao, The duration of nuclear residence of NFAT determines the pattern of cytokine expression in human SCID T cells. *J. Immunol.* **165**, 297–305 (2000).
25. T. Yoshino, J. Ishikawa, K. Ohga, T. Morokata, R. Takezawa, H. Morio, Y. Okada, K. Honda, T. Yamada, YM-58483, a selective CRAC channel inhibitor, prevents antigen-induced airway eosinophilia and late phase asthmatic responses via Th2 cytokine inhibition in animal models. *Eur. J. Pharmacol.* **560**, 225–233 (2007).
26. M. Kaur, M. A. Birrell, B. Dekkak, S. Reynolds, S. Wong, J. De Alba, K. Raemdonck, S. Hall, K. Simpson, M. Begg, M. G. Belvisi, D. Singh, The role of CRAC channel in asthma. *Pulm. Pharmacol. Ther.* **35**, 67–74 (2015).
27. M. Sutovska, M. Kocmalova, I. Kazimierova, C. I. N. Forsberg, M. Joskova, M. Adamkov, S. Franova, Effects of inhalation of STIM-Orai antagonist SKF 96365 on ovalbumin-induced airway remodeling in guinea pigs. *Adv. Exp. Med. Biol.* , (2021).
28. A. Jairaman, C. H. Maguire, R. P. Schleimer, M. Prakriya, Allergens stimulate store-operated calcium entry and cytokine production in airway epithelial cells. *Sci. Rep.* **6**, 32311 (2016).
29. A. Jairaman, M. Yamashita, R. P. Schleimer, M. Prakriya, Store-operated Ca^{2+} release-activated Ca^{2+} channels regulate PAR2-activated Ca^{2+} signaling and cytokine production in airway epithelial cells. *J. Immunol.* **195**, 2122–2133 (2015).
30. W. W. Thompson, D. K. Shay, E. Weintraub, L. Brammer, N. Cox, L. J. Anderson, K. Fukuda, Mortality associated with influenza and respiratory syncytial virus in the United States. *JAMA* **289**, 179–186 (2003).
31. F. Krammer, G. J. D. Smith, R. A. M. Fouchier, M. Peiris, K. Kedzierska, P. C. Doherty, P. Palese, M. L. Shaw, J. Treanor, R. G. Webster, A. Garcia-Sastre, Influenza. *Nat. Rev. Dis. Primers* **4**, 3 (2018).
32. A. Pizzolla, T. H. O. Nguyen, J. M. Smith, A. G. Brooks, K. Kedzieska, W. R. Heath, P. C. Reading, L. M. Wakim, Resident memory CD8$^+$ T cells in the upper respiratory tract prevent pulmonary influenza virus infection. *Sci. Immunol.* **2**, eaam6970 (2017).
33. K. D. Zens, J. K. Chen, R. S. Guyer, F. L. Wu, F. Cvetkovski, M. Miron, D. L. Farber, Reduced generation of lung tissue-resident memory T cells during infancy. *J. Exp. Med.* **214**, 2915–2932 (2017).
34. T. M. Strutt, K. Dhume, C. M. Finn, J. H. Hwang, C. Castonguay, S. L. Swain, K. K. McKinstry, IL-15 supports the generation of protective lung-resident memory CD4 T cells. *Mucosal Immunol.* **11**, 668–680 (2018).
35. J. G. Cullen, H. A. McQuilten, K. M. Quinn, M. Olshansky, B. E. Russ, A. Morey, S. Wei, J. E. Prier, N. L. La Gruta, P. C. Doherty, S. J. Turner, CD4$^+$ T help promotes influenza virus-specific CD8$^+$ T cell memory by limiting metabolic dysfunction. *Proc. Natl. Acad. Sci. U.S.A.* **116**, 4481–4488 (2019).
36. S. Crotty, T follicular helper cell differentiation, function, and roles in disease. *Immunity* **41**, 529–542 (2014).
37. P. G. Thomas, S. A. Brown, W. Yue, J. So, R. J. Webby, P. C. Doherty, An unexpected antibody response to an engineered influenza virus modifies CD8+ T cell responses. *Proc. Natl. Acad. Sci. U.S.A.* **103**, 2764–2769 (2006).
38. S. Davidson, S. Crotta, T. M. McCabe, A. Wack, Pathogenic potential of interferon $\alpha\beta$ in acute influenza infection. *Nat. Commun.* **5**, 3864 (2014).
39. W. Fu, X. Liu, X. Lin, H. Feng, L. Sun, S. Li, H. Chen, H. Tang, L. Lu, W. Jin, C. Dong, Deficiency in T follicular regulatory cells promotes autoimmunity. *J. Exp. Med.* **215**, 815–825 (2018).
40. N. L. La Gruta, S. J. Turner, T cell mediated immunity to influenza: Mechanisms of viral control. *Trends Immunol.* **35**, 396–402 (2014).
41. S. J. Turner, E. Olivas, A. Gutierrez, G. Diaz, P. C. Doherty, Disregulated influenza A virus-specific CD8$^+$ T cell homeostasis in the absence of IFN-γ signaling. *J. Immunol.* **178**, 7616–7622 (2007).
42. T. Hussell, A. Pennycook, P. J. Openshaw, Inhibition of tumor necrosis factor reduces the severity of virus-specific lung immunopathology. *Eur. J. Immunol.* **31**, 2566–2573 (2001).
43. R. L. Peper, H. Van Campen, Tumor necrosis factor as a mediator of inflammation in influenza A viral pneumonia. *Microb. Pathog.* **19**, 175–183 (1995).
44. L. C. Denlinger, B. R. Phillips, S. Ramratnam, K. Ross, N. R. Bhakta, J. C. Cardet, M. Castro, S. P. Peters, W. Phipatanakul, S. Aujla, L. B. Bacharier, E. R. Bleecker, S. A. Comhair, A. Coverstone, M. DeBoer, S. C. Erzurum, S. B. Fain, M. Fajt, A. M. Fitzpatrick, J. Gaffin, B. Gaston, A. T. Hastie, G. A. Hawkins, F. Holguin, A. M. Irani, E. Israel, B. D. Levy, N. Ly, D. A. Meyers, W. C. Moore, R. Myers, M. T. Opina, M. C. Peters, M. L. Schiebler, R. L. Sorkness, W. G. Teague, S. E. Wenzel, P. G. Woodruff, D. T. Mauger, J. V. Fahy, N. N. Jarjour; National Heart, Lung, and Blood Institute's Severe Asthma Research Program-3 Investigators, Inflammatory and comorbid features of patients with severe asthma and frequent exacerbations. *Am. J. Respir. Crit. Care Med.* **195**, 302–313 (2017).
45. K. Nakagome, M. Nagata, Involvement and possible role of eosinophils in asthma exacerbation. *Front. Immunol.* **9**, 2220 (2018).
46. P. C. Fulkerson, C. A. Fischetti, M. L. McBride, L. M. Hassman, S. P. Hogan, M. E. Rothenberg, A central regulatory role for eosinophils and the eotaxin/CCR3 axis in chronic experimental allergic airway inflammation. *Proc. Natl. Acad. Sci. U.S.A.* **103**, 16418–16423 (2006).
47. L. M. Teran, M. Mochizuki, J. Bartels, E. L. Valencia, T. Nakajima, K. Hirai, J. M. Schroder, Th1- and Th2-type cytokines regulate the expression and production of eotaxin and RANTES by human lung fibroblasts. *Am. J. Respir. Cell Mol. Biol.* **20**, 777–786 (1999).
48. L. Li, Y. Xia, A. Nguyen, Y. H. Lai, L. Feng, T. R. Mosmann, D. Lo, Effects of Th2 cytokines on chemokine expression in the lung: IL-13 potently induces eotaxin expression by airway epithelial cells. *J. Immunol.* **162**, 2477–2487 (1999).
49. Q. Qin, J. Fan, R. Zheng, C. Wan, S. Mei, Q. Wu, H. Sun, M. Brown, J. Zhang, C. A. Meyer, X. S. Liu, Lisa: Inferring transcriptional regulators through integrative modeling of public chromatin accessibility and ChIP-seq data. *Genome Biol.* **21**, 32 (2020).
50. M. Lohoff, H. W. Mittrucker, S. Prechtl, S. Bischof, F. Sommer, S. Kock, D. A. Ferrick, G. S. Duncan, A. Gessner, T. W. Mak, Dysregulated T helper cell differentiation in the absence of interferon regulatory factor 4. *Proc. Natl. Acad. Sci. U.S.A.* **99**, 11808–11812 (2002).
51. J. Rengarajan, K. A. Mowen, K. D. McBride, E. D. Smith, H. Singh, L. H. Glimcher, Interferon regulatory factor 4 (IRF4) interacts with NFATc2 to modulate interleukin 4 gene expression. *J. Exp. Med.* **195**, 1003–1012 (2002).
52. B. C. Betz, K. L. Jordan-Williams, C. Wang, S. G. Kang, J. Liao, M. R. Logan, C. H. Kim, E. J. Taparowsky, Batf coordinates multiple aspects of B and T cell function required for normal antibody responses. *J. Exp. Med.* **207**, 933–942 (2010).
53. M. Kuwahara, W. Ise, M. Ochi, J. Suzuki, K. Kometani, S. Maruyama, M. Izumoto, A. Matsumoto, N. Takemori, A. Takemori, K. Shinoda, T. Nakayama, O. Ohara, M. Yasukawa, T. Sawasaki, T. Kurosaki, M. Yamashita, Bach2-Batf interactions control Th2-type immune response by regulating the IL-4 amplification loop. *Nat. Commun.* **7**, 12596 (2016).
54. G. Liu, Y. Lu, S. N. Thulasi Raman, F. Xu, Q. Wu, Z. Li, R. Brownlie, Q. Liu, Y. Zhou, Nuclear-resident RIG-I senses viral replication inducing antiviral immunity. *Nat. Commun.* **9**, 3199 (2018).
55. M. B. Graham, V. L. Braciale, T. J. Braciale, Influenza virus-specific CD4$^+$ T helper type 2 T lymphocytes do not promote recovery from experimental virus infection. *J. Exp. Med.* **180**, 1273–1282 (1994).
56. B. Upadhyaya, Y. Yin, B. J. Hill, D. C. Douek, C. Prussin, Hierarchical IL-5 expression defines a subpopulation of highly differentiated human Th2 cells. *J. Immunol.* **187**, 3111–3120 (2011).
57. J. Zhu, H. Yamane, J. Cote-Sierra, L. Guo, W. E. Paul, GATA-3 promotes Th2 responses through three different mechanisms: Induction of Th2 cytokine production, selective growth of Th2 cells and inhibition of Th1 cell-specific factors. *Cell Res.* **16**, 3–10 (2006).
58. R. Yagi, J. Zhu, W. E. Paul, An updated view on transcription factor GATA3-mediated regulation of Th1 and Th2 cell differentiation. *Int. Immunol.* **23**, 415–420 (2011).
59. A. Sahoo, S. Wali, R. Nurieva, T helper 2 and T follicular helper cells: Regulation and function of interleukin-4. *Cytokine Growth Factor Rev.* **30**, 29–37 (2016).
60. T. L. Murphy, R. Tussiwand, K. M. Murphy, Specificity through cooperation: BATF-IRF interactions control immune-regulatory networks. *Nat. Rev. Immunol.* **13**, 499–509 (2013).
61. H. Kurata, H. J. Lee, A. O'Garra, N. Arai, Ectopic expression of activated Stat6 induces the expression of Th2-specific cytokines and transcription factors in developing Th1 cells. *Immunity* **11**, 677–688 (1999).
62. J. Zhu, L. Guo, C. J. Watson, J. Hu-Li, W. E. Paul, Stat6 is necessary and sufficient for IL-4's role in Th2 differentiation and cell expansion. *J. Immunol.* **166**, 7276–7281 (2001).
63. J. Cote-Sierra, G. Foucras, L. Guo, L. Chiodetti, H. A. Young, J. Hu-Li, J. Zhu, W. E. Paul, Interleukin 2 plays a central role in Th2 differentiation. *Proc. Natl. Acad. Sci. U.S.A.* **101**, 3880–3885 (2004).

64. S. H. Ross, D. A. Cantrell, Signaling and function of interleukin-2 in T lymphocytes. *Annu. Rev. Immunol.* **36**, 411–433 (2018).
65. P. M. Renzi, S. Sapienza, S. Waserman, T. Du, R. Olivenstein, N. S. Wang, J. G. Martin, Effect of interleukin-2 on the airway response to antigen in the rat. *Am. Rev. Respir. Dis.* **146**, 163–169 (1992).
66. A. A. Milne, M. M. Teixeira, P. G. Hellewell, P. J. Piper, Induction of leucocyte recruitment and bronchial hyperresponsiveness in the guinea pig by aerosol administration of interleukin-2. *Int. Arch. Allergy Immunol.* **108**, 60–67 (1995).
67. R. T. Waldron, Y. Chen, H. Pham, A. Go, H. Y. Su, C. Hu, L. Wen, S. Z. Husain, C. A. Sugar, J. Roos, S. Ramos, A. Lugea, M. Dunn, K. Stauderman, S. J. Pandol, The Orai Ca2+ channel inhibitor CM4620 targets both parenchymal and immune cells to reduce inflammation in experimental acute pancreatitis. *J. Physiol.* **597**, 3085–3105 (2019).
68. M. P. DeBerge, K. H. Ely, R. I. Enelow, Soluble, but not transmembrane, TNF-α is required during influenza infection to limit the magnitude of immune responses and the extent of immunopathology. *J. Immunol.* **192**, 5839–5851 (2014).
69. K. M. Quinn, W. T. Kan, K. A. Watson, B. J. Liddicoat, N. G. Swan, H. McQuilten, A. E. Denton, J. Li, W. Chen, L. E. Brown, D. C. Jackson, P. C. Reading, P. C. Doherty, K. Kedzierska, L. Kedzierski, S. J. Turner, N. L. La Gruta, Extrinsically derived TNF is primarily responsible for limiting antiviral $CD8^+$ T cell response magnitude. *PLOS ONE* **12**, e0184732 (2017).
70. N. Baumgarth, A. Kelso, In vivo blockade of gamma interferon affects the influenza virus-induced humoral and the local cellular immune response in lung tissue. *J. Virol.* **70**, 4411–4418 (1996).
71. G. Karupiah, J. H. Chen, S. Mahalingam, C. F. Nathan, J. D. MacMicking, Rapid interferon γ–dependent clearance of influenza A virus and protection from consolidating pneumonitis in nitric oxide synthase 2-deficient mice. *J. Exp. Med.* **188**, 1541–1546 (1998).
72. M. B. Graham, D. K. Dalton, D. Giltinan, V. L. Braciale, T. A. Stewart, T. J. Braciale, Response to influenza infection in mice with a targeted disruption in the interferon gamma gene. *J. Exp. Med.* **178**, 1725–1732 (1993).
73. M. Q. Nicol, G. M. Campbell, D. J. Shaw, I. Dransfield, Y. Ligertwood, P. M. Beard, A. A. Nash, B. M. Dutia, Lack of IFNγ signaling attenuates spread of influenza A virus in vivo and leads to reduced pathogenesis. *Virology* **526**, 155–164 (2019).
74. H. Hammad, B. N. Lambrecht, The basic immunology of asthma. *Cell* **184**, 1469–1485 (2021).
75. G. Wei, L. Wei, J. Zhu, C. Zang, J. Hu-Li, Z. Yao, K. Cui, Y. Kanno, T. Y. Roh, W. T. Watford, D. E. Schones, W. Peng, H. W. Sun, W. E. Paul, J. J. O'Shea, K. Zhao, Global mapping of H3K4me3 and H3K27me3 reveals specificity and plasticity in lineage fate determination of differentiating $CD4^+$ T cells. *Immunity* **30**, 155–167 (2009).
76. J. Kock, S. Kreher, K. Lehmann, R. Riedel, M. Bardua, T. Lischke, M. Jargosch, C. Haftmann, H. Bendfeldt, F. Hatam, M. F. Mashreghi, R. Baumgrass, A. Radbruch, H. D. Chang, Nuclear factor of activated T cells regulates the expression of interleukin-4 in Th2 cells in an all-or-none fashion. *J. Biol. Chem.* **289**, 26752–26761 (2014).
77. E. Maier, A. Duschl, J. Horejs-Hoeck, STAT6-dependent and -independent mechanisms in Th2 polarization. *Eur. J. Immunol.* **42**, 2827–2833 (2012).
78. W. Liao, J. X. Lin, L. Wang, P. Li, W. J. Leonard, Modulation of cytokine receptors by IL-2 broadly regulates differentiation into helper T cell lineages. *Nat. Immunol.* **12**, 551–559 (2011).
79. J. Gomez-Rodriguez, F. Meylan, R. Handon, E. T. Hayes, S. M. Anderson, M. R. Kirby, R. M. Siegel, P. L. Schwartzberg, Itk is required for Th9 differentiation via TCR-mediated induction of IL-2 and IRF4. *Nat. Commun.* **7**, 10857 (2016).
80. C. A. McCarl, C. Picard, S. Khalil, T. Kawasaki, J. Rother, A. Papolos, J. Kutok, C. Hivroz, F. Ledeist, K. Plogmann, S. Ehl, G. Notheis, M. H. Albert, B. H. Belohradsky, J. Kirschner, A. Rao, A. Fischer, S. Feske, ORAI1 deficiency and lack of store-operated Ca^{2+} entry cause immunodeficiency, myopathy, and ectodermal dysplasia. *J. Allergy Clin. Immunol.* **124**, 1311–1318.e7 (2009).
81. U. Gowthaman, J. S. Chen, B. Zhang, W. F. Flynn, Y. Lu, W. Song, J. Joseph, J. A. Gertie, L. Xu, M. A. Collet, J. D. S. Grassmann, T. Simoneau, D. Chiang, M. C. Berin, J. E. Craft, J. S. Weinstein, A. Williams, S. C. Eisenbarth, Identification of a T follicular helper cell subset that drives anaphylactic IgE. *Science* **365**, (2019).
82. R. L. Coffman, J. Carty, A T cell activity that enhances polyclonal IgE production and its inhibition by interferon-γ. *J. Immunol.* **136**, 949–954 (1986).
83. J. Pene, J. F. Gauchat, S. Lecart, E. Drouet, P. Guglielmi, V. Boulay, A. Delwail, D. Foster, J. C. Lecron, H. Yssel, Cutting edge: IL-21 is a switch factor for the production of IgG1 and IgG3 by human B cells. *J. Immunol.* **172**, 5154–5157 (2004).
84. K. Ozaki, R. Spolski, C. G. Feng, C. F. Qi, J. Cheng, A. Sher, H. C. Morse III, C. Liu, P. L. Schwartzberg, W. J. Leonard, A critical role for IL-21 in regulating immunoglobulin production. *Science* **298**, 1630–1634 (2002).
85. X. Z. Shang, K. Y. Ma, J. Radewonuk, J. Li, X. Y. Song, D. E. Griswold, E. Emmell, L. Li, IgE isotype switch and IgE production are enhanced in IL-21-deficient but not IFN-γ-deficient mice in a Th2-biased response. *Cell. Immunol.* **241**, 66–74 (2006).
86. S. J. D'Souza, A. Pajak, K. Balazsi, L. Dagnino, Ca^{2+} and BMP-6 signaling regulate E2F during epidermal keratinocyte differentiation. *J. Biol. Chem.* **276**, 23531–23538 (2001).
87. M. Vaeth, Y. H. Wang, M. Eckstein, J. Yang, G. J. Silverman, R. S. Lacruz, K. Kannan, S. Feske, Tissue resident and follicular Treg cell differentiation is regulated by CRAC channels. *Nat. Commun.* **10**, 1183 (2019).
88. Y. Xiong, G. J. Hannon, H. Zhang, D. Casso, R. Kobayashi, D. Beach, p21 is a universal inhibitor of cyclin kinases. *Nature* **366**, 701–704 (1993).
89. M. Watanabe, K. D. Moon, M. S. Vacchio, K. S. Hathcock, R. J. Hodes, Downmodulation of tumor suppressor p53 by T cell receptor signaling is critical for antigen-specific $CD4^+$ T cell responses. *Immunity* **40**, 681–691 (2014).
90. C. R. Kahl, A. R. Means, Regulation of cell cycle progression by calcium/calmodulin-dependent pathways. *Endocr. Rev.* **24**, 719–736 (2003).
91. A. K. Khanna, J. D. Hosenpud, Cyclosporine induces the expression of the cyclin inhibitor p21. *Transplantation* **67**, 1262–1268 (1999).
92. D. M. Jelley-Gibbs, D. M. Brown, J. P. Dibble, L. Haynes, S. M. Eaton, S. L. Swain, Unexpected prolonged presentation of influenza antigens promotes CD4 T cell memory generation. *J. Exp. Med.* **202**, 697–706 (2005).
93. L. Desvignes, C. Weidinger, P. Shaw, M. Vaeth, T. Ribierre, M. Liu, T. Fergus, L. Kozhaya, L. McVoy, D. Unutmaz, J. D. Ernst, S. Feske, STIM1 controls T cell-mediated immune regulation and inflammation in chronic infection. *J. Clin. Invest.* **125**, 2347–2362 (2015).
94. W. C. Chang, C. H. Lee, T. Hirota, L. F. Wang, S. Doi, A. Miyatake, T. Enomoto, K. Tomita, M. Sakashita, T. Yamada, S. Fujieda, K. Ebe, H. Saeki, S. Takeuchi, M. Furue, W. C. Chen, Y. C. Chiu, W. P. Chang, C. H. Hong, E. Hsi, S. H. Juo, H. S. Yu, Y. Nakamura, M. Tamari, ORAI1 genetic polymorphisms associated with the susceptibility of atopic dermatitis in Japanese and Taiwanese populations. *PLOS ONE* **7**, e29387 (2012).
95. Y. C. Yeh, Y. P. Lin, H. Kramer, A. B. Parekh, Single-nucleotide polymorphisms in Orai1 associated with atopic dermatitis inhibit protein turnover, decrease calcium entry and disrupt calcium-dependent gene expression. *Hum. Mol. Genet.* **29**, 1808–1823 (2020).
96. A. S. Paller, J. M. Spergel, P. Mina-Osorio, A. D. Irvine, The atopic march and atopic multimorbidity: Many trajectories, many pathways. *J. Allergy Clin. Immunol.* **143**, 46–55 (2019).
97. M. Sutovska, M. Kocmalova, M. Joskova, M. Adamkov, S. Franova, The effect of long-term administered CRAC channels blocker on the functions of respiratory epithelium in guinea pig allergic asthma model. *Gen. Physiol. Biophys.* **34**, 167–176 (2015).
98. J. Di Capite, C. Nelson, G. Bates, A. B. Parekh, Targeting Ca^{2+} release-activated Ca^{2+} channel channels and leukotriene receptors provides a novel combination strategy for treating nasal polyposis. *J. Allergy Clin. Immunol.* **124**, 1014–1021.e1–3 (2009).
99. J. L. Di Capite, G. J. Bates, A. B. Parekh, Mast cell CRAC channel as a novel therapeutic target in allergy. *Curr. Opin. Allergy Clin. Immunol.* **11**, 33–38 (2011).
100. A. Somasundaram, A. K. Shum, H. J. McBride, J. A. Kessler, S. Feske, R. J. Miller, M. Prakriya, Store-operated CRAC channels regulate gene expression and proliferation in neural progenitor cells. *J. Neurosci.* **34**, 9107–9123 (2014).
101. S. Laffont, E. Blanquart, M. Savignac, C. Cenac, G. Laverny, D. Metzger, J. P. Girard, G. T. Belz, L. Pelletier, C. Seillet, J. C. Guery, Androgen signaling negatively controls group 2 innate lymphoid cells. *J. Exp. Med.* **214**, 1581–1592 (2017).
102. B. N. Melgert, D. S. Postma, I. Kuipers, M. Geerlings, M. A. Luinge, B. W. van der Strate, H. A. Kerstjens, W. Timens, M. N. Hylkema, Female mice are more susceptible to the development of allergic airway inflammation than male mice. *Clin. Exp. Allergy* **35**, 1496–1503 (2005).
103. U. Karakus, M. Crameri, C. Lanz, E. Yanguez, Propagation and titration of influenza viruses. *Methods Mol. Biol.* **1836**, 59–88 (2018).
104. A. Ballesteros-Tato, T. D. Randall, F. E. Lund, R. Spolski, W. J. Leonard, B. Leon, T follicular helper cell plasticity shapes pathogenic T helper 2 cell-mediated immunity to inhaled house dust mite. *Immunity* **44**, 259–273 (2016).
105. A. E. Kajon, A. P. Gigliotti, K. S. Harrod, Acute inflammatory response and remodeling of airway epithelium after subspecies B1 human adenovirus infection of the mouse lower respiratory tract. *J. Med. Virol.* **71**, 233–244 (2003).
106. C. A. Schneider, W. S. Rasband, K. W. Eliceiri, NIH Image to ImageJ: 25 years of image analysis. *Nat. Methods* **9**, 671–675 (2012).
107. D. I. Kim, M. K. Song, K. Lee, Comparison of asthma phenotypes in OVA-induced mice challenged via inhaled and intranasal routes. *BMC Pulm. Med.* **19**, 241 (2019).
108. W. Kujur, R. K. Gurram, N. Haleem, S. K. Maurya, J. N. Agrewala, Caerulomycin A inhibits Th2 cell activity: A possible role in the management of asthma. *Sci. Rep.* **5**, 15396 (2015).
109. J. Lian, M. Cuk, S. Kahlfuss, L. Kozhaya, M. Vaeth, F. Rieux-Laucat, C. Picard, M. J. Benson, A. Jakovcevic, K. Bilic, I. Martinac, P. Stathopulos, I. Kacskovics, T. Vraetz, C. Speckmann, S. Ehl, T. Issekutz, D. Unutmaz, S. Feske, ORAI1 mutations abolishing store-operated Ca^{2+} entry cause anhidrotic ectodermal dysplasia with immunodeficiency. *J. Allergy Clin. Immunol.* **142**, 1297–1310.e11 (2018).
110. A. M. Bolger, M. Lohse, B. Usadel, Trimmomatic: A flexible trimmer for Illumina sequence data. *Bioinformatics* **30**, 2114–2120 (2014).
111. A. Dobin, C. A. Davis, F. Schlesinger, J. Drenkow, C. Zaleski, S. Jha, P. Batut, M. Chaisson, T. R. Gingeras, STAR: Ultrafast universal RNA-seq aligner. *Bioinformatics* **29**, 15–21 (2013).

112. A. Subramanian, P. Tamayo, V. K. Mootha, S. Mukherjee, B. L. Ebert, M. A. Gillette, A. Paulovich, S. L. Pomeroy, T. R. Golub, E. S. Lander, J. P. Mesirov, Gene set enrichment analysis: A knowledge-based approach for interpreting genome-wide expression profiles. *Proc. Natl. Acad. Sci. U.S.A.* **102**, 15545–15550 (2005).
113. E. Y. Chen, C. M. Tan, Y. Kou, Q. Duan, Z. Wang, G. V. Meirelles, N. R. Clark, A. Ma'ayan, Enrichr: Interactive and collaborative HTML5 gene list enrichment analysis tool. *BMC Bioinformatics* **14**, 128 (2013).
114. A. Kramer, J. Green, J. Pollard Jr., S. Tugendreich, Causal analysis approaches in Ingenuity Pathway Analysis. *Bioinformatics* **30**, 523–530 (2014).
115. A. R. Abbas, D. Baldwin, Y. Ma, W. Ouyang, A. Gurney, F. Martin, S. Fong, M. van Lookeren Campagne, P. Godowski, P. M. Williams, A. C. Chan, H. F. Clark, Immune response in silico (IRIS): Immune-specific genes identified from a compendium of microarray expression data. *Genes Immun.* **6**, 319–331 (2005).
116. C. F. Schaefer, K. Anthony, S. Krupa, J. Buchoff, M. Day, T. Hannay, K. H. Buetow, PID: The pathway interaction database. *Nucleic Acids Res.* **37**, D674–D679 (2009).

Acknowledgments: We acknowledge technical support from the Experimental Pathology Research Laboratory (RRID:SCR_017928), Genome Technology Center (RRID: SCR_017929), and Cytometry and Cell Sorting Laboratory (RRID: SCR_017926) at NYU Langone Health. **Funding:** This study was funded by NIH grants AI097302 and AI130143 to S.F., AI150747 and AI121832 to P.G.T., and AI130343 and AI133076 to M.A.C.d.L. Additional funding was provided by postdoctoral fellowships from the German Research Foundation (DFG) to S.K. (KA 4514/1-1), M.V. (VA 882/1-1), and U.K. (KA 4083/2-1); postdoctoral fellowships from the SASS Foundation for Medical Research and the American Society of Hematology (ASH) to L.N.; and a Bernard Levine postdoctoral fellowship (NYU) to S.P.S. The Experimental Pathology Research Laboratory is partially supported by the Cancer Center Support Grant P30CA016087 at NYU Langone's Laura and Isaac Perlmutter Cancer Center. **Author contributions:** Y.-H.W., L.N., S.K., U.K., J.Z., M.M.-F., and M.V. conducted experiments. Y.-H.W., L.N., S.K., D.R., A.Y.T., U.K., M.M.-F., A.Y.T., I.S., F.Z., M.V., S.P.S., and S.F. analyzed data and interpreted the results. Y.-H.W., L.N., S.K., and S.F. designed the experiments. K.S., P.G.T., and M.A.C.d.L. provided reagents and expertise. S.K., L.N., and S.F. wrote the manuscript. All authors read and approved the final version of the manuscript. **Competing interests:** S.F. is a scientific cofounder of Calcimedica. K.S. is a co-founder and CSO of CalciMedica. P.G.T. is on the scientific advisory board of Immunoscape and Cytoagents and has consulted for Johnson and Johnson and PACT Pharma in the past 3 years. The other authors declare that they have no competing interests. **Data and materials availability**: All data needed to evaluate the conclusions in the paper are present in the paper and/or the Supplementary Materials. The RNA-seq data can be obtained in the Gene Expression Omnibus (GSE184228). CM4620 can be provided by CalciMedica pending scientific review and a completed material transfer agreement. Requests for the CM4620 should be submitted to: ken@calcimedica.com. A/HK/x31 can be provided by P.G.T. pending scientific review and a completed material transfer agreement. Requests for A/HK/x31 should be submitted to: paul.thomas@stjude.org.

Submitted 10 December 2021
Accepted 22 August 2022
Published 7 October 2022
10.1126/sciadv.abn6552

ScienceAdvances

Distinct roles of ORAI1 in T cell–mediated allergic airway inflammation and immunity to influenza A virus infection

Yin-Hu WangLucile NoyerSascha KahlfussDimitrius RaphaelAnthony Y. TaoUlrike KaufmannJingjie ZhuMarisa Mitchell-FlackIkjot SidhuFang ZhouMartin VaethPaul G. ThomasSean P. SaundersKenneth StaudermanMaria A. Curotto de LafailleStefan Feske

Sci. Adv., 8 (40), eabn6552. • DOI: 10.1126/sciadv.abn6552

Science Advances (ISSN) is published by the American Association for the Advancement of Science. 1200 New York Avenue NW, Washington, DC 20005. The title *Science Advances* is a registered trademark of AAAS.

Science Advances
AAAS

Supplementary Materials for

Distinct roles of ORAI1 in T cell–mediated allergic airway inflammation and immunity to influenza A virus infection

Yin-Hu Wang *et al.*

Corresponding author: Stefan Feske, feskes01@nyumc.org

Sci. Adv. **8**, eabn6552 (2022)
DOI: 10.1126/sciadv.abn6552

This PDF file includes:

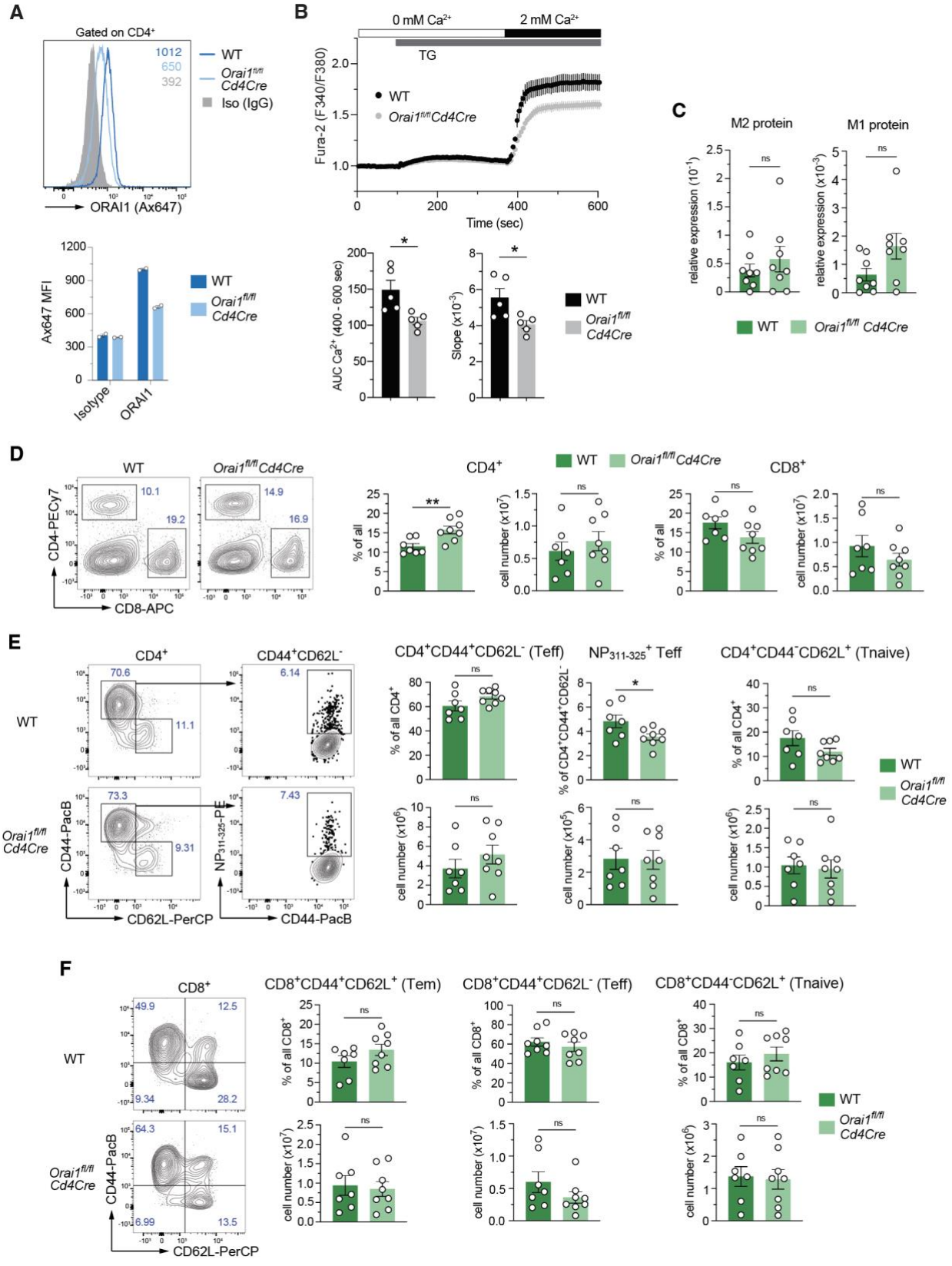

Supplementary Figure 1. Intact T cell mediated immune response to influenza A virus infection in in mice with T cell-specific deletion of *Orai1*. A, Representative flow cytometry plots and quantification of ORAI1 protein levels in *in vitro* differentiated Th2 cells from WT and *Orai1*$^{fl/fl}$*Cd4Cre* mice. Cell were

incubated with affinity-purified rabbit-anti-human ORAI1 antibody or rabbit IgG as isotype (iso) control. Data are representive of two repeat experiments. **B,** Cytosolic Ca^{2+} levels in naïve $CD4^+$ T cells isolated from the spleen of WT and *Orai1$^{fl/fl}$Cd4Cre* mice. T cells were loaded with Fura-2 and stimulated with 1 μM thapsigargin (TG) in Ca^{2+} free Ringer solution, followed by perfusion with 2 mM extracellular Ca^{2+}. Quantification of the area under the curve (AUC) and the slope of Ca^{2+} influx after Ca^{2+} readdition. Data are the mean ± SEM from 5 mice per genotype, pooled from 3 independent experiments. **C,** qRT-PCR analysis of IAV levels in total lung tissue from WT versus *Orai1$^{fl/fl}$Cd4Cre* mice at day 9 after infection with the x31 (H3N2) strain of influenza A virus (IAV). M2 and M1 proteins represent different genomic regions of IAV. **D,** Representative flow cytometry plots, frequencies and total numbers of $CD4^+$ and $CD8^+$ T cells in the lungs of WT and *Orai1$^{fl/fl}$Cd4Cre* mice 9 days after IAV infection. **E,** Representative flow cytometry plots, frequencies and numbers of total and IAV-specific (NP311-325 tetramer positive) $CD44^+CD62L^-$ effector (Teff) and $CD44^-CD62L^+$ naïve (Tnaive) $CD4^+$ T cells in lungs of WT and *Orai1$^{fl/fl}$Cd4Cre* mice at day 9 after IAV infection. **F**, Representative flow cytometry plots, frequencies and numbers of $CD44^+CD62L^+$ effector memory (Tem), $CD44^+CD62L^-$ effector (Teff) and $CD44^-CD62L^+$ naïve (Tnaive) $CD8^+$ T cells in lungs of WT and *Orai1$^{fl/fl}$Cd4Cre* mice at day 9 after IAV infection. Data in C are the mean ± SEM of 8 mice per cohort from 2 independent experiments. Data in D, E, F are the mean ± SEM from 7-8 mice per cohort from 2 independent experiments. Statistical analysis by paired (A) or unpaired (C-F) Student's t-test with the following significance levels: ***p<0.001 **p<0.01 *p<0.05. ns, not significant.

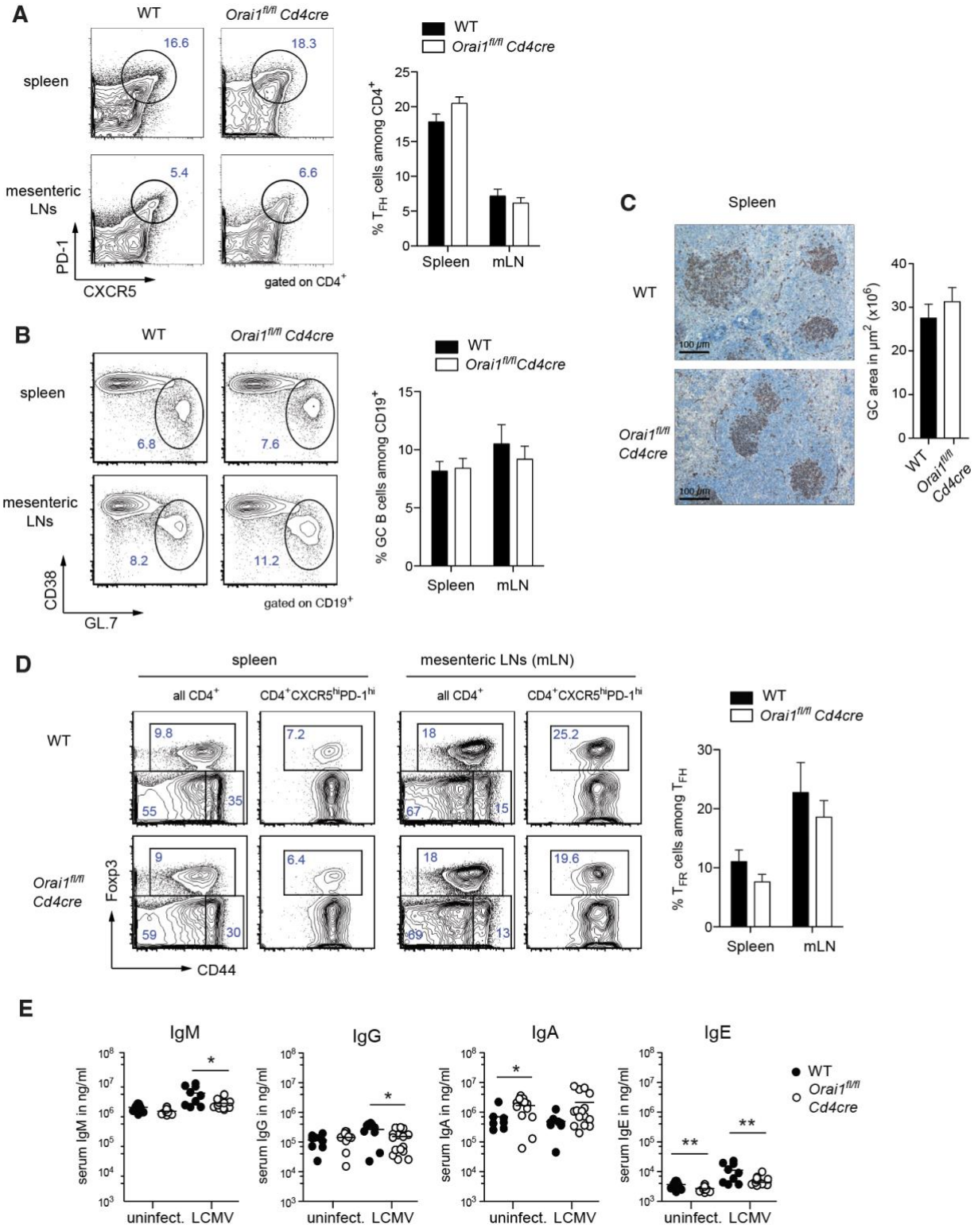

Supplementary Figure 2. T cell-specific deletion of *Orai1* does not impair adaptive immune responses to infection with lymphocytic choriomeningitis virus (LCMV). A, Frequencies of $CD4^+PD\text{-}1^{hi}CXCR5^{hi}$ T follicular helper (Tfh) cells in the spleens and mesenteric LNs (mLNs) of WT and *Orai1*$^{fl/fl}$*Cd4Cre* mice 10 days after infection with the Armstrong strain of LCMV. Data represent the mean ± SEM of 12-18 mice per group. **B,** Frequencies of $CD19^+CD38^-GL\text{-}7^+$ germinal center (GC) B cells in the spleens and mLNs of WT and *Orai1*$^{fl/fl}$*Cd4Cre* mice at day 10 p.i. Data are the mean ± SEM of 16-23 mice

per group. **C,** Representative immunohistochemistry staining for peanut agglutinin (PNA) of the spleens of WT and *Orai1*$^{fl/fl}$*Cd4Cre* mice 10 days after LCMV infection. **D,** Frequencies of CD4^{+}PD-1^{hi}CXCR5^{hi}CD44^{hi}FoxP3^{+} T follicular regulatory (Tfr) cells in the spleens and mLNs of WT and *Orai1*$^{fl/fl}$*Cd4Cre* mice at day 10 p.i. Data are the mean ± SEM of 12-16 mice per group. **E,** Total serum levels of IgM, IgG, IgA and IgE in WT and *Orai1*$^{fl/fl}$*Cd4Cre* mice before and 10 days after LCMV infection. Data are the mean ± SEM of 7-15 individual serum samples. Statistical analysis by unpaired Student's t-test with the following significance levels: *p<0.05, **p<0.01.

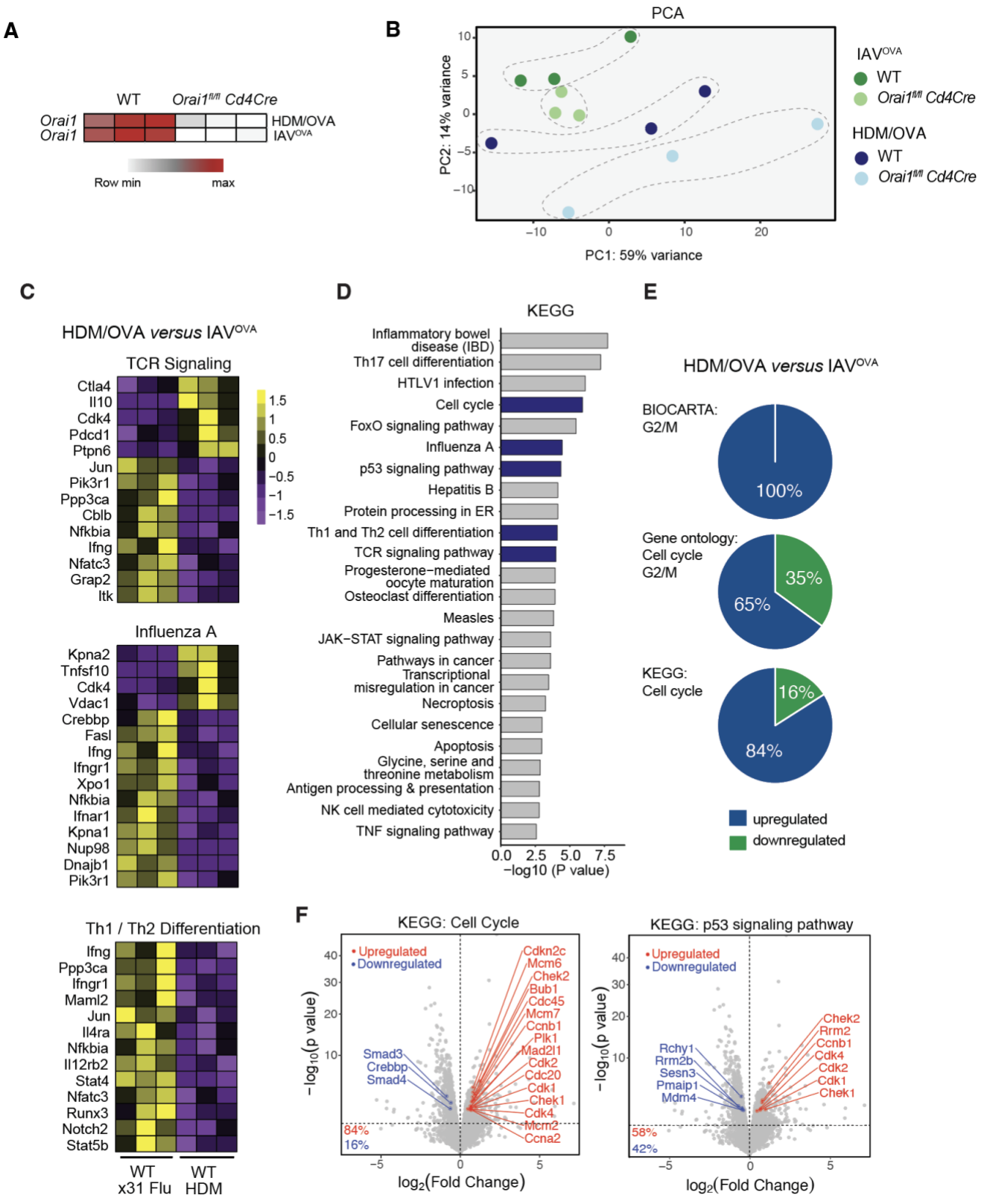

Supplementary Figure 3. ORAI1 regulates differential expression of cell cycle-associated genes in CD4$^+$ T cells after induction of allergic airway inflammation by HDM/OVA. A-B, RNA-Seq analysis of differentially expressed genes (DEG) in CD4$^+$ T cells of WT OT-II and *Orai1$^{fl/fl}$Cd4Cre* OT-II donor mice in

response to HDM/OVA immunization and IAV^{OVA} infection. The experimental designs are shown in Figure 3A,B. **A,** Heatmap showing normalized *Orai1* mRNA expression in $CD4^+$ T cells after HDM/OVA immunization or IAV^{OVA} infection. **B**, Principal component analysis (PCA) of the indicated groups. **C**, Heatmaps comparing expression of genes contained in the KEGG pathways *TCR signaling*, *Influenza A* and *Th1/Th2 Differentiation* in WT OT-II T cells after IAV^{OVA} infection and HDM/OVA treatment. **D**, Differentially regulated KEGG pathways in OT-II T cells from IAV^{OVA} infected and HDM/OVA treated mice ranked by the $-\log_{10}$ of *p* values. Statistical analysis by Fisher's exact test: $p < 0.1$. **E**, Percentage of up- and downregulated genes in the BIOCARTA pathway *Cell cycle G2M Checkpoint*, the Gene ontology pathway *Cell cycle G2/M* and the KEGG pathway *Cell cycle* in OT-II T cells from IAV^{OVA} infected and HDM/OVA treated mice. **F**, Differentially expressed genes (DEG) in OT-II T cells from IAV^{OVA} infected and HDM/OVA treated mice. DEG belonging to the KEGG pathways *Cell cycle* and *p53 signaling* that are up- and downregulated are indicated in red and blue, respectively. Data are from WT OT-II and *Orai1*$^{fl/fl}$*Cd4Cre* OT-II donor T cells isolated from 3 IAV^{OVA}-infected and 3 HDM/OVA-treated $TCR\alpha^{-/-}$ mice. Statistical analysis in D and F by Fisher's exact test using a *p* value cut-off < 0.1.

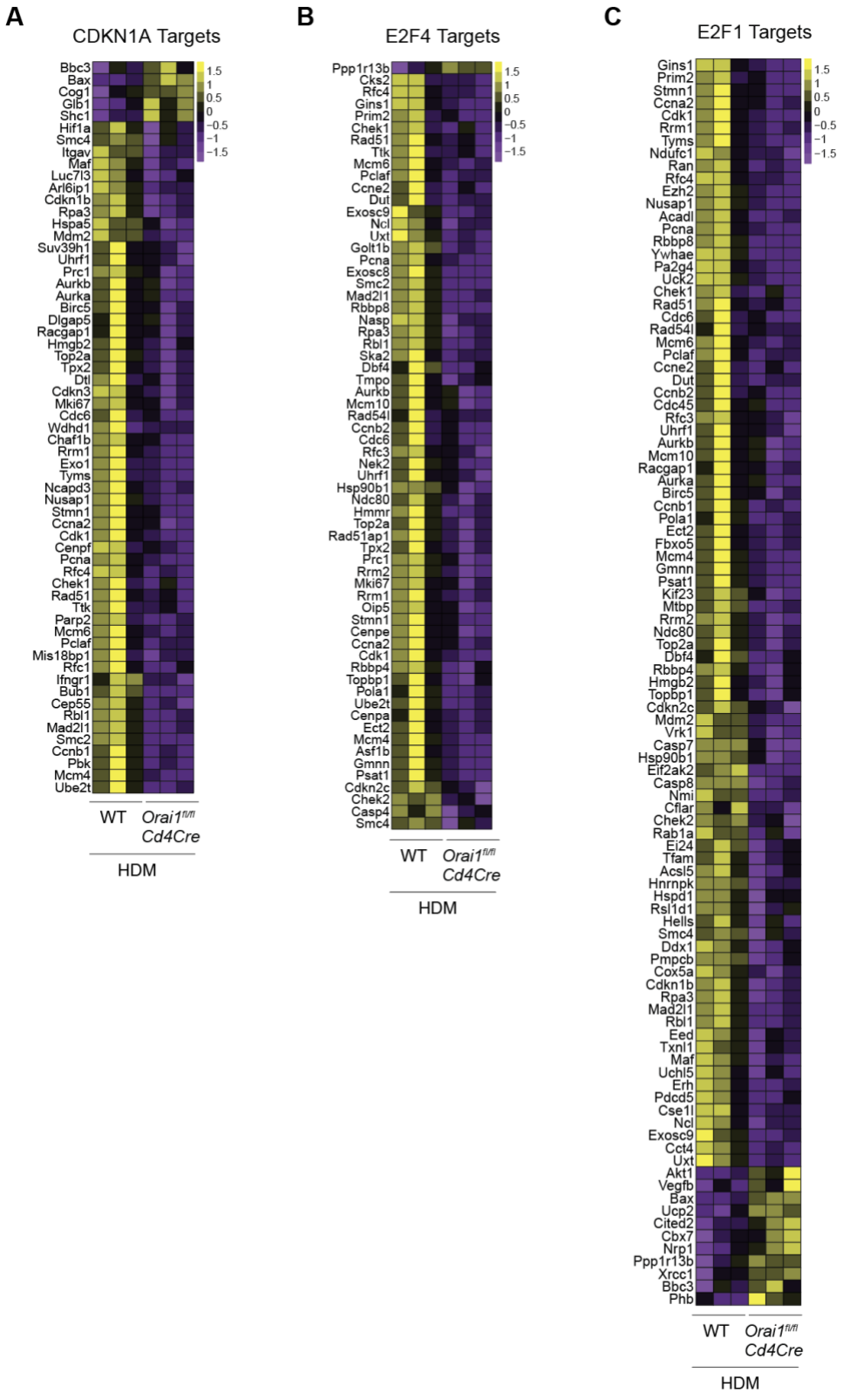

Supplementary Figure 4. ORAI1 regulates differential expression of targets genes of the cell cycle-regulators CDKN1A, E2F4 and E2F1 in pulmonary CD4$^+$ T cells after immunization with HDM/OVA. RNA-Seq data are from the same experiment described in Supplementary Fig.4. Heatmaps of DEG regulated by CDKN1A **(A)**, E2F4 **(B)** and E2F1 **(C)** in WT and *Orai1*-deficient CD4$^+$ T cells after HDM/OVA immunization. Colors represent the Z score expression relative to average expression per row.

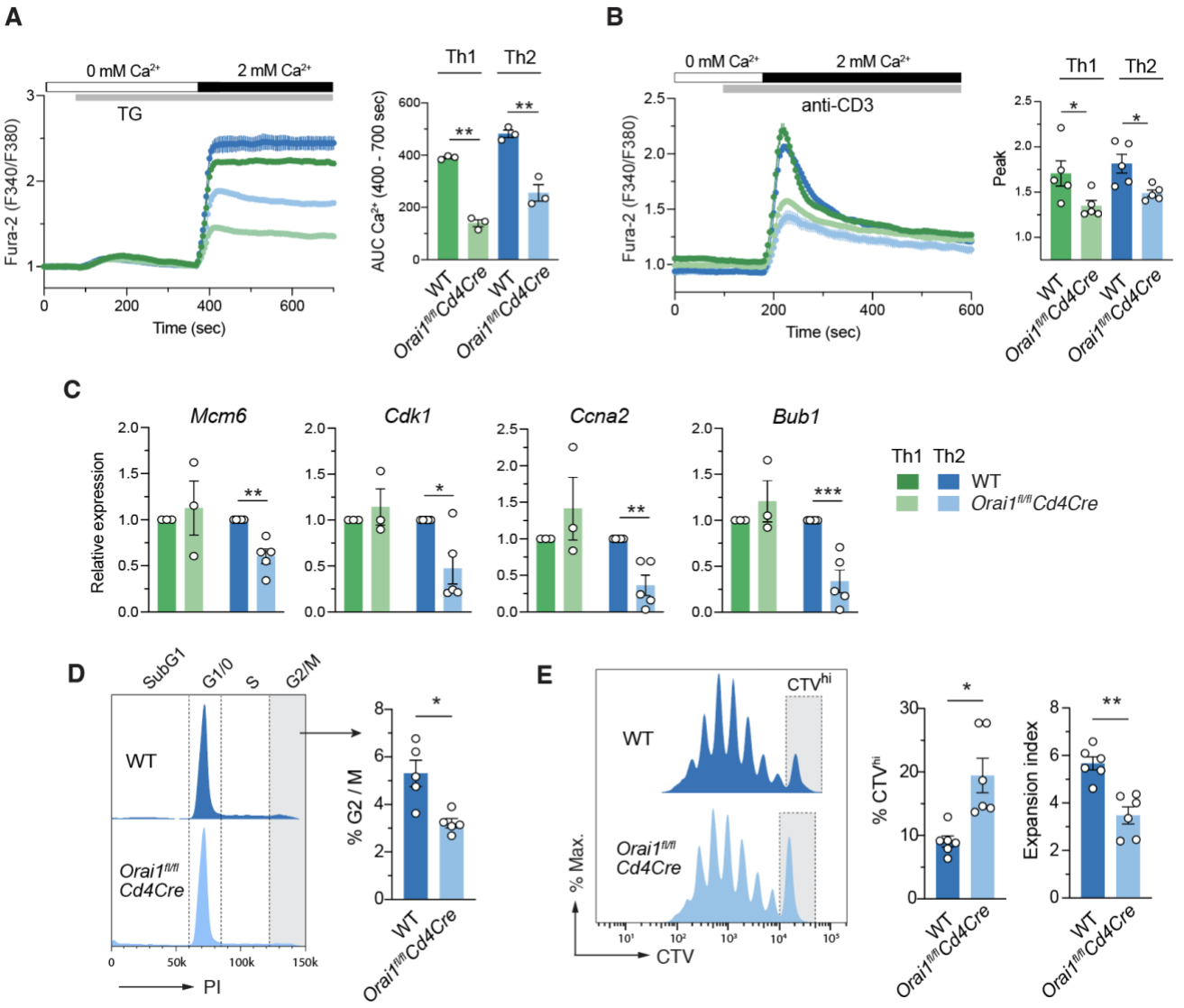

Supplementary Figure 5. ORAI1 regulates the expression of cell cycle-regulating genes and the proliferation of Th2 cells. A-B, Cytosolic Ca^{2+} levels in Th1 and Th2 cells derived from $CD4^+$ T cells of WT and *Orai1*$^{fl/fl}$*Cd4Cre* mice. T cells were loaded with Fura-2 and stimulated with 1 μM thapsigargin (TG) **(A)** or anti-CD3 crosslinking **(B)** in Ca^{2+} free Ringer solution, followed by readdition of 2 mM extracellular Ca^{2+}. Quantification of the area under the curve (AUC, in **A**) or peak (**B**) following Ca^{2+} readdition. **C**, Cell cycle-regulating genes identified by RNA-Seq were analyzed for mRNA levels by qRT-PCR in Th1 and Th2 cells of WT and *Orai1*$^{fl/fl}$*Cd4Cre* mice at day 5 of *in vitro* polarization. Expression levels were normalized to *Rpl32* house keeping gene and WT T cells. **D,** Cell cycle analysis of WT and *Orai1*$^{fl/fl}$*Cd4Cre* mice 3 days following stimulation with anti-CD3 and anti-CD28 dynabeads (T cell : dynabead ratio of 1:4) in the presence of IL-4 and anti-IFNγ. Cells were stained with propidium iodide on day 3 post-stimulation. **E,** Proliferation of Th2 cells of WT and *Orai1*$^{fl/fl}$*Cd4Cre* mice following stimulation as in (C). T cells were loaded with CellTrace Violet (CTV) and analyzed at day 4 post-stimulation. Data in A-E are the mean ± SEM from 3-6 mice per genotype, pooled from 3-4 independent experiments. Statistical analysis by paired (A,B,D,E) or unpaired (C) Student's t-test with the following significance levels: ***p<0.001 **p<0.01 *p<0.05.

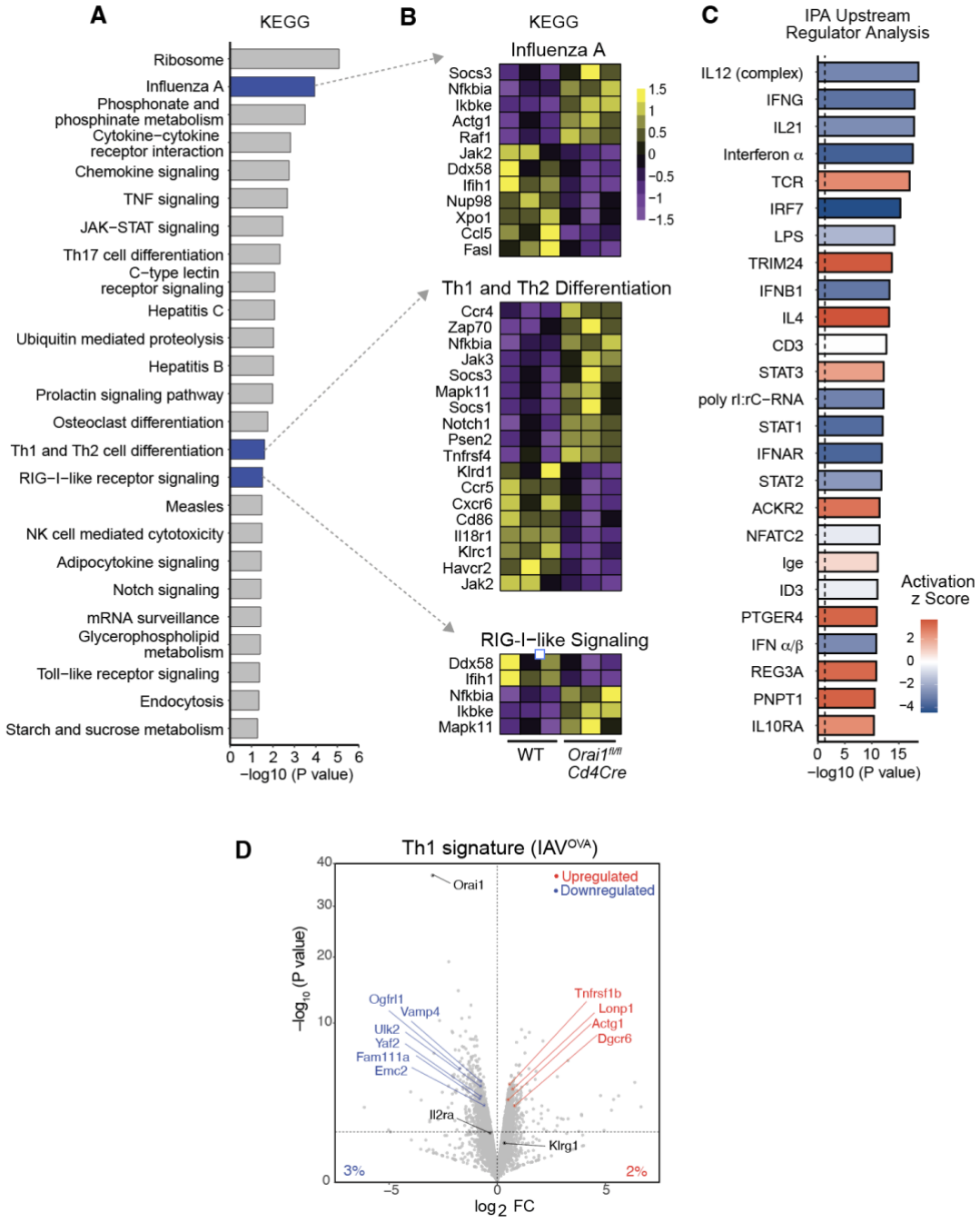

Supplementary Figure 6. Dysregulated gene expression and signaling pathways in *Orai1*-deficient T cells after IAV infection. Analysis of differentially expressed genes (DEG) and pathways in WT OT-II and *Orai1*$^{fl/fl}$*Cd4Cre* OT-II donor CD4^{+} T cells isolated from TCR$\alpha^{-/-}$ recipient mice following IAV^{OVA} infection. The experimental design is shown in Figure 3A. **A,** KEGG pathway analysis comparing WT and Orai1-deficient T cells. Shown are the top 25 deregulated pathways ranked by *p* value. **B**, Heatmaps of DEG included in the KEGG pathways *Influenza A*, *Th1/Th2 Differentiation* and *RIG-I-like Signaling* shown in (A). **C**, IPA Upstream Regulator Analysis of DEG in WT OT-II and *Orai1*$^{fl/fl}$*Cd4Cre* OT-II CD4^{+} T cells after IAV^{OVA} infection. Upstream regulators are ranked by *p* value. Colors indicate the activation Z score. **D,** Volcano plot of DEG (in gray) in WT OT-II and *Orai1*$^{fl/fl}$*Cd4Cre* OT-II CD4^{+} T cells following infection with IAV^{OVA}. DEG belonging to the Th1 signature *Th1 vs naive CD4 Tcell up* (M3376) published in *(76)* that are upregulated in *Orai1*-deficient T cells are indicated in red; downregulated DEG are shown in blue. Data in A-D are from 3 IAV^{OVA} infected mice per cohort. Statistical analysis in A and C by Fisher's exact test using a *p* value cut-off < 0.1.

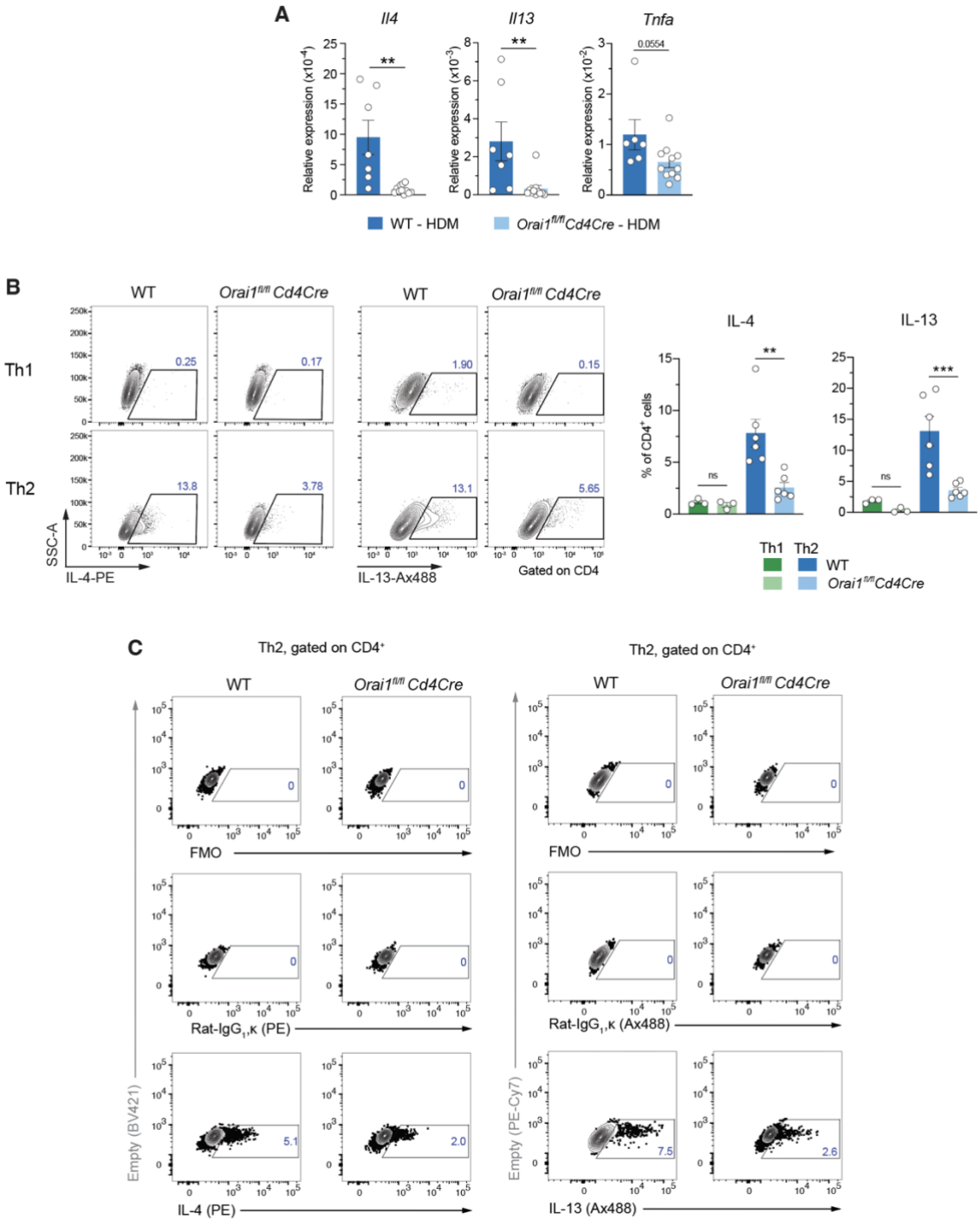

Supplementary Figure 7. ORAI1 is required for the production of cytokines by Th2 cells *in vitro* and *in vivo*. A, Expression of cytokine genes in whole lung tissue of WT and *Orai1*$^{fl/fl}$*Cd4Cre* mice after HDM challenge analyzed by qRT-PCR. **B,** Representative flow cytometry plots and frequencies of intracellular IL-4 and IL-13 cytokine staining in CD4$^+$ T cells of WT and *Orai1*$^{fl/fl}$*Cd4Cre* mice that were polarized into Th1 and Th2 cells *in vitro* and analyzed after 5 days and stimulation with PMA/ionomycin for 4h. **C**, Representative flow cytometry plots of IL-4 and IL-13 production by CD4$^+$ T cells from WT and *Orai1*$^{fl/fl}$*Cd4Cre* mice that were differentiated into Th2 cells for 5 days *in vitro* and stimulated with PMA/ionomycin for 4h. The isotype control antibodies are rat IgG$_{1,\kappa}$ conjugated with PE or Ax488. Fluorescence minus one (FMO) was determined by staining with anti-CD4 (APC-Cy7), and LIVE/DEAD™ Fixable Blue Dead Cell Stain without either anti-IL-4 or anti-IL-13. Data are the mean ± SEM of 3-6 mice per genotype from at least 3 independent experiments. Statistical analysis by unpaired Student's t-test with the following significance levels: ***$p < 0.001$; **$p < 0.01$; *$p<0.05$.

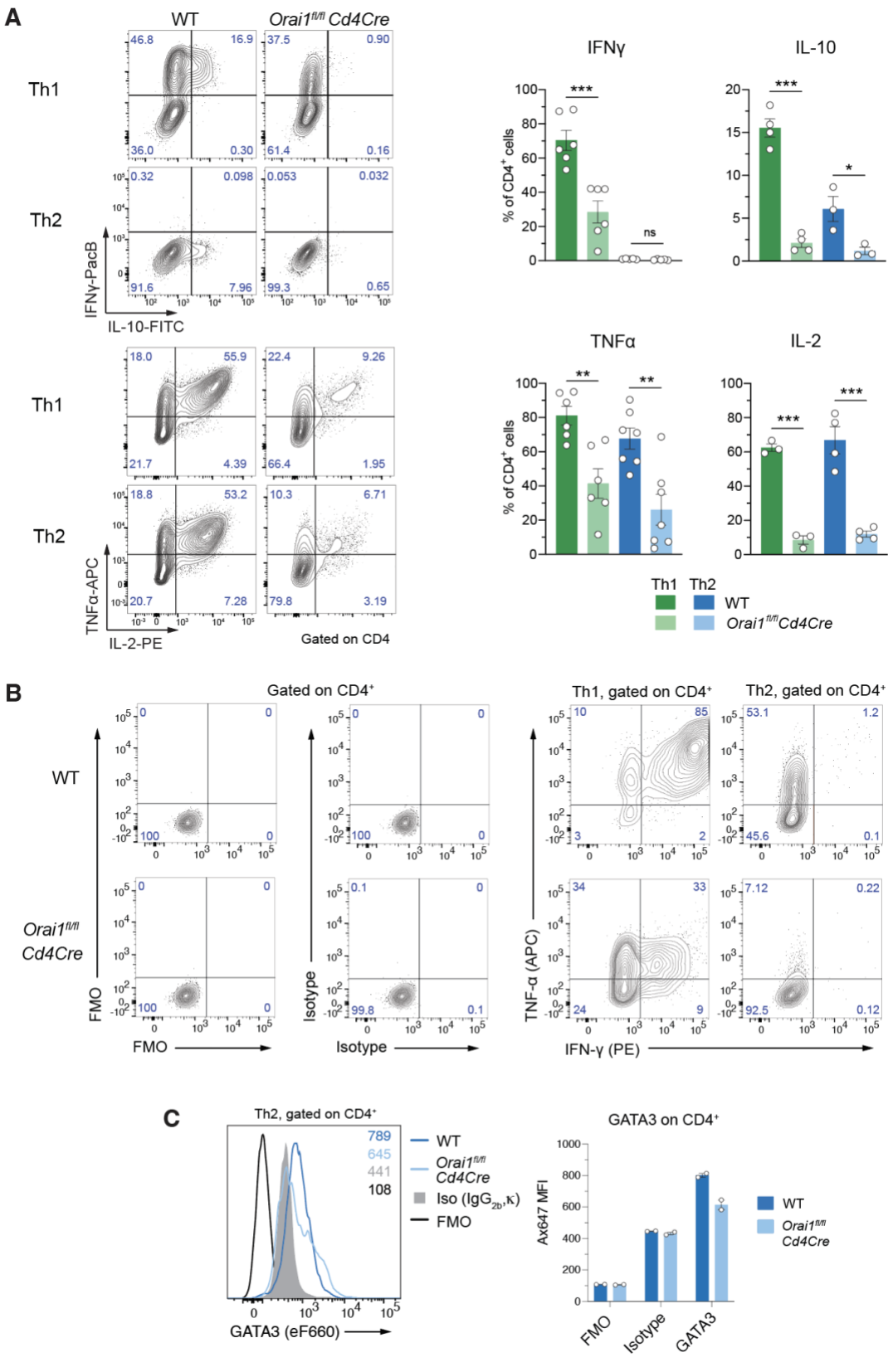

Supplementary Figure 8. ORAI1 is required for cytokine production by Th1 and Th2 cells. A, Representative flow cytometry plots and frequencies of IFNγ, IL-10, TNFα and IL-2 producing $CD4^+$ Th1 and Th2 cells *in vitro* that were analyzed after 5 days of polarization *in vitro* and stimulation with PMA/ionomycin for 4h. **B,** Representative flow cytometry plots of TNFα and IFNγ producing $CD4^+$ T cells

from WT and *Orai1*$^{fl/fl}$*Cd4Cre* mice that were differentiated into Th1 and Th2 cells *in vitro* for 3 days. The isotype control for cytokine antibodies was rat IgG_1,κ conjugated with APC or PE. FMO was determined by staining with anti-CD4 (APC-Cy7), and LIVE/DEAD™ Fixable Blue Dead Cell Stain without either anti-TNF-α or anti-IFN-γ. **C,** GATA3 protein levels in $CD4^+$ T cells from WT and *Orai1*$^{fl/fl}$*Cd4Cre* mice that were differentiated into Th2 cells for 5 days *in vitro.* The isotype control for anti-GATA3 antibody is rat IgG_2b,κ conjugated with eF660. FMO was determined by staining with anti-CD4 (APC-Cy7) antibody without anti-GATA3 (eF660). Data are the mean ± SEM of 3-7 mice per genotype from at least 3 independent experiments. Statistical analysis by unpaired Student's t-test with the following significance levels: ***$p < 0.001$; **$p < 0.01$; *$p<0.05$.

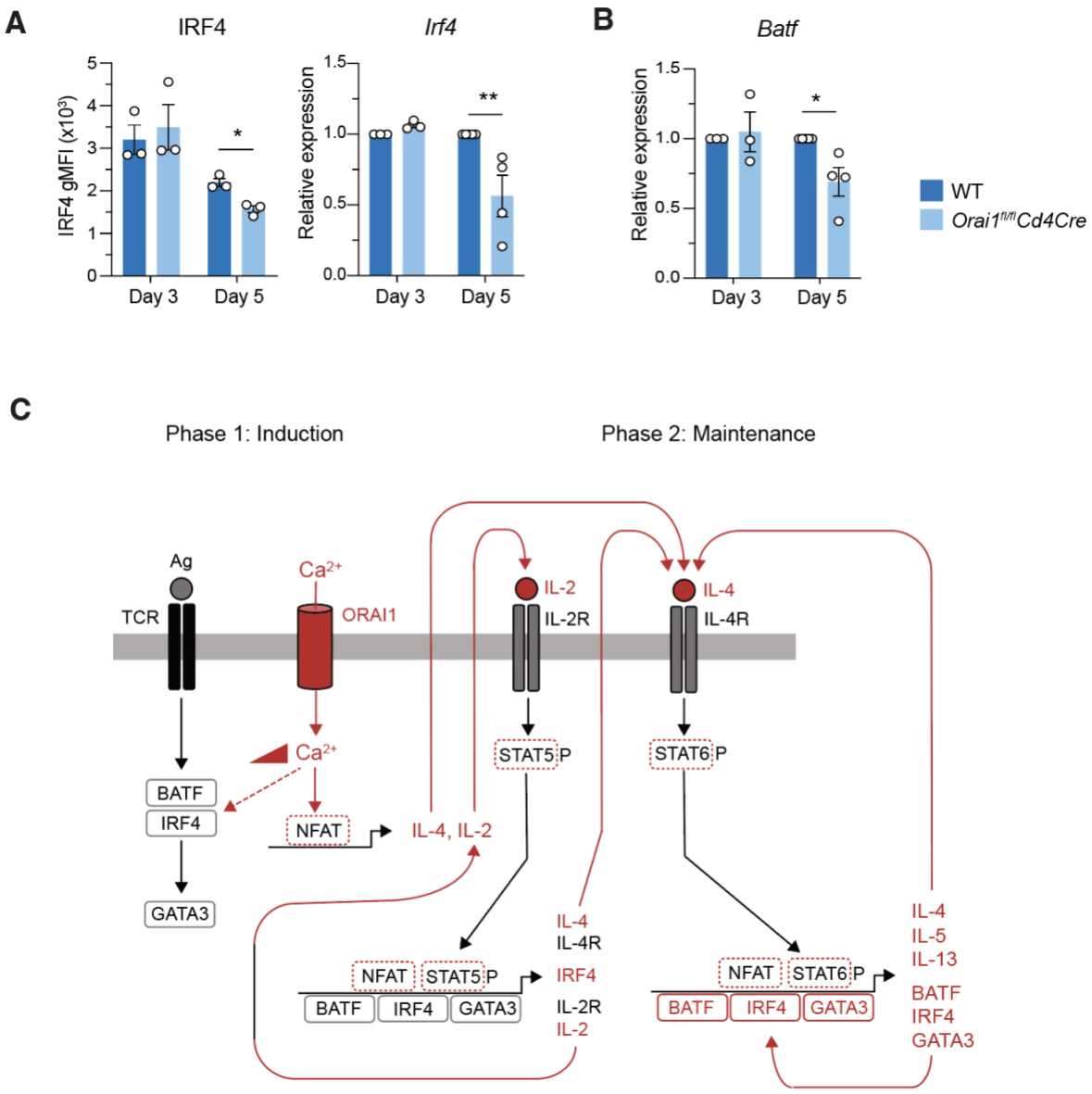

Supplementary Figure 9. ORAI1 is required for the maintenance of GATA3, IRF4 and BATF expression by Th2 cells *in vitro*. A,B, Analysis of IRF4 and BATF expression by $CD4^+$ T cells of WT and *Orai1$^{fl/fl}$Cd4Cre* mice that were polarized into Th2 cells (IL-4, anti-IFNγ) *in vitro* and analyzed at days 3 and 5 in culture. **A,** Representative histogram plots and quantification of IRF4 protein levels (MFI) analyzed by flow cytometry (left) and *Irf4* mRNA expression analyzed by qRT-PCR (right), normalized to RPL32 and WT. **B**, *Batf* mRNA expression analyzed by qRT-PCR, normalized to *Rpl32* house keeping gene and WT T cells. Data in A and B are the mean ± SEM of 3-4 mice per genotype from at least 3 representative experiments. Statistical analysis by 2-way ANOVA with Sidak's multiple comparison (mRNA in A,B) and paired Student's t-test (protein in A). ***p<0.001 **p<0.01 *p<0.05. **C,** Proposed model of the effects of ORAI1 and SOCE on Th2 cell differentiation and maintenance. Cytokines, transcription factors and pathways shown in red are decreased in the absence of ORAI1. Dashed red boxes indicate molecules whose function is presumed to be impaired but that were not measured directly. The red triangle and dashed line downstream of Ca^{2+} indicate that BATF and IRF4 expression requires SOCE as shown in *(9)* but is not impaired in the absence of ORAI1 and partial reduction of SOCE during initial T cell activation.

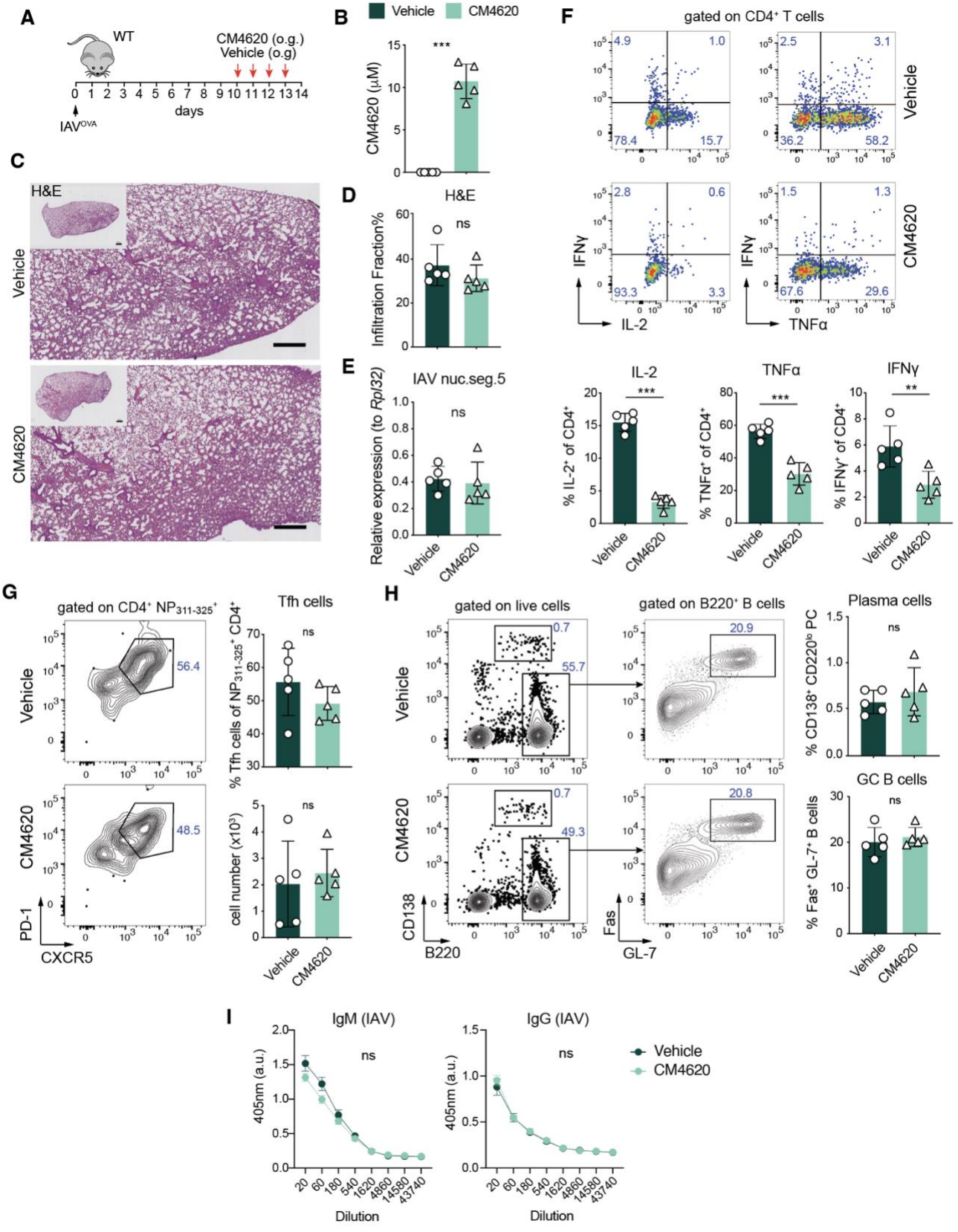

Supplementary Figure 10. Pharmacological CRAC channel inhibition does not compromise adaptive immunity to influenza A virus infection. A, Protocol used for infection of wildtype (WT) C57BL/6J mice with the x31 (H3N2) strain of influenza A virus (IAV). Mice were treated with 25 mg per kg

bodyweight of CM4620 or vehicle alone by oral gavage (o.g.) on four consecutive days and analyzed 14 days p.i. **B,** Concentrations of CM4620 in the serum of mice measured by LC-MS. **C**, Representative H&E stains of lung sections of mice. Scale bars represents 500 µm. **D,** Percentage of lung area with leukocyte infiltration based on H&E stains in (C). **E,** Virus burdens in the lungs of mice treated with CM4620 or vehicle at day 14 p.i. measured by qRT-PCR of nuclear segment 5 of IAV. **F,** Frequencies of $CD4^+$ T cells producing IL-2, IFN-γ and TNF-α. T cells were isolated from the lungs of mice at day 14 p.i. and restimulated *in vitro* with PMA / ionomycin for 4h and analyzed by flow cytometry. **G,** Frequencies and total numbers of PD-1^+ $CXCR5^+$ T follicular helper (Tfh) cells specific for nuclear protein (NP) antigen of IAV that were isolated from the mediastinal lymph nodes (mLNs) of mice 14 days p.i. **H,** Frequencies of $B220^+$ GL-7^+ Fas^+ germinal center (GC) B cells and $B220^{int}$ $CD138^+$ plasma cells (PC) in the mLNs of mice. **I,** Serum levels of IAV-specific IgM and IgG antibodies at day 14 p.i. measured by ELISA. Data in D-I are the mean $\pm$ SEM of 5 mice per cohort from 2 independent experiments. Statistical analysis by unpaired Student's t-test: ***$p < 0.001$; **$p < 0.01$; *$p < 0.05$. ns, not significant.

SUPPLEMENTARY TABLES

Supplementary Table 1. Primers for realtime PCR.

Gene	Forward primer	Reverse primer
Il4	CGAGCTCACTCTCTGTGGTG	TGAACGAGGTCACAGGAGAA
Il13	CACACTCCATACCATGCTGC	TGTGTCTCTCCCTCTGACCC
Il5	CCCACGGACAGTTTGATTCT	GCAATGAGACGATGAGGCTT
Il6	TAGTCCTTCCTACCCCAATTTCC	TTGGTCCTTAGCCACTCCTTC
Tnfa	AGGGTCTGGGCCATAGAACT	CCACCACGCTCTTCTGTCTAC
Il33	ACTATGAGTCTCCCTGTCCTG	ACG TCA CCCCTTTGA AGC
Mcp1 (Ccl2)	TGATCCCAATGAGTAGGCTGGAG	ATGTCTGGACCCATTCCTTCTTG
Mcp3 (Ccl7)	CCTGGGAAGCTGTTATCTTCAA	TGGAGTTGGGGTTTTCATGTC
Eotaxin1 (Ccl11)	GCGCTTCTATTCCTGCTGCTCACGG	GTGGCATCCTGGACCCACTTCTTC
Eotaxin2 (Ccl24)	GCCTCCTTCTCCTGGTAGCCTGC	ATGGCCCTTCTTGGTGATGAAGAT
Rantes (Ccl5)	ATGAAGATCTCTGCAGCTGCCCT	ACTTCTTCTCTGGGTTGGCACACA
M2 protein (Ion channel)	AAGACCAATCCTGTCACCTCTGA	CAAAGCGTCTACGCTGCAGTCC
M1 protein (Matrix)	CCGAGATCGCACAGAGACTTGAAGAT	GGCAAGTGCACCAGCAGAATAACT
Segment 5 (nucleoprotein)	GCACGGTCAGCACTCATTCTGAG	GACCAAATGAAAACCCAGCTCA
Segment 7 (pre-mRNA M1 and M2)	AGCCAAGTGTACAGCCTAATC	CTTCAAATGCGGCAGAATGG
Segment 7 (pre-mRNA M1 and M2)	CAGATGGAGACTGATGGAGAAC	GGTGCACATTTGGATGTAGAATC
Gata3	AGGATGTCCCTGCTCTCCTT	GCCTGCGGACTCTACCATAA
Irf4	GCAATGGGAAACTCCGACAGT	CAGCGTCCTCCTCACGATTGT
Batf	GCGTTCTGTTTCTCCAGGTC	AGAGAGAAGAATCGCATCGC
Ccna2	GTGGTGATTCAAAACTGCCA	AGAGTGTGAAGATGCCCTGG
Mcm6	TGCACGAGCCTCTTCCCTACT	TCCCGCATGTCCATCTTATCA

Bub1	AGAATGCTCTGTCAGCTCATCT	TGTCTTCACTAACCCACTGCT
Cdk1	AGAAGGTACTTACGGTGTGGT	GAGAGATTTCCCGAATTGCAGT

Supplementary Table 2. Antibodies for flow cytometry.

Antigen	**Manufacturer**	**Clone**	**Conjugation**
B220	eBioscience	RA3-6B2	FITC
B220	eBioscience	RA3-6B2	PB
B220	Biolegend	RA3-6B2	BV510
BCL6	eBioscience	BCL-DWN	PE
BrdU	eBiosience	BU20A	FITC
CCR7	eBiosience	4B12	APC
CD11b	eBioscience	M1/70	PE-Cy7
CD11c	Biolegend	N418	FITC
CD16/32 (Fc block)	eBioscience	93	Non-conjugated
CD16/32 (Fc block)	BioXcell	2.4G2	Non-conjugated
CD38	eBioscience	90	APC
CD38	Biolegend	T10	PE-Cy7
CD4	eBioscience	GK1.5	PB
CD4	Biolegend	GK1.5	APC-Cy7
CD4	eBioscience	GK1.5	PE-Cy7
CD44	eBioscience	IM7	FITC
CD44	eBioscience	IM7	PB
CD44	eBioscience	IM7	PerCP-Cy5.5
CD44	eBioscience	IM7	PE-Cy7
CD62L	Biolegend	Mel-14	PerCP-Cy5.5
CD69	eBiosience	H1.2F3	FITC
CD69	eBiosience	H1.2F3	PE
CD8	eBioscience	53-6.7	PB
CD8	eBioscience	53-6.7	APC
CD8	eBioscience	53.6-7	PE
CD95(Fas)	BD Bioscience	Jo2	BV421
CD138	Biolegend	281-2	PE
CXCR5	eBioscience	SPRCL5	PerCP-eFluor™ 710
CXCR5	Biolegend	L138D7	BV421
FOXP3	eBioscience	FJK-16s	PE
GATA3	eBioscience	TWAJ	eFluor® 660

GL-7	Biolegend	GL7	Alexa-Fluor647
GL-7	Biolegend	GL7	FITC
GR-1 (Ly6G)	Biolegend	1A8	Alexa-Fluor647
IFN-γ	eBioscience	XMG1.2	APC
IFN-γ	Biolegend	XMG1.2	PE
IFN-γ	eBioscience	XMG1.2	PE
IFN-γ	Biolegend	XMG1.2	BV421
IL-10	Biolegend	JES5-16E3	FITC
IL-13	eBioscience	eBio13A	Alexa-Fluor488
IL-17A	Biolegend	TC11-18H10.1	FITC
IL-17A	eBioscience	eBio17B7	PerCP-Cy5.5
IL-2	eBioscience	JES6-5H4	FITC
IL-2	Biolegend	JES6-5H4	PE
IL-21	eBiosience	mhalx21	PE
IL-4	eBioscience	11B11	PE
IL-5	Biolegend	TRFK5	PE
IRF4	eBioscience	3E4	eFluor® 660
MHC II	eBioscience	25UG	PB
PD-1	Biolegend	29F.1A12	PE-Cy7
PD-1	eBioscience	J43	APC
Siglec-F	BD Biosciences	E50-2440	PE
T-bet	eBioscience	eBio4B10	PerCP-Cy5.5
T-bet	eBioscience	eBio4B10	PE
TNF-α	eBioscience	MP6-XT22	APC
Rat IgG1, κ Isotype Ctrl (for IL-13)	eBioscience	eBRG1	Alexa-Fluor488
Rat IgG1, κ Isotype Ctrl (for IL-4)	eBioscience	eBRG1	PE
Rat IgG1, κ Isotype Ctrl (for TNF-α)	eBioscience	eBRG1	APC
Rat IgG1, κ Isotype Ctrl (for IFN-γ)	Biolegend	RTK2071	PE
Rat IgG2b, κ Isotype Control (for GATA3)	eBioscience	eB149/10H5	eFluor 660
ORAI1 (custom-made)	Yenzym Antibodies	Polyclonal (YZ6856)	Non-conjugated
Normal rabbit IgG	Cell Signaling	Polyclonal (2729)	Non-conjugated
Goat anti rabbit IgG	Thermo Fisher	Polyclonal (A21244)	Alexa-Fluor647

Supplementary Table 3. MHC class II tetramers for flow cytometry.

Tetramer	Source	Model	Conjugation
I-A(b)AQVYSLIRPNENPAHK (NP311-25)	NIH Tetramer Core Facility	IVA	PE
I-A(b)AQVYSLIRPNENPAHK (NP311-25)	NIH Tetramer Core Facility	IVA	Alexa-Fluor647
I-A(b) / CQIYPPNVNKI (Derp1)	NIH Tetramer Core Facility	HDM	APC
I-A(b) / CQIYPPNVNKI (Derp1)	NIH Tetramer Core Facility	HDM	PE